Regulation of the ESCRT-III membrane scission machinery in *Saccharomyces cerevisiae*

By
Natalie K Johnson
B.A. Boston University, 2008

A thesis submitted to the
Faculty of the Graduate School of the
University of Colorado in partial fulfillment
of the requirement for the degree of
Doctor of Philosophy
Department of Molecular, Cellular, and Developmental Biology
2016

This thesis entitled:

Regulation of the ESCRT-III membrane scission machinery in *Saccharomyces cerevisiae*

written by Natalie K Johnson

has been approved for the

Department of Molecular, Cellular, and Developmental Biology

_____

Greg Odorizzi, Ph.D., Advisor

_____

Corrie Detweiler, PhD., Chair

Date: _____

The final copy has been examined by the signatories and we find that both the content and the form meet the acceptable presentation standards of scholarly work in the above mentioned disipline

Johnson, Natalie K. (Ph.D., Molecular, Cellular, and Developmental Biology)

Regulation of the ESCRT-III membrane scission machinery in *Saccharomyces cerevisiae*

Thesis directed by Professor Greg Odorizzi

Endosomal sorting complexes required for transport (ESCRTs) function at late endosomal multivesicular bodies (MVBs) to sort ubiquitinated transmembrane proteins into intraluminal vesicles (ILVs) prior to fusion with lysosomes, or the homologous organelle in yeast, the vacuole. There are four distinct ESCRT complexes (ESCRT-0, -I, -II, and -III) that each transiently associate with the cytosolic surface of endosome membranes without getting consumed by the forming ILV. ESCRT-0, -I, and -II each contain one or more subunits that bind ubiquitin to collectively sequester cargo into microdomains on the membrane. Were as ESCRT-0, -I, and -II are constitutively assembled complexes, electrostatic interactions within individual ESCRT-III subunits maintain the proteins as monomers in the cytosol. Autoinhibition of the ESCRT-III subunit Vps20 is relieved after binding ESCRT-II at endosomes, when then nucleates homo-polymerization of the most abundant protein of the ESCRT-III complex, Snf7. Cargo deubiquitination must precede membrane scission to replenish free ubiquitin levels available to the cell, and Doa4 is the hydrolase in *S. cerevisiae* to do this. I first show that ESCRT-III polymerization can be uncoupled from ILV formation if the cargo-sorting arm of the ESCRT pathway is disabled. I later show that Doa4 has an additional, non- catalytic function that stalls Snf7 depolymerization, and hence, ILV scission. Activated Vps20 directly binds Doa4 to inhibit both its catalytic and membrane scission stalling functions. My data provides insight into the relationship between cargo sorting, cargo deubiquitination, ESCRT-III assembly/ disassembly cycles, and ILV scission.

Table of Contents

Tables

Figures

Abbreviations

2μ	high copy number overexpression plasmid
Δ	deletion strain
β2AR	beta 2 adrenergic receptor
A_{600}	Absorbance at 600 nm
AAA	ATPase associated with a variety of cellular activities
ACAP1	ARF GAP with coiled-coil ankryin repeat and PH domain containing protein 1
ALIX	ALG-2 interacting protein X
AMSH	Associated molecule with the SH3 domain of STAM
AP	Adapter protein
ART	Arrestin related trafficking
ATP	Adenine triphosphate
BOD	Bro1 domain
Bro1	Bck1-like resistance to osmotic shock
CBZ-pheleu	dipeptide N-CBZ-L-phenyalanyl-L-leucine
CCVs	clathrin coated vesicles
CEN	centromeric low copy expression plasmid
CHMP	charged multivesicular body protein
CPS	carboxy peptidase S
CPY	carboxy peptidase Y
DIC	Differential interference contrast
DID	Doa4 independent degradation
DUB	deubiquitinating enzyme
EGFR	Epidermal growth factor receptor
ENaC	epithelial Na+ channel
Eps15	Epidermal growth factor receptor substrate 15
Epsin	Eps15 interacting protein
ER	endoplasmic reticulum
ESCRT	Endosomal sorting complex required for transport
GGA	Golgi-localized, gamma-ear-containing, Arf-binding
GLUE	GRAM-like ubiquitin binding in EAP45
GST	Glutathione S-transferase
HIV	human immunodeficiency virus
Hrs	hepatocyte growth factor receptor substrate
Hse	heat shock element
IB	immunoblot
ILV	intralumenal vesical
IP	immunoprecipitation
MIM	MIT interacting motif
MIT	microtubule interacting and trafficking
MPR	mannose-6-phosphate receptor
MVB	multivesicular body
NZF	Npl14 zinc finger
PBS	phosphate buffered saline

PH	plexstrin homology
PI3P	phosphatidyl inositol-3-phosphate
PRD	proline rich domain
Snf7	sucrose non-fermenting 7
STAM	signal transducing adapter molecule
TCA	trichloracteic acid
TEM	tranmission electron microscopy
TEN	tubular endosomal network
TfR	transferrin receptor
TGN	Trans Golgi network
Tsg	tumor suppressor gene
Ub	ubiquitin
UBD	ubiquitin binding domain
Vpl	vacuolar protein localization
Vps	vacuolar protein sorting
VPT	vacuolar protein targeting
VTE	vesicular tubular endosome
WT	wild-type

Chapter 1: Introduction

Endosomal vesicular transport

Vesicular trafficking is a primary mechanism to transfer proteins and lipids between subcellular compartments, such as the plasma membrane, the ER, the Golgi complex, endosomes, and the major hydrolytic organelle, lysosomes (or the homologous organelle in yeast, the vacuole). Endosome biogenesis results form the fusion of vesicles derived from the plasma membrane and the TGN. Entry to endosomes from the plasma membrane is achieved by a variety of mechanisms, including clathrin-mediated endocytosis, caveolin-mediated endocytosis, phagocytosis, and pinocytosis (Mellman 1996). Clathrin-mediated endocytosis has been studied in the greatest mechanistic detail and is considered to be the primary mechanism for internalization of receptors and other non-receptor transmembrane proteins from the plasma membrane. Clathrin coated vesicles (CCVs) from the TGN carry biosynthetic protein cargoes to endosomes, and although the details are more obscure, the sorting mechanisms for this route bear similarity to clathrin-mediated endocytosis.

Mature endosomes fuse with lysosomes, but prior to fusion, transmembrane protein cargoes are sorted for degradation or recycling at morphologically distinct domains: the vacuolar endosome and the tubular endosomal network (TEN). Degradation requires that all domains of the protein, both soluble and insoluble, be exposed to the lysosome lumen, which is achieved by sorting the cargoes into intralumenal vesicles (ILVs) that bud from the limiting membrane of the vacuolar

endosome into the lumen. Upon fusion between endosomes and lysosomes, ILVs and their transmembrane cargoes are exposed to the hydrolytic interior of the lysosome lumen. The TEN branches into multiple vesicular export pathways directed back to the plasma membrane and the Golgi (Bonifacino et al., 2006) (Figure 1.1).

Cytosolic factors recruited to the donor compartment remodel the membrane to generate a vesicle. Clathrin coats form vesicles (CCVs) that traffic between endosomes, the TGN, and the plasma membrane, and clathrin adapter proteins coordinate vesicle formation with cargo selection through interactions with ubiquitin (discussed below) or linear peptide motifs located on the cytosolic domains of target proteins (Bonifacino and Traub, 2003). One such clathrin adapter that sorts cargo for endocytosis is the AP-2 complex, which binds tyrosine or dileucine based motifs and interacts with additional adapters that bind ubiquitin (Bonifacino 2004; Kelley et al., 2011; Polo et al., 2002; MacGurn et al., 2012). Another clathrin adapter, the mammalian ARF GAP with coiled-coil ankyrin repeat and PH domain-containing protein 1 (ACAP1), recognizes phenyalanine-based sequences on transmembrane proteins at endosomes (Dai et al., 2004; Hsu et al., 2012). A model cargo that traverses this pathway is the human transferrin receptor (TfR), which is endocytosed and recycled to the plasma membrane in CCVs associated with AP-2 and ACAP1, respectively (Hsu et al., 2012).

Mannose-6-phosphate receptors (MPRs) are type-I integral membrane proteins that recognize the mannose-6-phosphate modifications received by newly synthesized soluble hydrolases in the mammalian Golgi (Seaman 2008). The monomeric Golgi-

localized, γ –Ear-containing, Arf-Binding (GGA) proteins are a family of clathrin adapters that bind ubiquitin (discussed below) and acidic cluster dileucine motifs to sort MPRs,

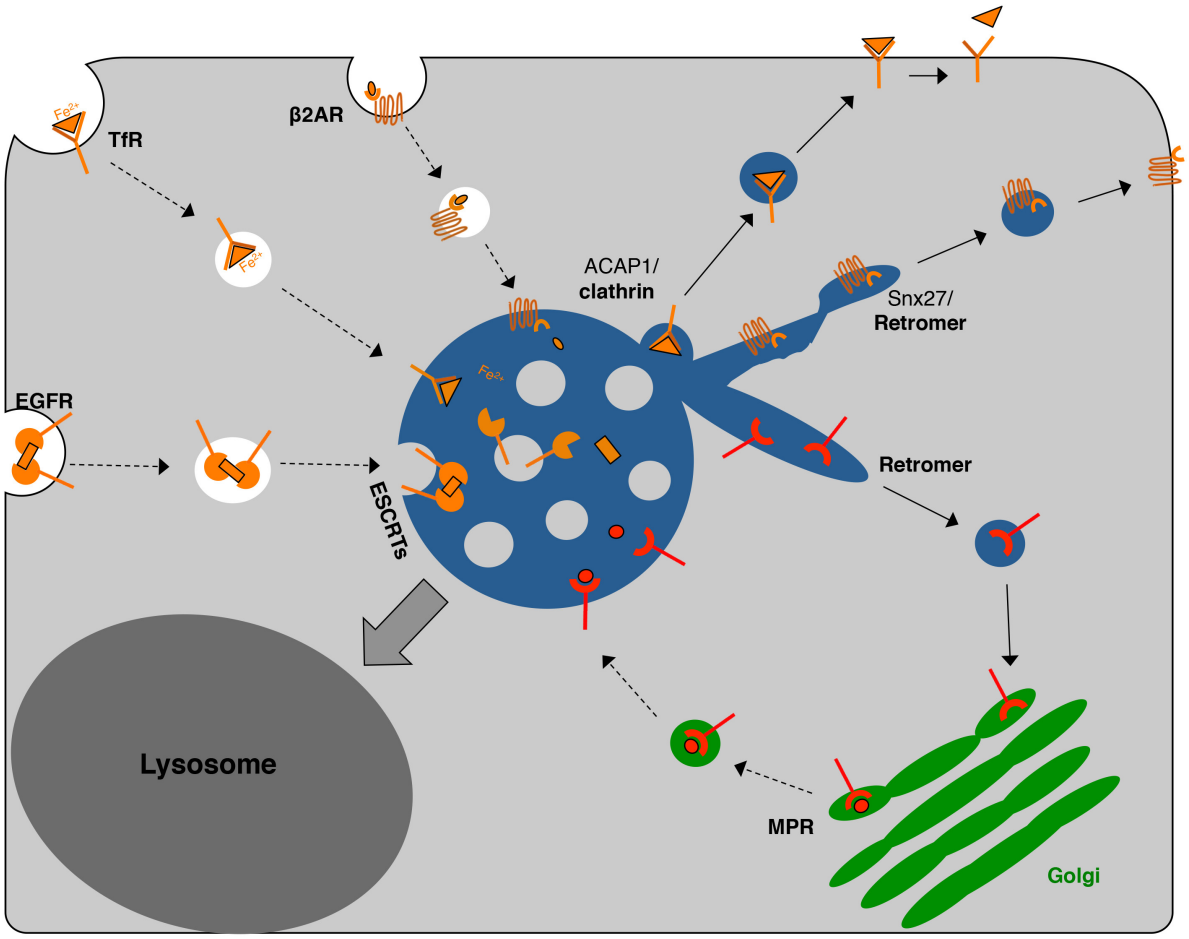

Figure 1.1. Endosomal vesicular transport pathways.
Diagram highlighting various vesicular transport pathways to and from endosomes in a mammalian cell. Clathrin coated vesicles (CCVs) originate from the plasma membrane carrying transmembrane cargoes such as activated signaling receptors (like EGFR or β2AR) or transporters (the TfR), or from the Golgi carrying transmembrane cargoes such as acid-hydrolase receptors (like mannose-6-phosphate receptors (MPR), and fuse with endosomes. Soluble ligands dissociate and transmembrane cargoes can be ensnared by the ESCRTs for entry into the ILV degradative pathway or sorted into various recycling pathways. Transmembrane cargo export from endosomes is mediated by retromer, clathrin, and various adapter proteins. Mature endosomes ultimately fuse with lysosomes and ILV content is degraded.

as well as the functionally equivalent vacuolar hydrolase receptor in yeast, Vps10, at the TGN for transport to endosomes (Seaman 2008; Marcusson et al., 1994; Cooper et al., 1996; Puertollano et al., 2001; Doray et al., 2002; Guo et al., 2014; Misra et al., 2002). Retromer is a coat-like protein complex that was initially shown to recycle Vps10 from endosomes to the TGN in yeast, and it was later shown to function similarly in MPR recycling in mammals (Johannes et al., 2008; Seaman et al., 1998; Seaman et al., 2004; Arighi et al., 2004). Historically, retromer is best known for its role in recycling transmembrane cargoes to the TGN, but it has more recently been shown to recycle the beta 2-adrenergic receptor (β2AR) from endosomes to the plasma membrane in mammalian cells (Temkin et al., 2011). It is not fully clear how retromer recognizes cargo for retrieval to the TGN, but interactions with hydrophobic peptide sequences have been implicated (Nothwher et al., 2000; Arighi et al., 2004; Seaman 2012). SNX27 is a retromer adaptor that binds the PSD95/Dlg1/ZO-1 (PDZ) domain of β2AR for plasma membrane recycling (Cao et al., 1999; Temkin et al., 2011).

Transmembrane cargo sorted for the alternative fate, degradation, are targeted by the Endosomal Sorting Complexes Required for Transport (ESCRTs), which are a cytosolic protein network that generate ILVs and bind ubiquitin to select for cargo. While ubiquitination and linear peptide motifs can redundantly target many transmembrane proteins to endosomes, ubiquitination is critical to target most transmembrane proteins into ILVs, and it is at this stage where ubiquitin's role in determining the fate of a transmembrane protein is greatest (Hurley 2011; Babst 2014). ESCRTs are discussed in more detail below.

Ubiquitin-mediated transmembrane protein trafficking

Ubiquitin is a 76 amino acid peptide that is post translationally conjugated to substrate proteins as a sorting signal. Ubiquitination targets transmembrane proteins into ILVs in a manner analogous to which ubiquitination targets soluble cytosolic proteins for degradation by proteasomes. Ubiquitin-mediated endocytosis remodels cellular responsiveness to extracellular stimuli by initiating down-regulation of activated signaling receptors as well as non-receptor transmembrane proteins, such as ion channels, transporters, and gap junction proteins (Hurley 2010). Ultimately, even long-lived transmembrane proteins or damaged transmembrane proteins are turned over via this mechanism as the means for their disposal.

Ubiquitination is a dynamic modification regulated by the activities of ubiquitin conjugating and deconjugating enzymes (Kelley et al., 2011; Clague et al., 2012). Ubiquitin forms an isopeptide bond with a lysine in the target protein by the sequential actions of three enzymes: a ubiquitin-activating enzyme (E1), a ubiquitin-conjugating enzyme (E2), and a ubiquitin-ligase (E3). E3 ligases impart substrate specificity for ubiquitin conjugation reactions (MacGurn et al., 2012; Clague et al., 2012). The ubiquitin modification is removed by the action of deubiquitinating proteases (DUBs), which catalyze hydrolysis of the covalent bond between ubiquitin and the target protein.

Ubiquitin ligases can engage transmembrane protein targets directly or indirectly. For example, WW domains on the ubiquitin ligase Nedd4-2 directly engage PY motifs (PPxY) on the mammalian epithelial sodium channel (ENaC) to initiate ubiquitin-dependent endocytosis (MacGurn et al., 2012). Rsp5 is the yeast Nedd4 homolog and

the sole ubiquitin ligase to function in the endolysosomal pathway. Several well-characterized Rsp5 substrates at the plasma membrane include the mating factor receptors Ste2 and Ste3, which like many Rsp5 substrates, lack PY motifs (Dunn and Hick, 2001). WW domains on Rsp5 engage PY motifs on adapter proteins of the arrestin-related trafficking (ART) family to mediate ubiquitin-dependent endocytosis (MacGurn et al., 2012; Lin et al., 2008).

How do ubiquitin ligases or ubiquitin ligase adapters in the cytosol recognize transmembrane proteins that are misfolded, or in need of downregulation? A recent study in yeast shows that ARTs drive ubiquitin conjugation in response to factors that are intrinsic to the target protein, such as misfolding, as well as by external factors, such as nutrient availability and ligand binding. (Keener and Babst, 2013; Babst 2014). The emerging model proposes that cell surface transmembrane proteins intrinsically detect any conformational change that deviates from the ground state (i.e. substrate binding or misfolding) and respond by exposing specific lysines to E3 ligases in the cytosol.

Discovery and characterization of Vacuolar Protein Sorting genes

The machinery that sorts ubiquitinated transmembrane cargoes into ILVs make up a subset of the vesicular trafficking genes that were identified from genetic screens in yeast looking at carboxy peptidase Y (CPY) secretion as a metric for vesicular trafficking fidelity in the biosynthetic pathway. CPY is a soluble hydrolase trafficked from the TGN to the vacuole via endosomes by the continuously recycled receptor Vps10 (discussed above), but CPY accumulates in the TGN and enters the default

secretory pathway when endosomal sorting is compromised (Stevens et al., 1982). To identify genes that function in biosynthetic trafficking, one research group mutatgenized a leucine-auxotrophic strain and screened for growth on media containing N-CBZ-L-phenylalanyl-L-leucine (CBZ-phleu), because CPY secretion liberates leucine from CBZ-phleu. The identified mutants fell into 19 complementation groups dubbed vacuolar protein localization genes (VPL) (Rothman and Stevens 1986). Another research group utilized a CPY-invertase fusion construct to identify spontaneous mutants that grow on sucrose as the only fermentable carbon source, because invertase hydrolyzes sucrose into glucose and fructose. 33 CPY-invertase secreting complementation groups were identified and named vacuolar protein targeting (VPT) genes (Bankaitis et al., 1986). 12 of the VPT complementation groups were also identified in the Stevens study, and the remaining 21 novel VPT complementation groups were pooled with the 19 VPL complementation groups and re-named vacuolar protein sorting (VPS) genes (Robinson et al., 1988).

Phenotypic analysis of vacuole morphology was used to functionally characterize the different VPS genes, which were then binned into 6 classes, A-F (Raymond et al., 1992, Seaman 2008). A subset of the VPS complementation groups, the class E VPS mutants, accumulate the transmembrane vacuolar hydrolase carboxy peptidase S (CPS) and the G-protein coupled mating factor receptor Ste2 at aberrant endosomal structures dubbed class E compartments, indicating the biosynthetic and endocytic transport pathways converge at endosomes prior to vacuole fusion (Odorizzi et al., 1998). The proteins encoded by the class E VPS genes make up the Endosomal Sorting Complexes Required for Transport (ESCRTs), which have the dual

responsibility of remodeling the endosomal limiting membrane to generate ILVs and for selecting transmembrane proteins to include in ILVs.

The ESCRT pathway to Lysosomal degradation

The budding of ILVs commences at early endosomes and seemingly proceeds throughout endosomal maturation, giving rise to late endosomes filled with ILVs; because of this distinctive morphology, late endosomes were originally termed multivesicular bodies (MVBs) in early electron microscopy studies (Palade 1955; Sotelo and Porter 1959). Both the budding of ILVs and the selection of ubiquitinated transmembrane protein cargoes are executed by the ESCRTs (Figure 1.2). Four distinct ESCRT complexes (ESCRT-0, -I, -II, and -III) and Vps4, a member of the AAA family of ATPases broadly thought to function in the disassembly, dissociation, or remodeling of macromolecular complexes, makeup this machinery that is transiently recruited to the cytosolic surface of the endosomal limiting membrane (Hurley 2010). The first ESCRT complex identified was yeast ESCRT-I, followed by yeast ESCRT complexes 0, II, and III (Katzmann et al., 2001; Bilodeau et al., 2002; Babst et al., 2002a; Babst et al., 2002b). A subset of the ESCRTs sort cargo, while others drive membrane remodeling, and through the combined actions of ESCRT-III and Vps4, the ILV is released into the endosome lumen.

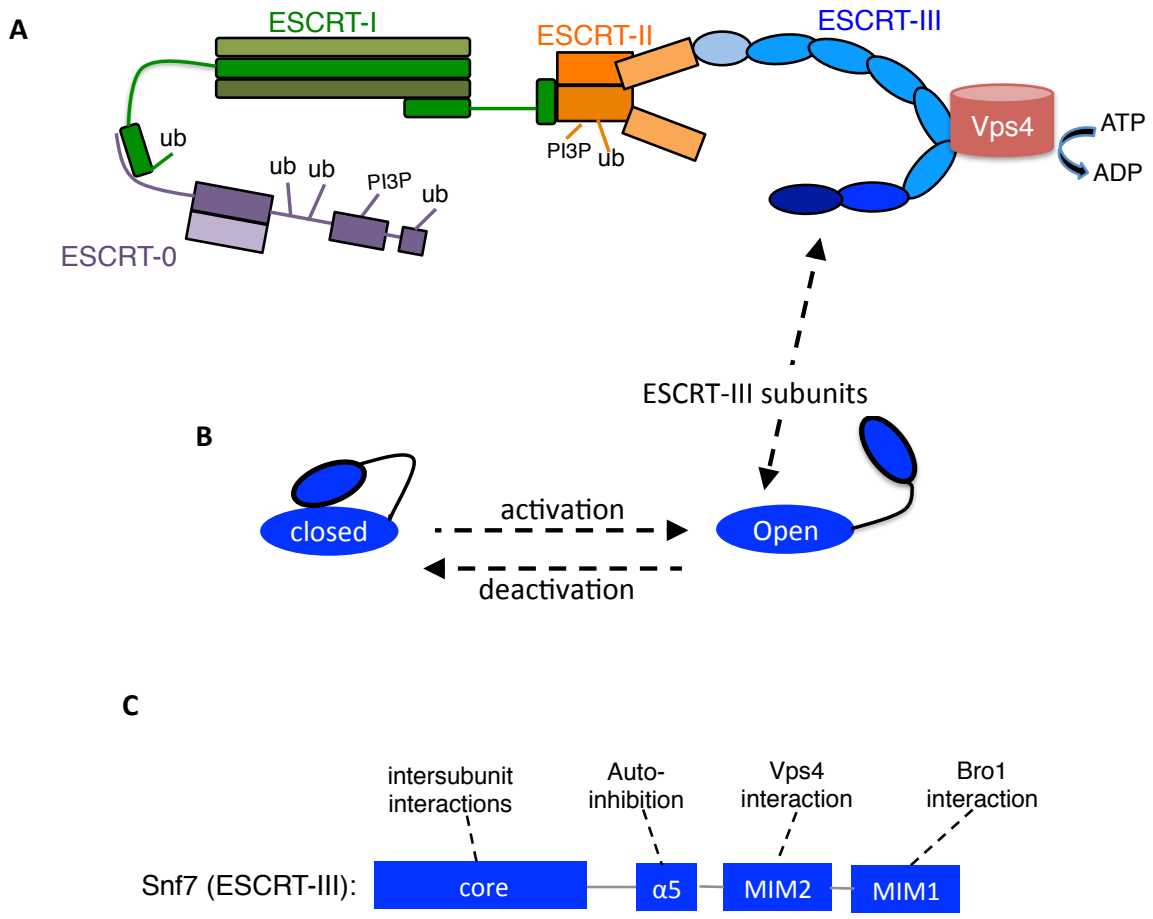

Figure 1.2. Domain interactions of the ESCRT complexes.
(A) Cartoon of the domain organization and interactions between ESCRT-0, -I, -II, -III, and the Vps4 oligomer. Adapted from Tang et al., 2016. (B) Model of ESCRT-III subunit conformations. (C) Domain organization and interactions of Snf7. Adapted from Tang et al., 2015.

Ubiquitinated transmembrane proteins delivered to endosomes engage ESCRT-0, -I, and –II, which each contain one or more subunits with ubiquitin-binding domains (UBDs), but the domains appear to be functionally redundant in yeast as cargo sorting is impaired only when multiple UBDs have been disabled in unison (Bilodeau et al., 2002; Katzmann et al., 2001; Alam et al., 2004; Shields et al., 2009). ESCRT-0 is a heterodimeric complex composed of Vps27 and Hse1 proteins in yeast, or their orthologs in mammals, HRS and STAM (Bilodeau et al., 2002; Bache et al., 2003*).* ESCRT-0 associates with early endosomes by virtue of the FYVE domain in its HRS/Vps27 subunit, which binds to PI(3)P enriched in endosomal membranes (Stahelin et al., 2002; Raiborg et al., 2001; Katzmann et al., 2003*)*. ESCRT-I is a heterotetrameric complex composed of Vps23, Vps28, Vps37, and Mvb12 proteins in yeast, or their orthologs in mammals TSG101, VPS28, VPS37, and MVB12, that form an extended stalk-like structure with ESCRT-0 bound at one end, and ESCRT-II bound at the other end (Katzmann et al., 2001; Kostelansky et al., 2007). ESCRT-II is a heterotetrameric complex composed of Vps22, Vps36, and two Vps25 proteins (Babst et al., 2002b). Current models based on studies of the yeast ESCRT complexes suggest that ESCRT-0 mediates recruitment of a super-complex comprised of ESCRT-I and –II. However, ESCRT-II can associate with endosomes and function independently of ESCRT-I, at least in yeast, and chapter 2 elaborates on the unique role of ESCRT-II in coordinating cargo selection with vesicle formation (Katzmann et al., 2003; Hurley 2010, Babst et al., 2002b; Im et al., 2008; Kostelansky et al., 2006; Mageswaren et al., 2015). In vitro studies using purified yeast ESCRT complexes added to synthetic

membranes indicate that ESCRT-I and -II have the potential to initiate ILV bud formation (Wollert et al., 2010; Rozycki et al., 2012). Incipient ILV buds, however, ultimately require ESCRT-III for their detachment into the compartment lumen (Wollert et al., 2009; 2010).

Unlike ESCRT-0, -I, and -II, ESCRT-III lacks UBDs and exists only transiently as a complex when its subunits are membrane-associated (Babst et al., 2002b). ESCRT-III subunits are homologous to one another. The subunits are highly flexible, consisting of six alpha helices, a basic N-terminus, and an acidic C-terminus that interacts in cis to prevent formation of higher order structures (Babst et al., 2002a). The closed/inactive conformation of each ESCRT-III subunit switches to an active conformation upon displacement of its autoinhibitory carboxyl (C)-terminus (Shim et al., 2007; Saksena et al., 2009). ESCRT-III in yeast consists of four core subunits and three peripheral subunits. Humans express 12 ESCRT-III subunits, also referred to as charged multi-vesicular body proteins (CHMPs). CHMPs are grouped into seven families of which CHMP1-6 have yeast orthologs (Hurley 2010).

Studies of yeast ESCRT-III proteins suggest initiation of complex assembly is driven by ESCRT-II binding the ESCRT-III subunit, Vps20 (CHMP6 in humans), which responds by switching to its open/active conformation (Babst et al., 2002a). Activated Vps20, in turn, nucleates the activation and homopolymerization of the ESCRT-III

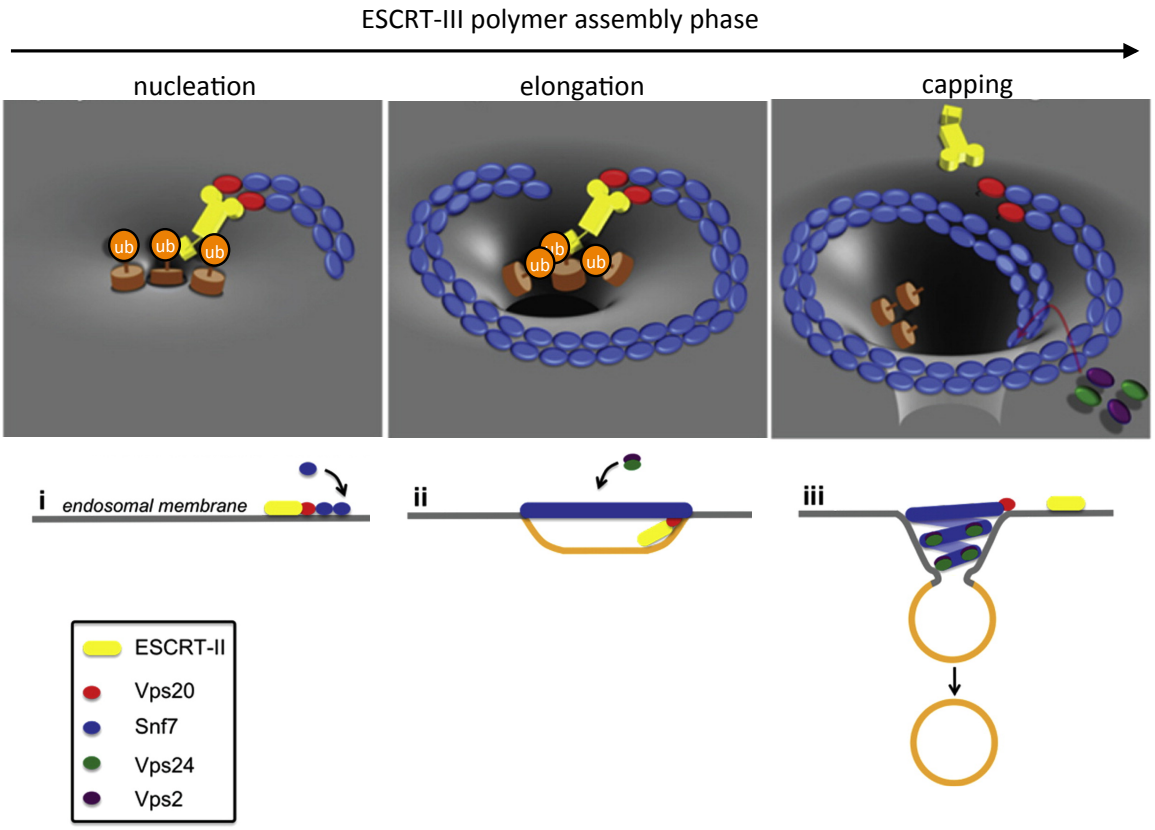

Figure 1.3. Phases of ESCRT-III oligomerization. (Top) Model of ubiquitinated transmembrane cargo, ESCRT-II, and ESCRT-III protein organization throughout ESCRT-III complex assembly as viewed from the surface of the endosomal limiting membrane. (Bottom) Model of the above cartoon from a “side” view highlighting the position of the budding ILV relative to the limiting membrane and lumen. Adapted from Henne et al., 2012.

subunit Snf7 (CHMP4A, 4B, and 4C in humans), which physically comprises the bulk of the ESCRT-III complex (Saksena et al., 2009; Teis et al., 2008). Termination, or capping, of Snf7 homo-polymerization occurs upon its association with the other two core subunits of ESCRT-III, Vps24 (CHMP3 in humans) and Vps2 (CHMP2A and 2B humans), and is followed by recruitment of Vps4 (Saksena et al., 2009). The biophysical mechanism by which ESCRT-III drives membrane scission is unresolved. ESCRT-III assembly is sufficient to catalyze ILV scission in vitro, but in vivo studies suggest a role for Vps4 (Wollert et al., 2009; Nickerson et al., 2010; Wemmer et al., 2011; Adell et al., 2014).

Among ESCRTs, the most deeply conserved are subunits of the ESCRT-III complex and its regulatory ATPase, Vps4, orthologs of which are in Archaea, where they function in cell division (Samson et al., 2008). This role is conserved in eukaryotes, where the ESCRT-III/Vps4 machinery functions during cytokinesis to constrict and sever the membrane necks connecting daughter cells (Carlton and Martin-Serrano, 2007). This activity is exploited by HIV and other retroviruses, which recruit ESCRT-III/Vps4 to bud from the plasma membrane of infected cells (Garrus et al., 2001). The membrane scission activity of ESCRT-III/Vps4 might also be involved in other processes in which this machinery has more recently been found to be required, including plasma membrane wound repair (Jimenez et al., 2014), nuclear pore complex quality control (Webster et al., 2014), and post-mitotic nuclear envelope reformation (Olmos et al, 2015; Vietri et al, 2015).

The amino terminus of Vps4 consists of a microtubule interacting and trafficking (MIT) domain that binds two distinct MIT-interacting motifs (MIM1 or MIM2) located at or

near the carboxy termini of each ESCRT-III subunit (Obita et al., 2007; Stuchell-Brereton et al., 2007; Kieffer et al., 2008). Like other AAA proteins, Vps4 oligomerizes into a multimeric ring with a central pore, through which it extrudes individual ESCRT-III subunits to mediate disassembly of the complex and allow for further rounds of polymerization (Babst et al., 1998; Hurley and Yang, 2014). Of the Core ESCRT-III proteins, the MIM1 site of Vps2 has the highest affinity for the Vps4 MIT domain (Obita et al., 2007). Vps2 and Did2 (CHMP1A and 1B in humans), a peripheral ESCRT-III protein that binds Vps24, recruit Vps4 to ESCRT-III (Babst et al., 2002a; Nickerson et al., 2006). The MIM2 site of Snf7 binds the Vps4 MIT domain, and although the interaction is not required for Vps4 recruitment, it is important for Vps4 function in disassembling the ESCRT-III complex (Shestakova et al., 2010; Adell et al., 2014). The MIM1 site of Snf7 binds the structurally dissimilar 'Bro1 domain' located at the N-terminus of the class E Vps protein Bro1 (discussed below) (Kim et al., 2005).

Prior to its role in membrane scission, ESCRT-III polymerization encircles ILV cargoes at the ILV bud site for deubiquitination, which maintains free ubiquitin levels in the cytosol that are necessary for cell viability (Teis et al., 2008; Swaminathan et al., 1999). Doa4, or its closest mammalian ortholog UBPY, remove ubiquitin from ILV cargoes prior to membrane scission (Figure 1.4) (Dupre and Haguenauer-Tsapis, 2001; Katzmann et al., 2001; Mizuno et al., 2005; Row et al., 2006). Temporal coordination of cargo deubiquitination with ESCRT-III polymerization prevents cargo form diffusing into recycling pathways, and ESCRT-III proteins regulate UBPY and Doa4 to ensure this. UBPY is recruited through its MIT domain, which binds CHMP4C, CHMP1A/1B, and CHMP7 (Row et al., 2007). Bro1 stimulates Doa4 catalytic activity, and Bro1

recruitment is driven through its interaction with Snf7 (Richter et al., 2007; Kim et al., 2005; Wemmer et al., 2011). ILV scission follows deubiquitination, and chapter 3 shows how this is regulated in yeast: Doa4 stalls ILV scission by inhibiting Vps4 activity towards ESCRT-III (Figure 1.5).

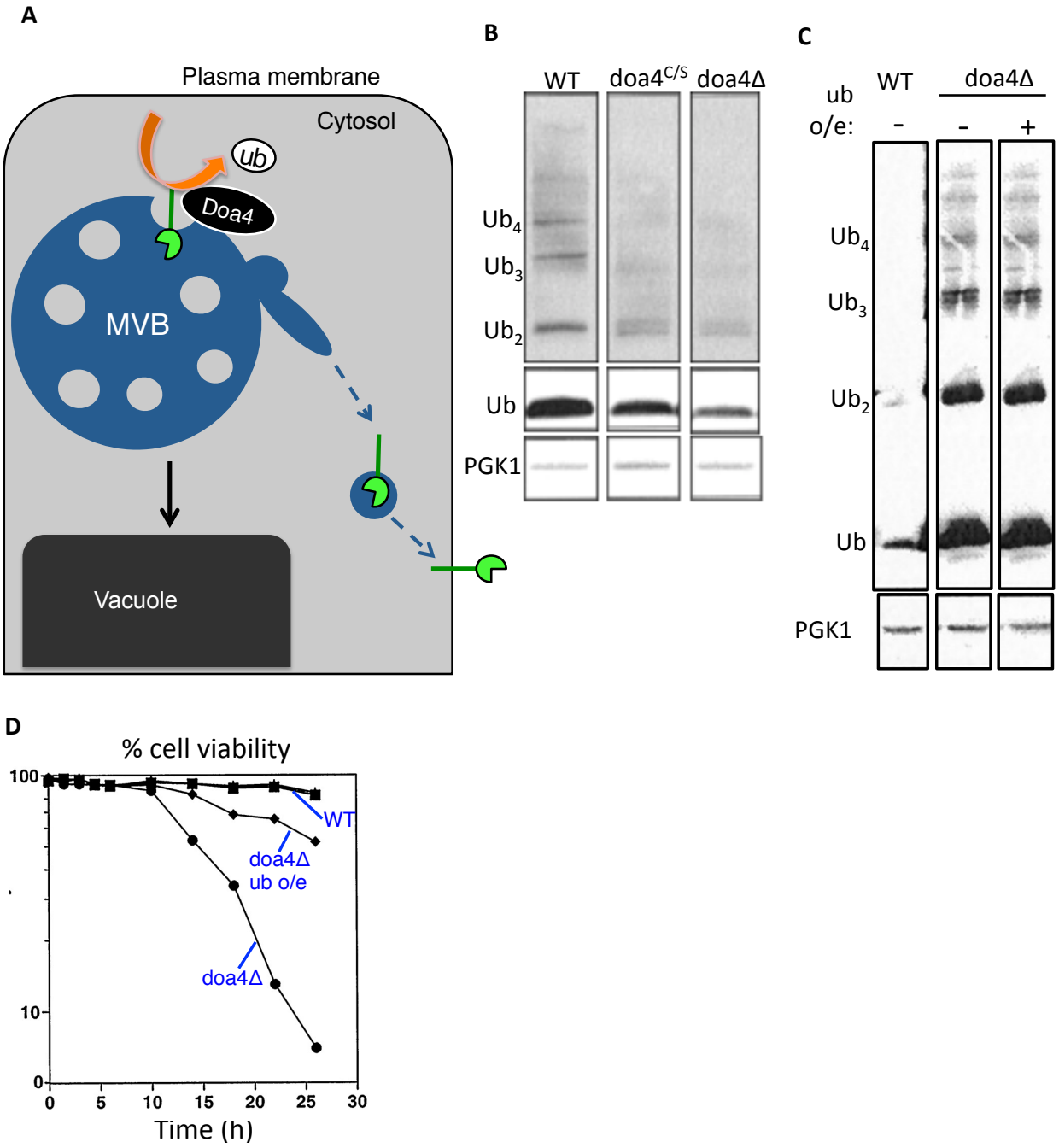

Figure 1.4. The importance of deubiquitination regulation in the ILV budding pathway. (A) Cartoon of transmembrane cargo recycling when deubiquitination occurs prematurely. (B) anti-ubiquitin western blot of yeast extracts (from stationary phase cells) showing that Doa4 deubiquitination activity is required to maintain ubiquitin levels. (C) anit-ubiquitin blot as in B with ubiquitin overexpression where indicated. (D) Percent cell viability at the indicated time points as measured by propidium iodide staining. Adapted from Swaminathan et al., 1999.

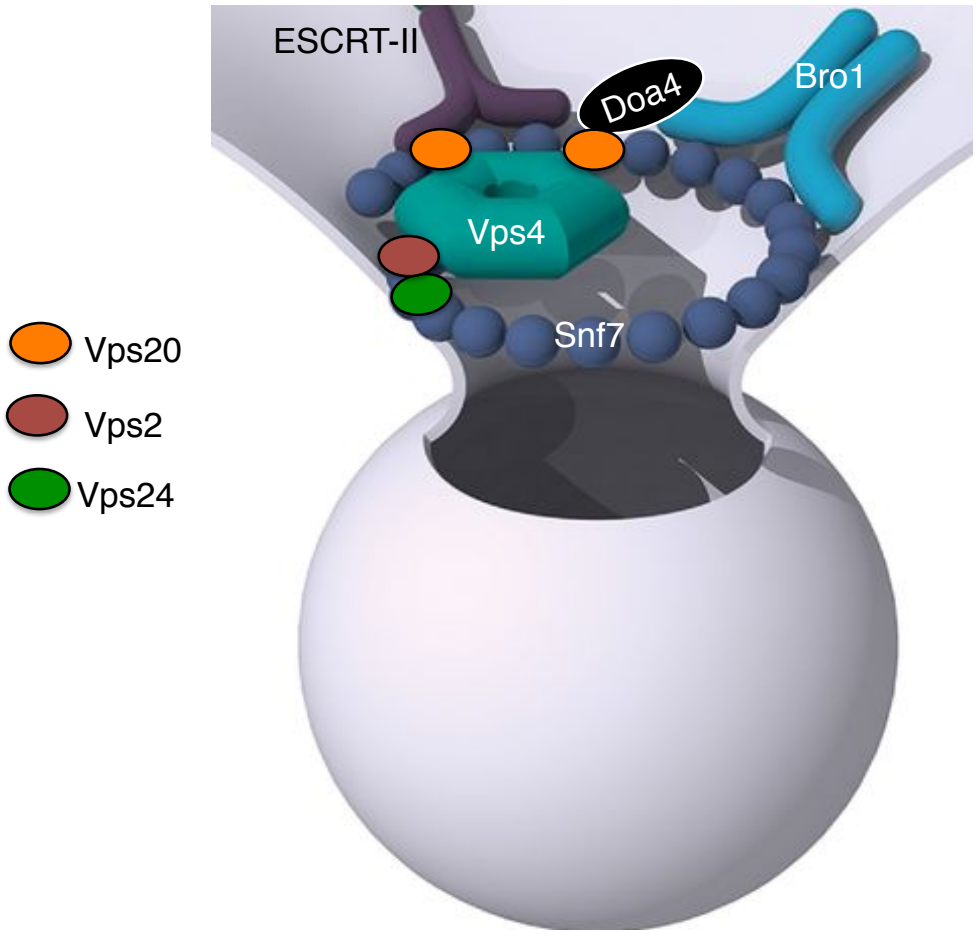

Figure 1.5. Model of ESCRT and deubiquitination machinery interactions at the ILV scission site. Adapted from Hurley 2015.

Chapter 2: ESCRT-II regulates ESCRT-III assembly to coordinate cargo sorting with ILV formation

Introduction

The ESCRT machinery is composed of five multimeric complexes: ESCRT-0, ESCRT-I, ESCRT-II, ESCRT-III, and the Vps4 complex (reviewed in Henne et al., 2011). These soluble complexes are recruited from the cytosol to the MVB, where they function in cargo sorting and ILV formation. "Early-acting" ESCRT complexes (ESCRT-0 and ESCRT-I) possess numerous ubiquitin-binding domains and are therefore proposed to concentrate ubiquitinated cargo on the endosomal membrane (Bilodeau et al., 2002, 2003; Pornillos et al., 2002; Shih et al., 2002; Mizuno et al., 2003; Shields et al., 2009; Ren and Hurley, 2010). The later-acting ESCRT-III proteins form helical and circular filaments that can deform membrane both in vivo and in vitro (Hanson et al., 2008; Bodon et al., 2011; Henne et al., 2012). The Vps4 complex then disassembles ESCRT-III, and ATP-dependent activity that seems to drive ILV abscission (Babst et al., 1998, 2002a,b; Adell et al., 2014). Therefore these "late-acting" ESCRTs are implicated in the formation of ILVs. ESCRT-II links the cargo sorting activity of the early-acting ESCRTs to ILV formation mediated by the late-acting ESCRTs. However, mechanistic insights are lacking as to how ESCRT-II executes this process.

ESCRT-II is a heterotetrameric protein complex consisting of one copy of Vps36 and Vps22 and two copies of Vps25 (Hierro et al., 2004; Teo et al., 2004). The N-terminal GRAM-like ubiquitin-binding in Eap45 (GLUE) domain (Slagsvold et al., 2005) of Vps36 interacts with ubiquitin (either on cargo proteins or other ubiquitinated ESCRT

proteins; Meyer et al., 2002; Alam et al., 2004), with the endosomal lipid phosphatidylinositol 3-phosphate (PI3P; Slagsvold et al., 2005; Teo et al., 2006), and with the Vps28 C-terminus of ESCRT-I (Teo et al., 2006; Gill et al., 2007). These interactions are predicted to play an important role in the recruitment of ESCRT-II to the MVB. Furthermore, an ESCRT-I–ESCRT-II supercomplex has been described that is proposed to function in the membrane deformation process leading to the formation of ILVs (Wollert and Hurley, 2010; Boura et al., 2012). Finally, the Vps25 subunits of ESCRT-II bind to Vps20, a myristoylated subunit of ESCRT-III (Ashra et al., 1998; Teo et al., 2004). This interaction between ESCRT-II and Vps20 is believed to initiate the assembly of the ESCRT-III filament (Teis et al., 2008).

In this study, we report that ESCRT-II is regulated not only by recruitment to the MVB but also by an ESCRT-I–mediated activation step. However, this regulatory function of ESCRT-I is not essential for the MVB pathway and can be partially bypassed by a constitutively active ESCRT-II mutant. Furthermore, we show that assembly of ESCRT-III, which is considered the core ESCRT machinery, is not sufficient for efficient ILV formation and that cargo concentration may be essential for this process.

Results

Regulation of ESCRT-II recruitment and function

The early ESCRTs (ESCRT-0 and -I) contain numerous ubiquitin-binding domains and are thus likely to be involved in cargo sorting (reviewed in Henne et al., 2011). ESCRT-III and Vps4 have been proposed to function in membrane scission, severing the neck of the forming MVB vesicles. ESCRT-II links these early and late functions of the ESCRT machinery by initiating ESCRT-III formation in an ESCRT-I–

dependent manner. This interaction between ESCRT-I and ESCRT-II seems to be regulatory, since the MVB sorting defect observed in an ESCRT-I–deletion strain can be partially bypassed by overexpressing ESCRT-II (Babst et al., 2002b). ESCRT-I binds to ESCRT-II via the Vps36 GLUE domain, a domain that also interacts with PI3P and ubiquitin (Figure 2.1; Meyer et al., 2002; Alam et al., 2004; Slagsvold et al., 2005; Teo et al., 2006; Gill et al., 2007). We tested if these three GLUE domain interactions regulate ESCRT-II function by aiding the recruitment of ESCRT-II from the cytoplasm to the MVB.

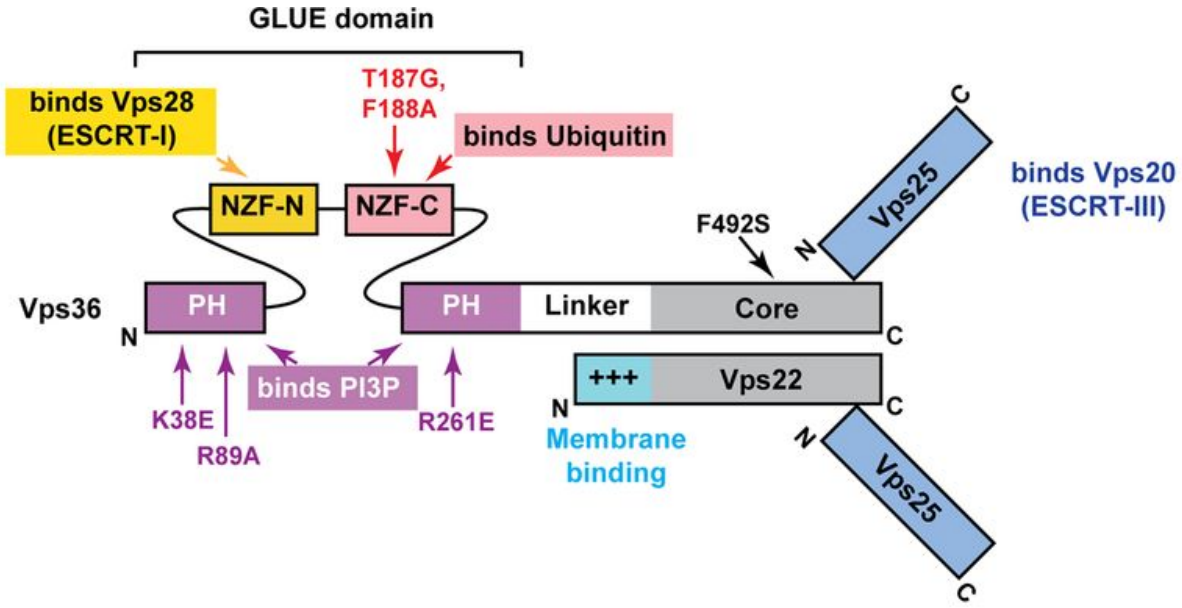

Figure 2.1. ESCRT-II binding partners.
A schematic of ESCRT-II domain architecture, interacting partners, and point mutations used in this study to disrupt these interactions. Adapted from Mageswaran and Johnson et al., 2015.

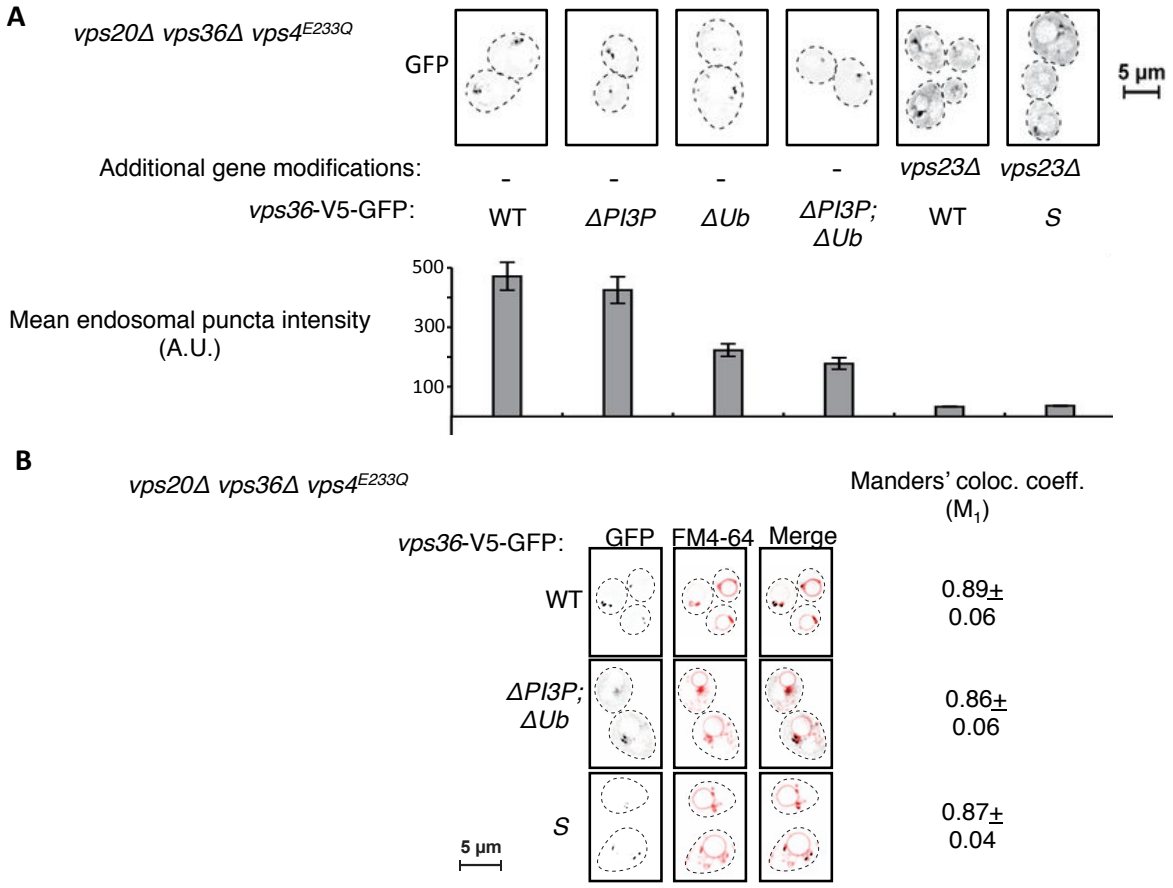

Figure 2.2. The role of ESCRT-II binding partners in ESCRT-II localization.
All strains in this figure lack genomic *VPS36* and express tagged versions of wild-type (WT) or mutant *VPS36* from a low-copy CEN plasmid under native promoter. (A) Endosomal localization of ESCRT-II by fluorescence microscopy and its quantification. Microscopic images are presented in inverted gray scale, where black denotes GFP signal. The GFP puncta represent endosomes since they colocalized with FM4-64 as shown in B. n = 552, 544, 545, 558, 521, and 461 (in the order of strain presentation). Error bars denote the 95% confidence intervals over mean. (B) Colocalization of Vps36 fusion proteins with FM4-64. M1 is the Manders' colocalization coefficient for GFP signal with FM4-64. N=3, 3, and 4 (in the order of strain presentation). Values denote mean +/- range for 95% confidence interval. Adapted from Mageswaran and Johnson et al., 2015.

Previous studies suggested that endosomal localization of ESCRT-II is dependent on the GLUE–PI3P interaction (Teo et al., 2006) or the combination of both PI3P binding and the interaction of a positive-charged helix of Vps22 with negative-charged phospholipids (Im and Hurley, 2008). Furthermore, a study showed that deletion of ESCRT-I did not impair MVB recruitment of ESCRT-II (Babst et al., 2002b). These localization studies were performed either with just the GLUE domain or in absence of functional Vps4, an ATPase that recycles ESCRTs back to the cytoplasm. Lack of Vps4 results in accumulation of ESCRT-II–ESCRT-III complexes that are thoroughly anchored on the endosomal membrane (Babst et al., 2002b). Because of this trapping effect, even strong defects in ESCRT-II recruitment to the endosome would not be detectable. To circumvent these problems, we performed the localization studies using a green fluorescent protein (GFP)–tagged version of full-length Vps36 in a strain that lacked both the ESCRT-III subunit Vps20 (to prevent anchoring by ESCRT-III) and a functional Vps4 (expressing dominant- negative vps4 (E233Q) to accumulate endosomal membranes) in addition to lacking genomic *VPS36*. ESCRT-II localization to endosomes was quantified by measuring the fluorescence intensity of the accumulated endosomes (class E compartments) found in ~500 cells. The GFP puncta were identified as class E compartments on the basis of their colocalization with FM4-64, a lipophilic dye that labels the endocytic pathway, as seen in Figure 2.2B.

We first tested the contribution of the PI3P-binding domain to the recruitment of ESCRT-II by constructing the double mutant *vps36* (*R89A,R261A*)-V5-GFP, which, based on data from a previous report, was predicted to abolish PI3P binding (Teo et al., 2006). Surprisingly, this mutant form of ESCRT-II was as efficiently recruited to

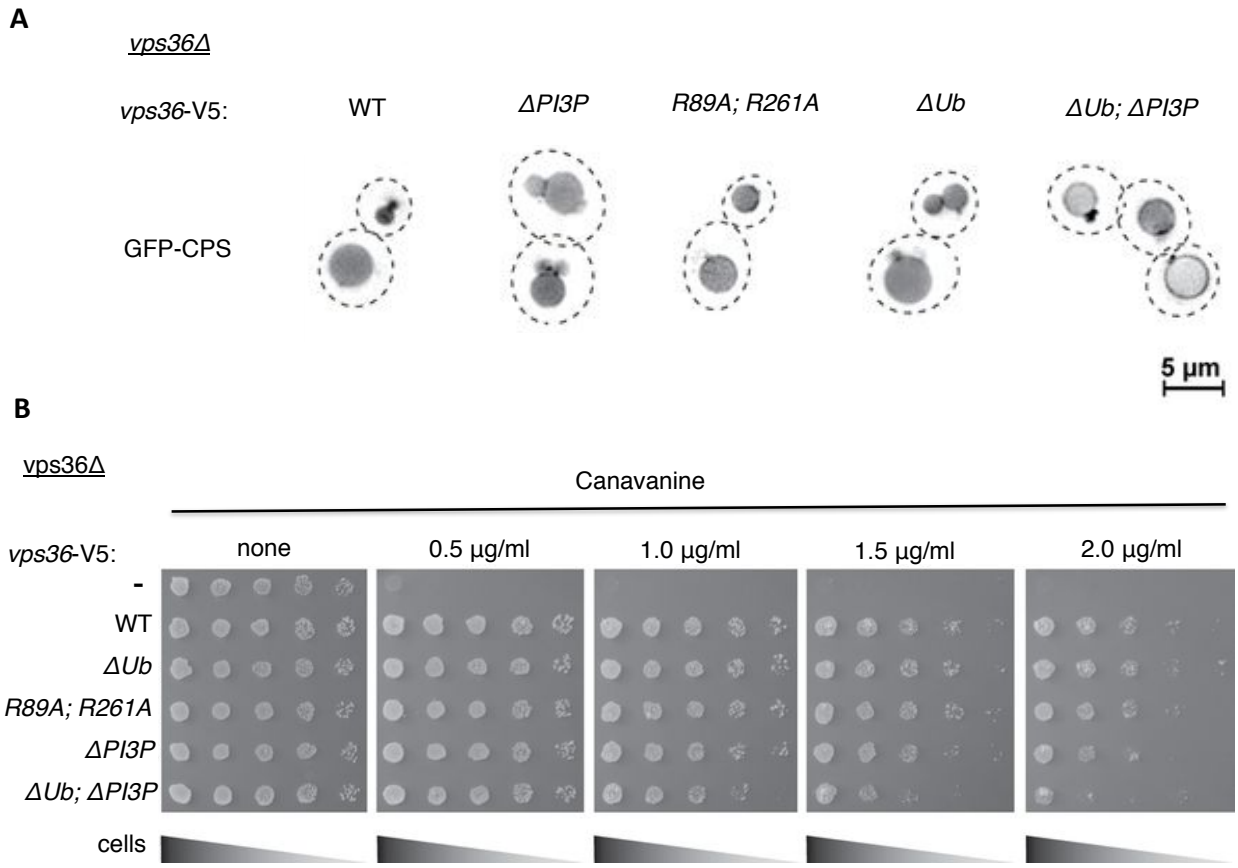

Figure 2.3. The role of ESCRT-II binding partners in ESCRT-II function. As in figure 2.2, all strains in this figure lack genomic *VPS36* and express tagged versions of wild-type (WT) or mutant *VPS36* from a low-copy CEN plasmid under native promoter. (A) Localization of GFP-CPS1 in different vps36-mutant strains (B) Growth assays from serial dilutions of cells plated on agar containing different concentrations of canavanine. Adapted from Mageswaran and Johnson et al., 2015.

endosomes as the wild-type complex (data not shown). Therefore a triple mutant was constructed (K38E, R89A, R261E) that replaced two key positively charged amino acids of the PI3P-binding pocket with glutamate (referred to as *ΔPI3P*). As observed for the double mutant, cells expressing *vps36* (*ΔPI3P*)-V5- GFP showed wild type-like localization of ESCRT-II to endosomes (Figure 2.2A). Together these data suggested that the PI3P interaction does not significantly contribute to the endosomal recruitment of ESCRT-II.

Consistent with the localization data, we found that both *vps36* (*R89A, R261A*)-V5 and vps36 (ΔPI3P)-V5 complemented the MVB-sorting defect of a *VPS36*-deletion strain. Both Vps36 mutants were able to function in the efficient delivery of GFP-Cps1, a cargo of the MVB pathway (Odorizzi et al., 1998), to the vacuolar lumen (Figure 2.3A). Furthermore, both PI3P- binding mutants complemented the growth defect of a *VPS36*-deletion strain on canavanine-containing plates (Figure 2.3B). Canavanine, a toxic arginine analogue, is imported by yeast via the transporter Can1. Because Can1 is regulated in part by degradation via the MVB pathway, ESCRT mutants stabilize Can1 and thus show increased canavanine sensitivity compared with wild-type cells (Teis et al., 2010). Together this data indicates that interaction of Vps36 and PI3P plays a minor role in the localization and activity of ESCRT-II. At this point, we are not able to reconcile why our results contradict previously published data (Teo et al., 2006).

Next we analyzed the importance of the ubiquitin-binding site of Vps36 by introducing the mutations T187G and F188A (a double mutant we refer to as (*ΔUb*; Figure 2.1A). These mutations were previously shown to block binding of the Vps36 GLUE domain to ubiquitin (Shields et al., 2009). Localization studies of strains

expressing *vps36* (*ΔUb*)-V5-GFP indicated that loss of ubiquitin binding caused a ~50% drop of ESCRT-II association with the endosomal membrane (in *vps20Δ vps36Δ* in the presence of *vps4* (*E233Q)* (Figure 2.2A). However, this recruitment defect did not result in a MVB-sorting phenotype. Both the vacuolar delivery of GFP-Cps1 and growth on canavanine were found to be wild type–like in cells expressing *vps36* (*ΔUb*)-V5 (Figure 2.3A and B). This result was consistent with previously published data (Shields et al., 2009).

The combination of the ubiquitin-binding mutations along with the PI3P-binding mutations (*vps36* (*ΔPI3P ΔUb*)-V5-GFP) resulted in no additional ESCRT-II recruiting defect compared with the ubiquitin-binding mutation alone (Figure 2.2A). However, cells expressing *vps36* (*ΔPI3P ΔUb*)-V5 exhibited partial missorting of GFP-Cps1 to the vacuolar membrane and marginally increased canavanine sensitivity (Figure 2.3A and B), suggesting a possible regulatory role for ubiquitin and PI3P binding independent of their function in ESCRT-II recruitment. In addition, the lack of any observable GFP-Cps1 sorting defect with either *ΔUb* or *ΔPI3P* alone suggests redundant functions for ubiquitin and PI3P binding.

To analyze the importance of ESCRT-I, we deleted *VPS23*, the gene encoding the major subunit of the ESCRT-I protein complex. In the strain *vps23Δ vps20Δ vps36Δ* $vps4^{E233Q}$, GFP-tagged WT copy of ESCRT-II localized mainly to the cytoplasm, and endosomal recruitment was <10% compared to the recruitment in cells with functional ESCRT-I (Figure 2.2A). This result suggested that ESCRT-I provides a significant recruitment signal for ESCRT-II, most likely through direct interaction of the Vps28 C-terminus (ESCRT-I) with the Vps36 GLUE domain (ESCRT-II).

In summary, the analysis of the Vps36 GLUE-domain mutants indicated that the interaction between ESCRT-I and ESCRT-II plays a key role in the endosomal recruitment of ESCRT-II. Binding of the GLUE domain to ubiquitin further contributes to recruitment efficiency. In contrast, the interaction of the GLUE domain with PI3P seems to be less relevant for ESCRT-II localization or function.

Evidence for redundant ESCRT-0, -I, and -II functions

The data presented so far suggested that the ESCRT-I interaction is important for localization of ESCRT-II. However, the observed suppression of the ESCRT-I phenotype by overexpression of ESCRT-II suggested that ESCRT-I is not an essential component of the ESCRT machinery, but that it plays a regulatory role (Babst et al., 2002b). Using fluorescence microscopy, we confirmed the previously published results that ESCRT-II overexpression restores GFP-CPS1 sorting to the vacuolar lumen in vps23 deletions (Babst et al., 2002b; Alam et al., 2004; Figure 2.4A).

To study further the potential regulatory role of ESCRT-I on ESCRT-II function, we performed a genetic screen to identify an ESCRT-II mutant that suppresses the MVB-sorting defect caused by loss of ESCRT-I. We randomly mutagenized plasmid-encoded *VPS36* and expressed these mutants in a strain deleted for *VPS36* and *VPS23*. The resulting strains were grown in the presence of canavanine at a concentration that is lethal for *vps23*Δ. This screen identified *vps36(F492S*) (Phe at 492 to Ser, referred to as *vps36(S)*; Figure 2.1A) as a mutant that suppresses the canavanine sensitivity of *vps23*Δ (Figure 2.4B). Using a functional V5-tagged version of Vps36, western blot analysis showed that the mutation did not affect the expression

levels of the Vps36 protein (data not shown). Additionally, *vps36(S)* suppressed the canavanine sensitivity phenotype of a strain deleted for the ESCRT-0 subunit Vps27, but not for strains deleted for any of the ESCRT-III subunits (Figures 2.4B). Transmission election microscopy (TEM) analysis of endosomes in *vps23*Δ *vps36(S)* cells showed ILV formation was dramatically improved by this hyperactive ESCRT-II mutant (Figure 2.4C, and Figure2.6).

To better quantify the sorting defects, we analyzed GFP-Cps1 sorting by Western blot using anti-GFP antibodies. When GFP-Cps1 enters the vacuolar lumen, the resident hydrolases clip the protein and release free GFP. In contrast, the proteolytic clipping of GFP-Cps1, which mislocalizes to the vacuolar membrane and class E compartments, causes the accumulation of heavier GFP fusion products. The ratio of the free GFP signal to the total GFP signal from proteolytic processing indicates the extent of GFP-Cps1 sorting into the MVB pathway, and Figure 2.4D shows these quantifications. Consistent with our canavanine sensitivity data, *vps36(S)* suppressed the GFP-CPS1 sorting phenotype in ESCRT-0 or -I deletion strains (Figure 2.4D). Furthermore, just as canavininve sensitivity in ESCRT-III deletions was not suppressed by *vps36(S*), GFP-CPS1 sorting in a *vps4* deletion was not suppressed by *vps36(S)* (Figure 2.4D). Surprisingly, the suppression of ESCRT-0Δ by *vps36(S)* was greatly impaired in the absence of the ESCRT-I subunit *VPS23* (Figure 2.4D), suggesting that at least one of the early ESCRTs has to be present for a functioning MVB pathway and that the functions of ESCRT-0 and ESCRT-I seemed to be redundant. Together the phenotypic analyses indicated that expression of 2μ ESCRT-II or the *vps36(S)*- mutant partially bypassed the need for the early ESCRTs (ESCRT-0 or ESCRT-I) but remained

dependent on the function of the late ESCRTs.

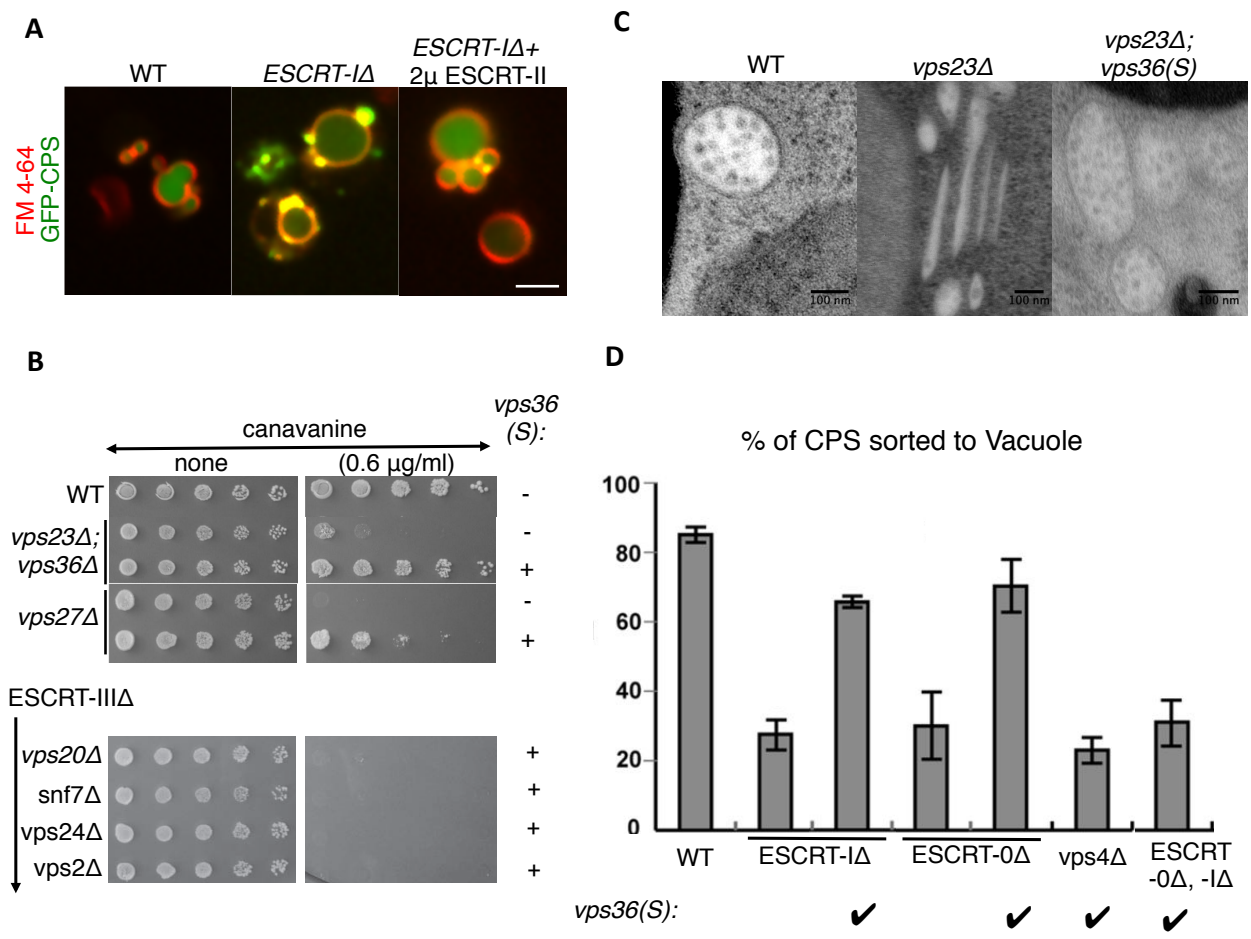

Figure 2.4. Evidence for redundant ESCRT-0, I, and -II functions. (A) Fluorescent images of FM 4-64 stained yeast expressing GFP-CPS1. 2μ = high copy number overexpression plasmid. Bar, 2 μM (B) Growth assays from serial dilutions of cells plated on agar containing different concentrations of canavanine. Expression of vps36(S) from a low copy plasmid is indicated to the right of the panel. (C) Representative TEM images of endosomes from 90 nm thin sections. (D) Quantification GFP-CPS1 sorting to the vacuole lumen from western blots of whole cell yeast extracts probing for CPS1 in the indicated strains. Low-copy plasmid encoded *vps36(S)* expression is indicated along the bottom. Adapted from Mageswaran and Johnson et al., 2015.

ESCRT-II can independently drive ESCRT-III polymerization but functionality requires upstream ESCRTs

Suppression of the ESCRT-I–mutant phenotype was not due to improved endosomal recruitment of ESCRT-II in this strain. Localization studies in *vps23*Δ *vps20*Δ *vps36*Δ *vps4*^{E233Q} cells expressing *vps36(S)*-V5- GFP as the only copy of *VPS36* indicated that the bypass mutation did not improve the amount of endosome-associated ESCRT-II over the wild-type copy (Figure 2.2). This result suggested that ESCRT-II function was regulated not only by endosomal recruitment but also by a mechanism that switched membrane-associated ESCRT-II from an inactive to an active form. In the case of wild-type ESCRT-II, this activation might be triggered by the interactions of the Vps36 GLUE domain with ESCRT-I, PI3P, and ubiquitin. In contrast, the vps36(S)-mutant form of ESCRT-II seemed to be constitutively active and is therefore independent of the upstream factors for activation.

To test if *vps36(S)* is able to initiate ESCRT-III formation without ESCRT-I interaction, we analyzed the oligomeric state (Figure 2.5A) of the most common ESCRT-III subunit, Snf7, using a glycerol density gradient centrifugation assay. In these experiments, the monomeric Snf7 protein was found in the top fractions of the gradient, and the oligomers were found throughout the lower fractions (consistent with previously published data; Teis et al., 2008). Similar to the previously published results, we found that wild-type cells contained a monomeric and polymeric population of Snf7 at endosomes, whereas in cells lacking the ESCRT-III disassembly factor Vps4, the majority of Snf7 accumulated in the oligomeric form (Figure 2.5B). The *vps20*Δ strain contained no ESCRT-III oligomers, consistent with the model in which Vps20 initiates

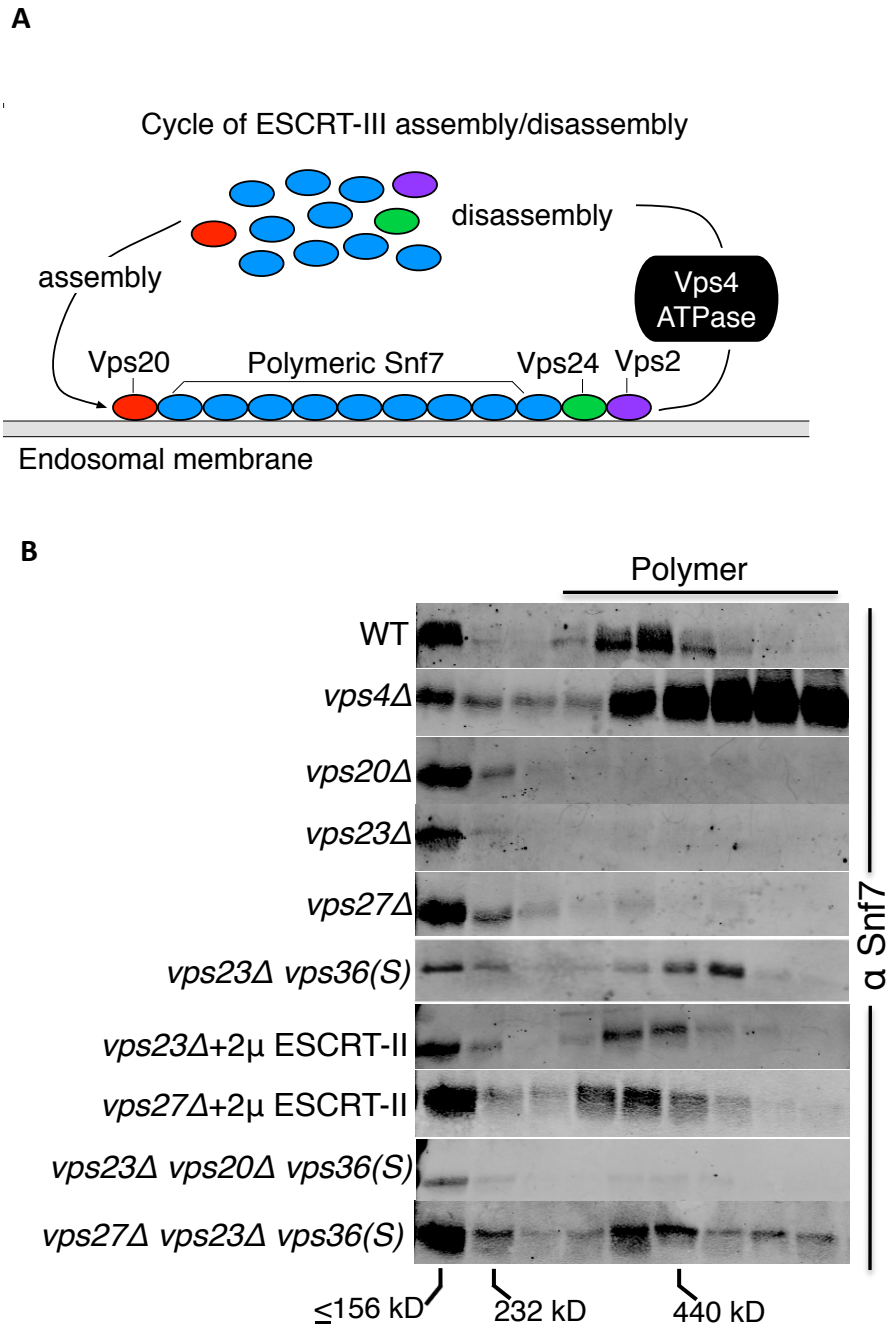

Figure 2.5. ESCRT-II can drive ESCRT-III polymerization independently of upstream ESCRTs. (A) Schematic diagram depicting ESCRT-III cycles of assembly and disassembly. (B) Western-blot analysis of the distribution Snf7 in density gradients resolved by rate-zonal density gradient centrifugation. Indicated below the bottom panel are the migrations of molecular-weight standards: Aldolase (156 kD), Catalase (232 kD), and Ferritin (440 kD). Also indicated above the top panel are the gradient fractions containing polymeric Snf7. Adapted from Mageswaran and Johnson et al., 2015.

Snf7 polymerization. Similarly, in cells lacking the ESCRT-II protein Vps36 (data not shown), the ESCRT-I protein Vps23, or the ESCRT-0 protein Vps27, Snf7 was predominantly monomeric, which indicates a defect in ESCRT- III assembly in these strains. However, expression of the bypass mutant *vps36(S)* in *vps23Δ*, expression of 2μ ESCRT-II in *vps23Δ*, expression of the bypass mutant *vps36(S)* in *vps27Δ* (data not shown), or expression of 2μ ESCRT-II in *vps27Δ* strains restored ESCRT-III oligomer assembly comparably to wild-type. Vps20 was required for this suppression of ESCRT-III formation, as a *vps23*Δ*vps20*Δ*vps36*Δ strain expressing *vps36(S)* showed greatly impaired Snf7 oligomerization.

Transmission election microscopy (TEM) was used to visualize the late endosomal compartments of the ESCRT-I and -II deletion strains. The cross-sections of *vps36Δ* cells showed no MVBs but instead showed class E compartments (Figure 2.6; Reider et al., 1996). *vps33Δ* cells showed a mixture of class E compartments and endosomes containing ILVs. TEM analysis of *vps23*Δ *vps36*Δ *vps36(S)* cells showed improvement of MVB morphology both in ILV number and endosomal morphology (fewer class E compartments and more globular endosomes) compared with *vps23*Δ (Figure 2.6). Of interest, the presence of vps36(S) triggered ESCRT-III oligomerization even in the absence of both VPS27 and VPS23 (Figure 2.5B), although the same strain was severely defective in MVB vesicle formation (Figure 2.6). This result suggested that ESCRT-III assembly is not sufficient to drive ILV formation in the absence of upstream ESCRT activity.

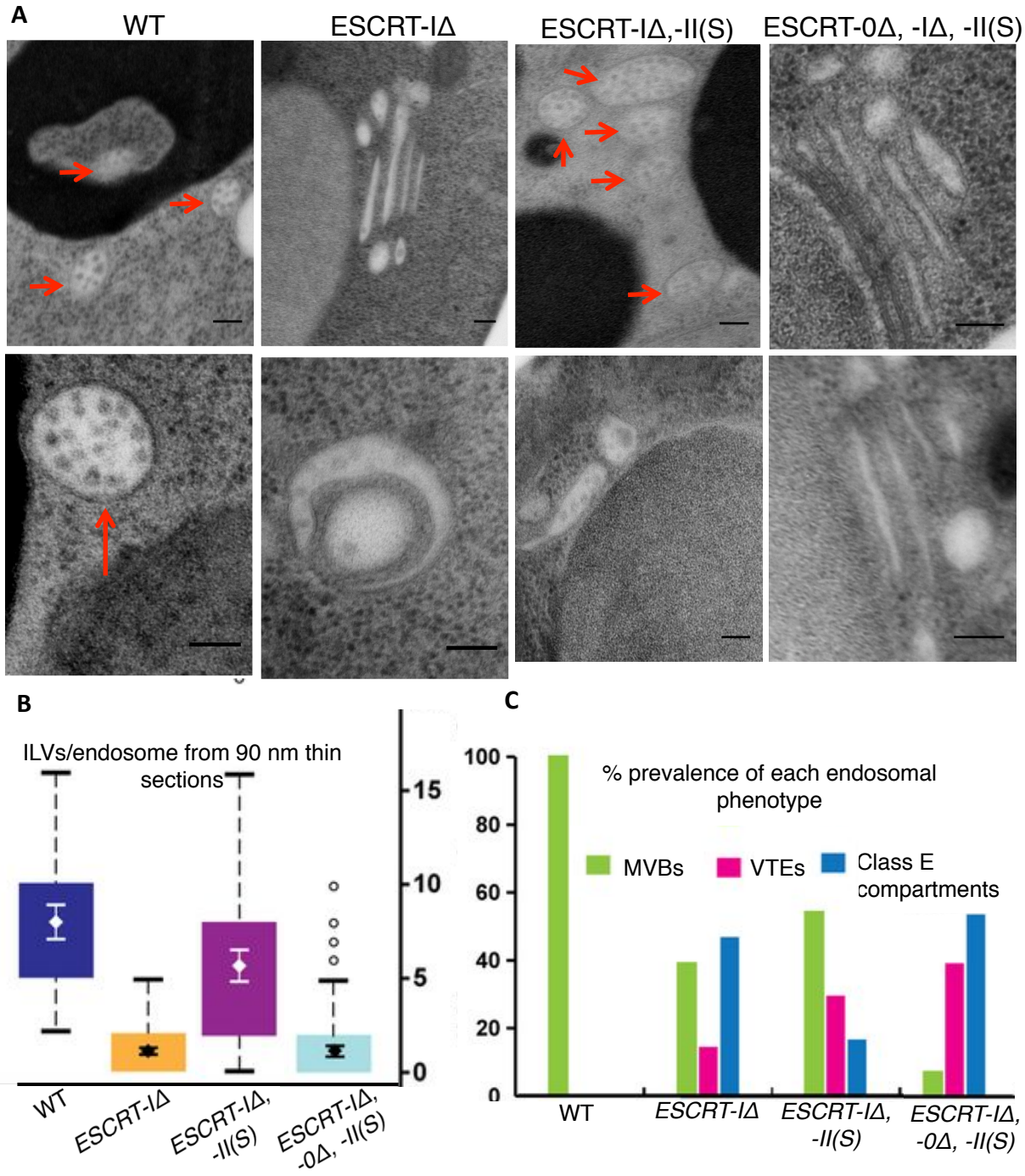

Figure 2.6. ESCRT-II requires upstream ESCRT activity to generate ESCRT-III polymers capable of ILV formation. (A) Representative TEM images of endosomes for each strain expressing the indicated plasmids. Red arrows indicate MVBs (B) ILVs/endosome observed in 90-nm thin sections shown as a box plot. The error bars show the 95% confidence interval over the mean. (C) Endosome morphology distribution. Number of endosome profiles counted for each strain: 52, 105, 34, 109, and 97 (in the order of strain presentation). Adapted from Mageswaran and Johnson et al., 2015.

Discussion

ESCRT-0 and ESCRT-I contain numerous ubiquitin-binding sites. In addition, ESCRT-0 seems to be able to form higher-ordered oligomers on the endosomal membrane (Mayers et al., 2011). These properties make these early ESCRTs prime candidates for the role of a cargo-capturing system. ESCRT-III polymers together with Vps4 seem to execute the membrane abscission reaction during both cytokinesis and HIV viral budding. Therefore it is likely that ESCRT-III/ Vps4 performs the same function at the MVB, constricting and severing the neck of the forming ILV. Besides its role in initiating ESCRT- III assembly, little is known about the function of ESCRT-II in ILV formation. Based on structural studies, a model has been proposed in which the ESCRT-I–ESCRT-II supercomplex is involved in deforming the membrane to drive the invagination of the forming ILV (Wollert and Hurley, 2010; Boura et al., 2012). However, direct evidence for this role of ESCRT-II in membrane bending is lacking.

A surprising conclusion from this chapter is the observation that ESCRT-0 and ESCRT-I are not essential for the MVB pathway but have redundant roles, most likely in cargo sorting and concentration. In contrast, the ESCRT-II–mediated initiation of ESCRT-III assembly is critical for this pathway. These observations suggested that the interactions of ESCRT-II with the upstream ESCRT-I complex are not essential for vesicle formation (e.g., driving membrane invagination) but play a regulatory role in ensuring ESCRT-III formation at the proper time and place. These data suggests that regulation of ESCRT-II function is mediated by both the recruitment of the complex from the cytoplasm to the MVB and an activation mechanism.

We identified the amino acid exchange F492S in Vps36 as a mutation that

seemed to result in a constitutively active form of ESCRT- II (referred to as ESCRT-II(S)). The localization of ESCRT-II(S) to endosomes was not increased compared with the wild-type complex, indicating that recruitment and activation of ESCRT-II are independent processes. ESCRT-II(S) was able to suppress the MVB-sorting phenotypes of an ESCRT-0 or ESCRT-I deletion by triggering ESCRT- III polymer formation in the absence of these upstream factors.

Another interesting observation from this chapter is that the constitutively active *vps36(S)* efficiently rescued ESCRT-III polymerization in the *vps23Δ vps27Δ* double mutant, but it showed only a marginal improvement in GFP-CPS1 sorting or ILV formation. This difference in phenotypic suppression suggested that some of the ESCRT-III polymers formed by ESCRT- II were unproductive, most likely because ESCRT-III polymerization was triggered at the wrong place and/or time. In addition, this result suggested that ESCRT-III alone is not sufficient to deform the membrane and cause vesicle budding. The concentration of cargo into a cargo–ESCRT patch at the endosome might play an important role in initiating vesicle formation. This is consistent with a previous study indicating that the presence of ubiquitinated cargo at the endosome is essential for ILV formation (MacDonald et al., 2012). Together these data suggest that ESCRT-0 and ESCRT-I have redundant functions and that at least one of these cargo-sorting complexes has to be present to drive ILV formation.

In summary, we propose a model in which the assembly of a cargo–ESCRT patch is an essential first step toward ILV formation (Figure 2.7). A cargo patch is formed by the interaction of ESCRT-0 and ESCRT-I with ubiquitinated transmembrane proteins. Because transmembrane proteins surround themselves with specific lipids, the

cargo patch is expected to have a unique lipid composition compared with the rest of the endosomal membrane. We propose that this assembly of ESCRTs, cargo, and lipids causes an inward deformation of the cargo patch (discussed in Babst, 2011). The ESCRT-I component of the cargo patch, together with ubiquitinated cargo and PI3P, recruits ESCRT-II by interacting with the GLUE domain. This interaction activates ESCRT-II, which in turn binds Vps20. ESCRT-II– bound Vps20 changes its conformation from the closed to the open state, which recruits Snf7 and initiates the polymerization of the ESCRT-III complex. Based on previous in vitro studies, the ESCRT-III polymer might form a corral that defines the boundaries of the forming vesicle (Henne et al., 2012). Finally, ESCRT-III, together with the Vps4 complex, drives the constriction of the membrane neck, which ultimately causes the abscission of the forming ILV (Figure 2.7).

In this model, constitutively active ESCRT-II(S) can partially bypass the loss of ESCRT-I by interacting with the ubiquitinated cargo, which ensures ESCRT-III formation at the proper place. However, deletion of ESCRT-0 or -I results in no cargo patch formation. As a consequence, ESCRT-III polymerization occurs randomly on the endosomal membrane, and only by chance will ESCRT-III form close to a cargo patch, explaining the inefficiency in ILV formation in this mutant strain.

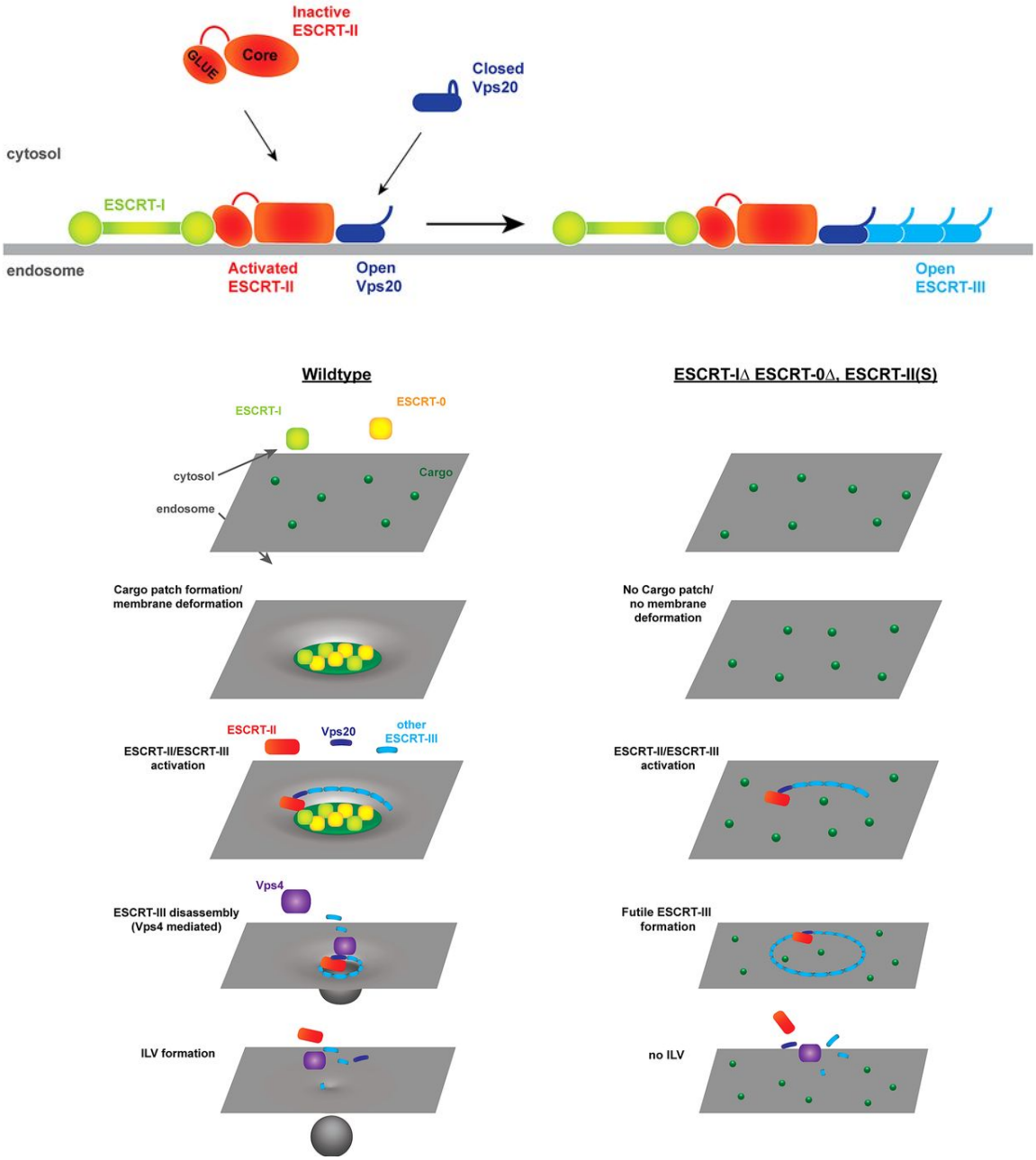

Figure 2.7. A model for ESCRT-II-mediated coupling of ILV formation with cargo sorting. The early ESCRT complexes (ESCRT-0 and -I) concentrate transmembrane cargo along with lipids interacting with the cargoes. The resulting cargo-ESCRT-lipid patch deforms the endosomal membrane. Subsequent recruitment and activation of ESCRT-II causes ESCRT-III polymerization. Vps4-mediated constriction of ESCRT-III results in deepening of the membrane invagination and ultimately fission of the ILV neck. In the absence of ESCRT-0 and -I, ESCRT-II (S) randomly initiates ESCRT-III polymerization. However, in the absence of a cargo patch, Vps4-mediated remodeling of ESCRT-III does not result in ILV formation. Adapted from Mageswaran and Johnson et al., 2015.

Materials and Methods

Strains, media, and plasmids

The strains and plasmids used in this study are described in Table 1. Yeast gene knockouts were constructed as previously described (Longtine et al., 1998). Yeast strain KFY7 was constructed in 6210.1 *WT* yeast by replacing *VPS36* with *URA3* gene and *VPS20* with *HIS3* gene. SKY1 strain was constructed by introducing *URA3* gene into the *VPS36* locus of EEY6-2. SKY8, SKY14, and SKY15 strains were constructed by further knocking out the genomic copy of *VPS20*, *VPS27*, or *SNF7* with G418 cassette (KanMX6) in SKY1. Plasmids were constructed using PCR/conventional restriction enzymes, the sequence and ligation-independent cloning (SLIC; Li and Elledge, 2007) method, or by QuikChange protocol. pSD2 and pSK211 were constructed by inserting the previously described GFP-Cps1 construct (Odorizzi et al., 1998) into pRS415 and pRS414 vectors, respectively. Similar vector swap was performed to construct pMB187 from the previously described pMB66 (Babst et al., 1998). F492S mutation in *VPS36* was isolated from the canavanine screen by using homologous recombination of error-prone PCR product of *VPS36* and a gapped plasmid of pMB131 that lacked most of the coding sequence of *VPS36* but retained the 5′ and 3′ untranslated regions. pSK163 was constructed by replacing the promoter region of the mutant *VPS36* isolated in the screen with wild-type promoter region. F492S mutation was introduced into pMB175 and its derivatives by QuikChange protocol using Phusion polymerase enzyme. Similar QuikChange protocol was used to make ubiquitin and PI3P mutants; linker deletions and V5- and GFP-tagged *VPS36* in

centromere (CEN) plasmids were derived from pMB131. V5 tagging of *VPS36* in pMB175 was performed by SLIC technique (using two PCR products for the vector and ESCRT-II sequences, whereas the V5 sequence was reconstituted by annealing two oligonucleotides). The GLUE domain deletions in pMB131, pMB175 and their derivatives were similarly made using SLIC technique using two PCR products for the vector and ESCRT-II sequences (without GLUE domain). Yeast strains were grown in rich yeast extract/peptone/dextrose (YPD) medium or in the appropriate synthetic drop-out media in yeast nitrogen base (YNB; Becton, Dickinson and Company, Sparks, MD) as published (Sherman et al., 1979). In every set of experiments, strains were grown in the same growth medium.

Fluorescence microscopy and quantification

Yeast cells were grown in YNB selective medium (Anachem Bio101 Systems, Luton, UK, and USBiological, Swampscott, MA) to logarithmic growth phase (0.7 OD_{600}). Fluorescence microscopy done in Figure 2.4A was done as described in chapter 3. All other fluorescence microscopy was performed at 100x magnification on a deconvolution microscope (DeltaVision; Applied Precision, Issaquah, WA) using the accompanying software. Images were taken as *Z*-stacks and deconvolved.

For quantification of endosomal localization of Vps36-V5-GFP, a projection of the *Z*-stacks (25 stacks, 5 μm total) of 500 cells was analyzed. The brightest intensity of puncta for each cell was recorded after background subtraction. For cells showing no discernible puncta, the value was recorded as zero. The error bars denote the 95% confidence interval over the mean for each strain.

For staining with FM4-64, cells in logarithmic growth phase were incubated with

the dye (at a final concentration of 1 µg/ml) at 30°C for 15 min. The cells were washed with fresh growth medium and incubated at 30°C for 30 min. Manders' colocalization coefficient (M_1) was used to quantify colocalization (Dunn et al., 2011). Deconvolved images from *Z*-stacks containing multiple cells were converted into a two-dimensional array of pixel intensities before background subtraction. For background subtraction, local background (median of a 40 x 40 region around the particular pixel) for each pixel was calculated. The local background value for each pixel was then subtracted from the respective pixel value. An additional small value was subtracted from each pixel to remove signal from nonspecific regions. M_1 was calculated over several images for each strain and presented as mean ± range for 95% confidence interval.

Canavanine plate assay

Yeast cells were grown in YNB (selective media wherever necessary) to logarithmic growth phase. After removal of the growth medium, cells were resuspended in 1 M sorbitol to final OD_{600} of 0.5. Serial dilutions were made for each strain in 96-well plates, so that the first column had 0.5 OD_{600} cells and every successive column was five times diluted from the preceding column. For each strain, 3 µl of cells were plated from the foregoing dilutions. Agar plates containing canavanine (Sigma-Aldrich, St. Louis, MO) were made with 2% glucose and 6.7 g/l YNB without arginine. In addition, uracil (20 µg/ml), leucine (30 µg/ml), histidine (20 µg/ml), adenine (20 µg/ml), lysine (30 µg/ml), and tryptophan (20 µg/ml) were provided wherever necessary to support the growth of auxotrophic strains.

Western blot analysis

For quantification of GFP-Cps1 sorting into vacuole, yeast cell extracts were obtained from strains grown to logarithmic phase. Cells were pelleted, resuspended in SDS–PAGE sample buffer (2% SDS, 0.1 M Tris, pH 6.8, 10% glycerol, 0.01% bromophenol blue, 5% β- mercaptoethanol), lysed using glass beads, and boiled for 5 min at 95°C. For Western blotting, monoclonal antibodies against GFP (anti- GFP antibody from Roche Diagnostics [Basel, Switzerland]) were used at 1:2500 dilutions. The anti-Snf7 antibody used was previously described (Babst et al., 1998). IRDye-conjugated secondary antibody was purchased from LI-COR Biosciences (Lincoln, NE), and Western blots were imaged using the accompanying Odyssey Imaging System.

Transmission electron microscopy

Yeast were grown at 30°C to logarithmic phase, transferred to aluminum hats, high-pressure frozen, and placed in vials with a freeze substitution solution of 0.1% uranyl acetate and 2% glutaraldehyde in anhydrous acetone. Vials were placed in an automatic freeze substitution device (EM AFS2; Leica, Buffalo Grove, IL) at –140°C and warmed to –80°C over 24 h. Cells were extracted from the hats at −80°C, placed in chilled tubes with fresh freeze substitution solution for 48 h, and then warmed to −60°C over 20 h. Fixative was replaced with Lowicryl HM20 over the next 96 h with three acetone washes, three washes of increasing HM20:acetone (1:3, 1:1, and 3:1), and six washes with 100% HM20. Polymerization with ultraviolet light began at −60°C for 12 h and continued up to 20°C over 36 h. The 90-nm sample thin sections were placed on rhodium-plated Formvar-coated copper grids and viewed with a Philips (Eindhoven, The

Netherlands) CM10 transmission electron microscope, and images were processed using ImageJ64.

Glycerol density gradient centrifugation assay

Thirty OD_{600} units of yeast cells were converted to spheroplasts, osmotically lysed in 1 ml ice- cold lysis buffer consisting of phosphate-buffered saline, pH 7.4 (PBS; 137 mM NaCl, 2.7 mM KCl, 10 mM Na_2HPO_4, 1.8 mM KH_2PO_4) that was supplemented with 0.5% Tween-20 and a protease inhibitor cocktail (Roche Diagnostics; Switzerland). The cells were then homogenized on ice before centrifugation at 16,100 x g for 10 min at 4℃ to pellet membranes. The membrane fraction was resuspended in 1 ml ice-cold lysis buffer and passed 5 times through a 25-gauge needle to generate a solubilized protein sample that was loaded at the top of a linear glycerol gradient (10%–40%) prepared in PBS and 0.5% Tween-20. The gradient was centrifuged at 100,000 x g for 4 hr at 4℃, after which, 1-ml fractions were collected from the top of the gradient, and 10% (vol/vol) trichloroacetic acid (TCA) was added to precipitate the proteins on ice for 20 min. The precipitates were harvested by centrifugation at 16,100 x *g* for 10 min at 4℃, then resuspended by sonication into ice-cold acetone, and incubated on ice for 20 min. Precipitates were harvested by centrifugation and sonication into acetone once more, after which, the pellets was dried by rotary evaporation, then each was resuspended by sonication into 100 µl Laemmli buffer (0.1% β-mercaptoethanol, 0.0005% bromophenol blue, 10% glycerol, 2% sodium dodecyl sulfate (SDS), 63 mM Tris-HCl, pH 6.8). The gradient fraction protein samples were boiled for 5 min, and 10 µl of each was resolved by SDS- polyacrylamide gel electrophoresis (SDS-PAGE), transferred to nitrocellulose, and analyzed by western blot using anti-Snf7 polyclonal

antiserum (Babst et al., 1998).

Statistical analysis

A Kolmogorov–Smirnov test was performed for endosomal localization of ESCRT-II in Figures 2.2A and for ILV counts in Figure 2.6B using the application R (www.r-project.org).

Chapter 3: ubiquitin hydrolase regulation of ESCRT-III activity at endosomes

Introduction

Doa4 is a yeast ubiquitin hydrolase that is essential for cells to maintain the cellular supply of free, nonconjugated ubiquitin (Swaminathan et al., 1999). The enzyme acts on both proteasomal and endosomal substrates, but of the 16 ubiquitin hydrolases found in *Saccharomyces cerevisiae*, Doa4 is the only one to act on ILV cargoes, making regulation of Doa4 activity at endosomes particularly important (Swaminathan et al., 1999; Katzmann et al., 2001). ESCRT-III assembly at endosomes traps ubiquitinated cargoes sorted by ESCRT-0, -I, and –II (Teis et al., 2010) and prevents their diffusion away from the site of ILV budding while the cargoes undergo deubiquitination. Bro1 promotes Doa4 localization to and regulates Doa4 catalytic function at endosomes (Luhtala and Odorizzi, 2004; Richter et al., 2007). Bro1 is recruited to ESCRT-III through direct interaction between its amino terminal 'Bro1 domain' and the MIM1 site in Snf7, while Vps4 binds the MIM2 site in Snf7 (Figure 3.1) (Kim et al., 2005; Wemmer et al., 2011). Identification of Bro1 as a candidate that regulates Doa4 came from a screen intended to gain incite into Bro1 function. Bro1 is a class E Vps gene, but the only class E Vps gene that is not a component of an ESCRT complex or the Vps4 machinery (Odorizzi et al., 2003). The screen revealed that Doa4 overexpression suppresses the class E compartment phenotype of a Bro1 deletion strain (Figure 3.2, A-C).

Overexpression restores Doa4 recruitment to endosomes in the absence of Bro1 (Richter et al., 2007; Luhtala and Odorizzi, 2004). Like other ubiquitin hydrolases,

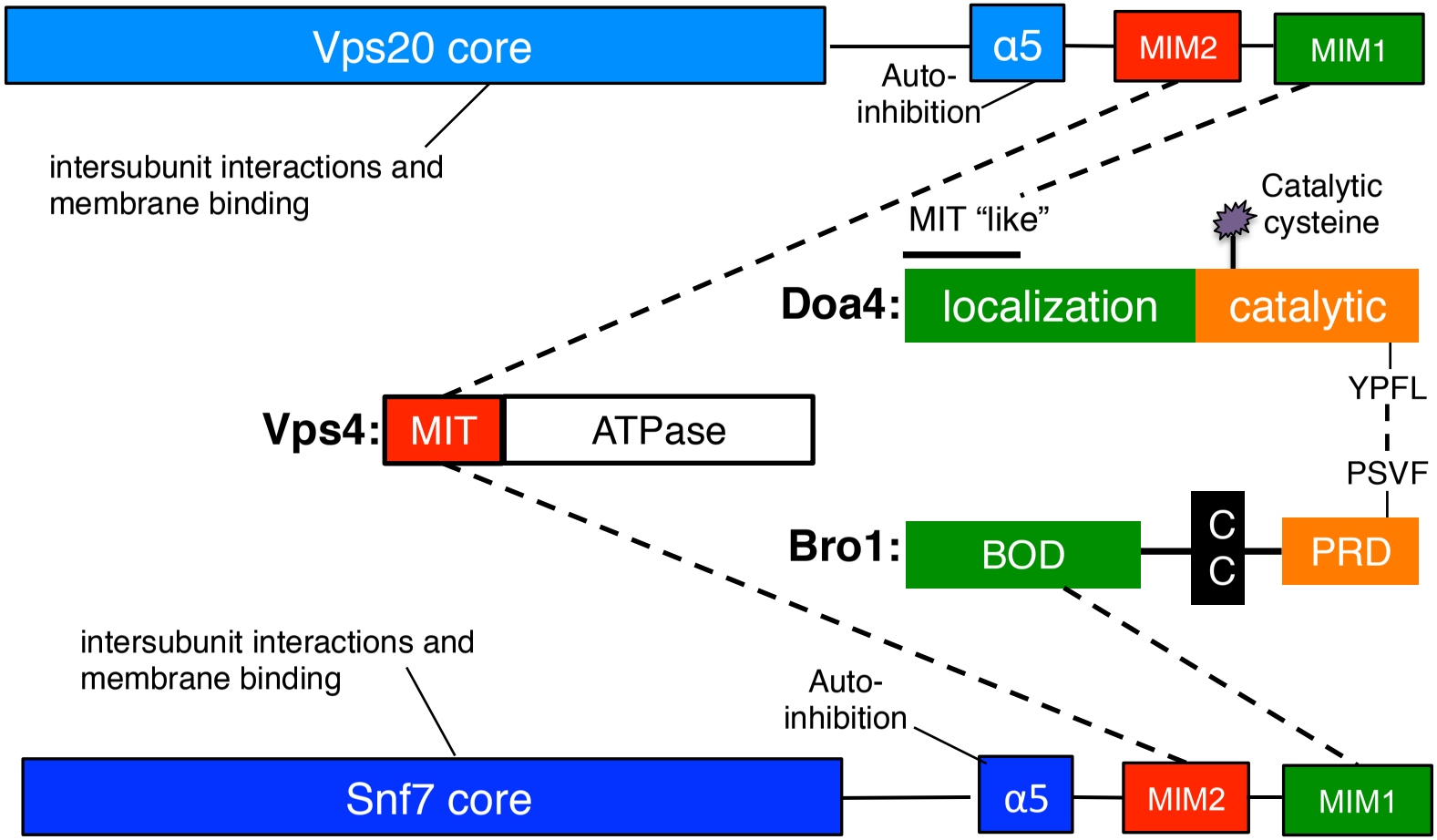

Figure 3.1. Domain interactions between ESCRT-III and ESCRT-III associated proteins. Model of known interaction domains between two core ESCRT-III proteins (Vps20 and Snf7) and three ESCRT-III associated proteins. Abbreviations: MIT-interacting motif (MIM), microtubule interacting and trafficking (MIT) domain, Bro1 domain (BOD), coiled-coil domain (CC), proline-rich domain (PRD). Adapted from Tang et al., 2015.

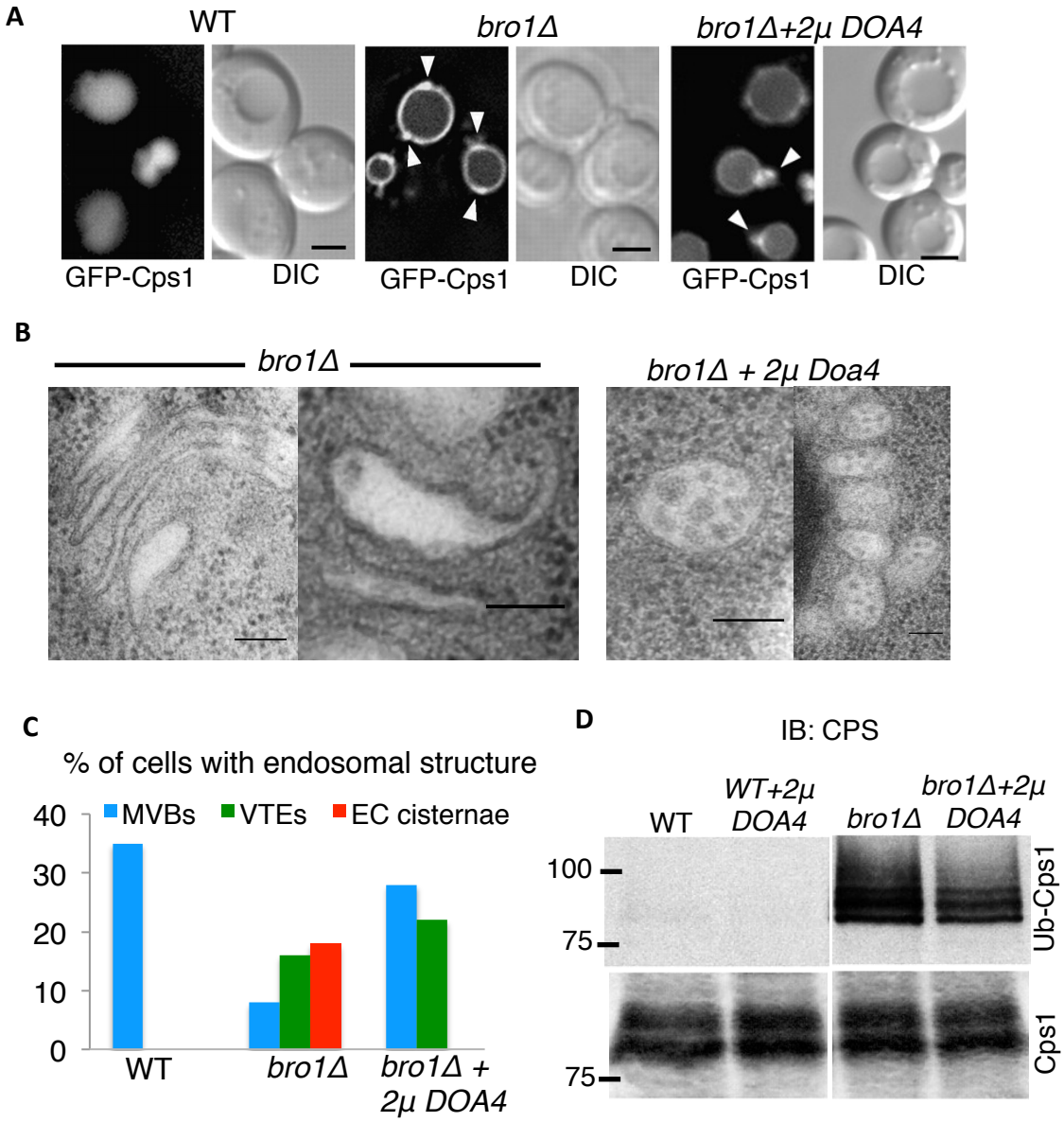

Figure 3.2. Doa4 overexpression suppresses class E compartment formation in *bro1* deletion strains. (A) Fluorescence and DIC microscopy of the indicated strains transformed with a low-copy-number plasmid encoding GFP-*Cps1* in addition to a high-copy-number plasmid (2μ) encoding *DOA4*. Arrowheads indicate class E compartments. Bars = 2 μM. (B) 90-nm thin section TEM images of endosomes form the indicated strains with or without 2μ *DOA4* expression. Scale bars = 100 nm. (C) Quantification of endosome morphologies from 100 cell counts by TEM as in B. (D) Western blot analysis of Cps1 immunoprecipitates probing for ubiquitin or Cps1. Note that Cps1 shows up as two bands due to differential glycosylation of the lumenal domain (Spormann et al., 1992). A and D adapted from Luhtala and Odorizzi, 2004).

Doa4 consists of an N-terminal localization domain and a C-terminal catalytic domain (Figure 3.1) (Kim et al., 2003; Richter et al., 2007). Fusion of the Doa4 localization domain with the catalytic domain of Ubp5, the yeast ubiquitin hydrolase most similar to Doa4, results in a hybrid protein that can localize to endosomes but cannot deubiquitinate ILV cargoes, indicating that regulation of Doa4 catalytic activity is key to its substrate specificity at ILVs (Richter et al., 2007). Bro1 stimulates Doa4 catalytic activity by directly binding a YPFL motif in its ubiquitin hydrolase domain (Figure 3.1) (Richter et al., 2007). Interaction with this motif is conserved in ALIX, the closest mammalian ortholog to Bro1, which binds YPxL motifs found in retroviral encoded Gag proteins to recruit ESCRTs (in a ubiquitin dependent manner) to the plasma membrane to mediate viral egress (Martin-Serrano et al., 2003; Morita and Sundquist, 2004).

While overexpression restores Doa4 recruitment to endosomes in the absence of Bro1, Doa4 catalytic activity is not restored in this context (Figure 3.2D) (Richter et al., 2007; Luhtala and Odorizzi, 2004). This finding complicated interpretation of the above mentioned screen to identify essential Bro1 properties that make it a class E Vps protein, but data hinted that an unknown, non-catalytic function of Doa4 mirrors an unknown function of Bro1 that influences ILV formation (Richter et al., 2007). In 2011, the lab showed that Bro1 domain-binding also protects Snf7 from disassembly by Vps4, and overexpression of *BRO1* in yeast inhibits ILV membrane scission (Wemmer et al., 2011), indicating that another Bro1 function is to regulate ESCRT-III membrane scission activity by controlling ESCRT-III disassembly. Here we show that overexpression of *DOA4* phenocopies the loss of Vps4 function by causing the accumulation of high-molecular-weight Snf7 polymers, which suggests that Doa4 stabilizes ESCRT-III by

protecting the complex from disassembly. We also show that *DOA4* overexpression strongly inhibits ILV membrane scission, consistent with ESCRT-III disassembly being coupled to the membrane scission activity of the complex.

The Vps4 MIT domain binds the MIM2 site in Vps20 (Figure 3.1), the ESCRT-III subunit that initiates complex assembly by nucleating Snf7 polymerization (Figure 2.5A) (Kieffer et al., 2008). Conversely, the MIM1 site in Vps20 binds an MIT-like domain at the amino terminus of Doa4 (Figure 3.1), and this interaction inhibits an unknown function of Doa4 that promotes ILV budding but does not involve Doa4 ubiquitin hydrolase activity (Richter et al., 2013). In this chapter, I show that Vps20-binding inhibits Doa4 from functioning non-catalytically to promote ESCRT-III stability and that overexpression of the Bro1 domain inhibits this interaction, revealing another mechanism by which Bro1 promotes Doa4 function. I further show that Doa4 preferentially binds the open/active conformation of Vps20 that nucleates Snf7 polymerization. Vps20 locked by mutation in its open/active conformation inhibits the MVB pathway, but ILV budding is restored if Doa4 binding to this mutant Vps20 is disabled. The constitutively open/active Vps20 mutant also inhibits ILV cargo deubiquitination by Doa4, signifying that Vps20-binding prevents Doa4 ubiquitin hydrolase function at MVBs. We propose that Vps20 negatively regulates Doa4 to prevent premature deubiquitination of ILV cargoes during the initiation of ESCRT-III assembly. The subsequent relief of inhibitory Vps20-binding to Doa4 by Bro1, coupled with Bro1 stimulation of Doa4 ubiquitin hydrolase activity, would allow Doa4 to inhibit ESCRT-III disassembly and forestall ILV membrane scission while it deubiquitinates transmembrane protein cargoes encircled by ESCRT-III.

RESULTS

Doa4 cooperates with Bro1 to stabilize ESCRT-III complexes

The stability of membrane-associated ESCRT-III complexes is determined by the rate of their assembly offset by the rate of their disassembly (Figure 2.5A). Thus, a measure of ESCRT-III complex stability is its abundance at steady state, which can be assayed by sedimentation of its most abundant subunit, Snf7, after rate-zonal centrifugation of detergent-solubilized membranes (Figure 2.5 A; Teis et al., 2008). Using this approach, we found a 50% decrease in the amount of polymeric Snf7 (i.e., ESCRT-III) upon deletion of *BRO1* (*bro1*Δ*;* Figure 3.3). Figure 3.3 also shows that overexpression of *DOA4* fully rescues ESCRT-III complex abundance in *bro1*Δ cells and that partial rescue was provided by overexpression of the catalytically inactive allele $doa4^{C571S}$, which fits nicely with a previous finding by the lab that DOA4 overexpression restores ILV budding in *bro1*Δ cells through an unknown, non-catalytic function (Figure 3.2). Our observations suggest that Doa4 functions to cooperate with Bro1 in promoting ESCRT-III complex stability. This hypothesis is supported by our observation that deletion of *DOA4* causes a strong reduction in ESCRT-III complexes, much like we see in *bro1*Δ cells (Figure 3.3). Furthermore, the abundance of ESCRT-III complexes in *doa4*Δ cells was restored to wild-type levels when *BRO1* was overexpressed, similar to the replenishment of ESCRT-III abundance in *bro1*Δ cells overexpressing *DOA4* (figure 3.3). Excess levels of either Doa4 or Bro1 can, therefore, maintain normal ESCRT-III complex stability when the other protein is absent.

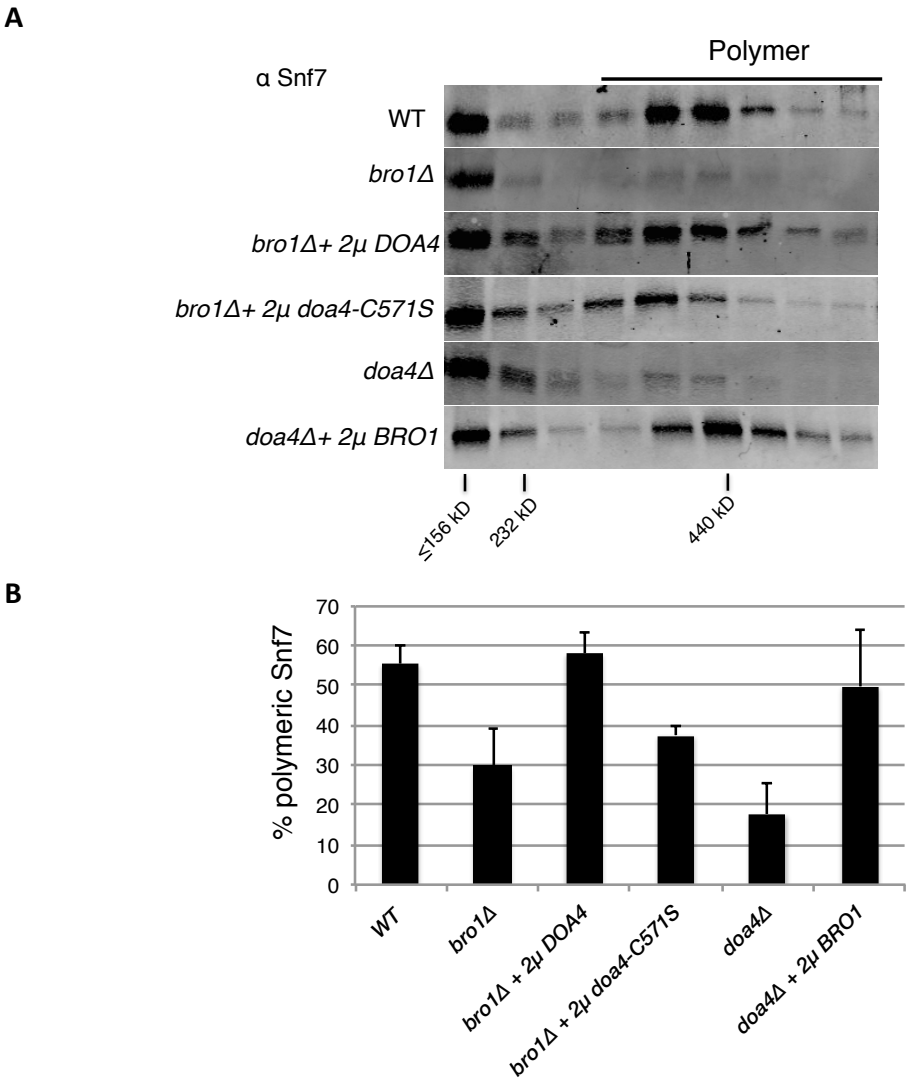

Figure 3.3. Doa4 cooperates with Bro1 to stabilize ESCRT-III complexes. (A) Western blot analysis of the distribution of Snf7 in fractions resolved by rate-zonal density gradient centrifugation. Indicated below the bottom panel are migrations of molecular-weight standards: aldolase (156 kD), catalase (232 kD), and ferritin (440 kD). (B) Quantifications from triplicate experiments of the percentage of Snf7 in all gradient fractions represented by polymeric Snf7/ESCRT-III seen fractions 4-9; this size range was previously established to correspond to assembled ESCRT-III complexes (Teis et al., 2008). Error bars represent standard deviations.

DOA4 overexpression causes accumulation of high-molecular-weight ESCRT-III complexes

The lab had previously seen a moderate increase in ESCRT-III complex abundance in wild-type cells when *BRO1* was overexpressed, consistent with Bro1 functioning to inhibit disassembly of the complex (Wemmer et al., 2011; figure 3.4 A and B). *DOA4* overexpression in wild-type cells had a similar effect (figure 3.4 A and B), which was not surprising, given that high-copy *DOA4* rescued ESCRT-III complex stability in cells lacking *BRO1* (figure 3.3). The abundance of ESCRT-III complexes also increased when $doa4^{C571S}$ was overexpressed in wild-type cells (figure 3.4 A and B), echoing the result in figure 3.3, which indicated that the ubiquitin hydrolase activty of Doa4 is not essential for it to promote ESCRT-III complex stability.

A notable difference upon overexpression of wild-type *DOA4* but not overexpression of $doa4^{C571S}$ or *BRO1* was the accumulation of higher molecular-weight ESCRT-III complexes, the size range of which was similar to that seen in cells lacking the Vps4 ATPase that disassembles ESCRT-III (*vps4*Δ*;* Figure 3.4 A and C). This observation suggested that *DOA4* overexpression boosts the abundance of ESCRT-III complexes by inhibiting their disassembly, although an alternative possibility is that Doa4 stimulates complex assembly. However, *DOA4* overexpression did not rescues ESCRT-III complex abundance either in *vps20*Δ cells or in $vps25^{T150K}$ cells (figure 3.4 E and F), the latter of which express a mutant version of the ESCRT-II complex that is unable to bind and activate Vps20 (Im et al., 2009; Teis et al., 2010). Doa4, therefore, cannot augment the canonical pathway for ESCRT-III complex assembly (Saksena et al., 2009; Teis et al., 2010), suggesting that Doa4 stabilizes ESCRT-III complexes by

inhibiting their disassembly rather than by stimulating complex disassembly.

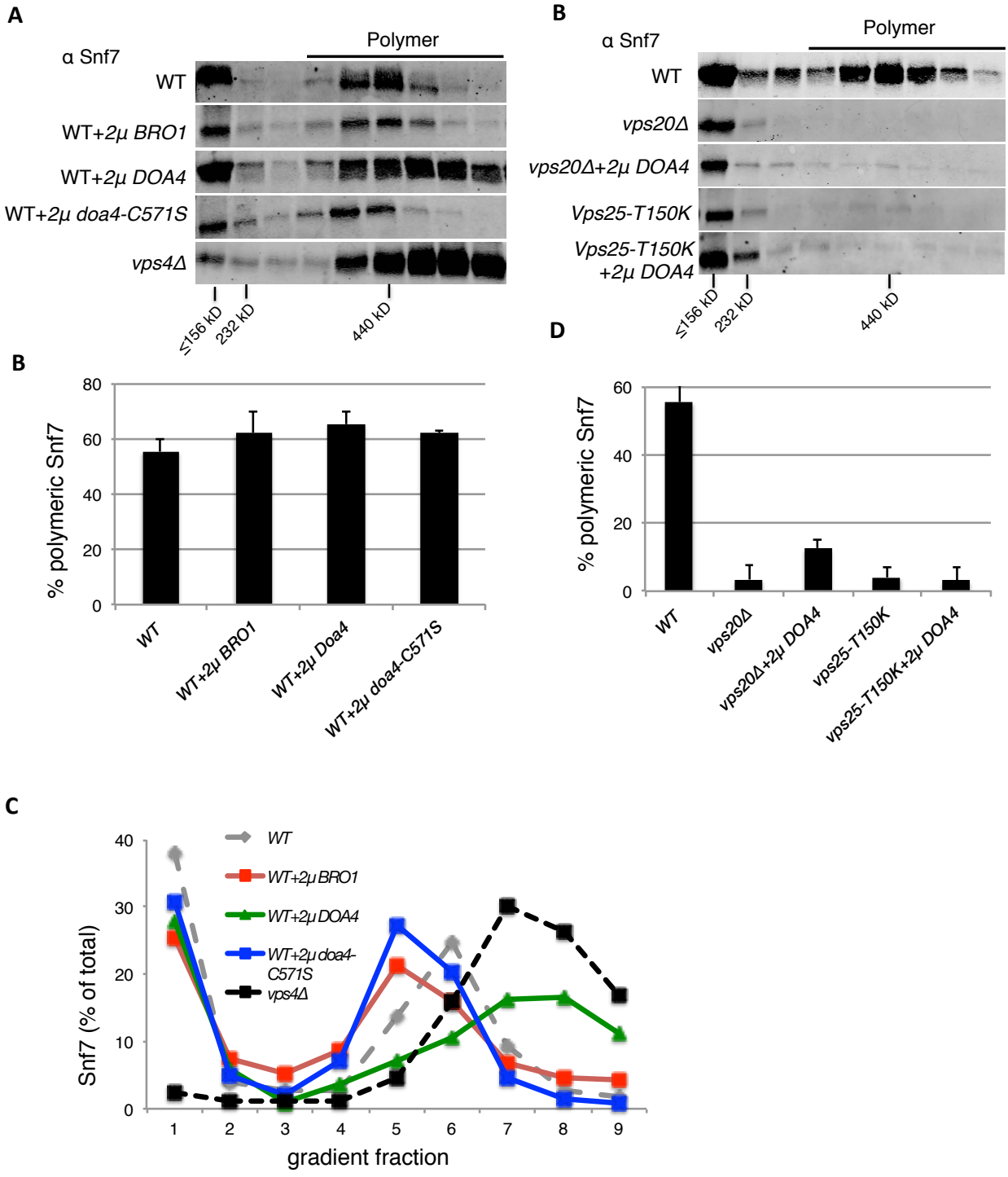

Figure 3.4. 2μ Doa4 causes accumulation of high molecular weight ESCRT-III complexes. (A) Western-blot analysis (A and D) and quantification (B and E) of polymeric Snf7 as described in Figure 3.2. (C) Line-graph representation of the mean percent of membrane-bound Snf7 in each gradient fraction from the indicated strains.

DOA4 overexpression inhibits ILV membrane scission

The lab had previously shown by electron tomography and three-dimensional modeling of yeast endosomal structures that *BRO1* overexpression in wild-type cells inhibits ILV membrane scission (Wemmer et al., 2011). Together with other studies (Sachse et al., 2004; Hanson et al., 2008; Adell et a., 2014; Cashikar et al., 2014; Shen et al., 2014), this observation was consistent with a model in which the membrane scission activity of ESCRT-III is coupled to disassembly of the complex by Vps4. We performed a similar examination of endosomal structures by tomography in wild-type yeast with or without *DOA4* overexpression to determine whether the inhibition of ESCRT-III disassembly by Doa4 affected ILV membrane scission.

As with the lab's previous study (Wemmer et al., 2011), we observed an average of 1.2 ILV budding profiles per MVB in wild-type cells (Figure 3.5, A and C), the frequency of which is nearly doubled by *BRO1* overexpression (Wemmer et al., 2011; Figure 3.5C). A concomitant reduction in the amount of lumenal membrane caused by *BRO1* overexpression (Wemmer et al., 2011; Figure 3.5D) signified that excess levels of Bro1 inhibits ILV membrane scission. Compared to *BRO1* overexpression, however, *DOA4* overexpression had a much stronger effect. MVBs had an average of 5.0 ILV budding profiles in wild-type cells overexpressing *DOA4*, which is > 4.5-fold the amount normally seen and > 2.5-fold the amount observed upon *BRO1* overexpression (Figure 3.5, B and C).

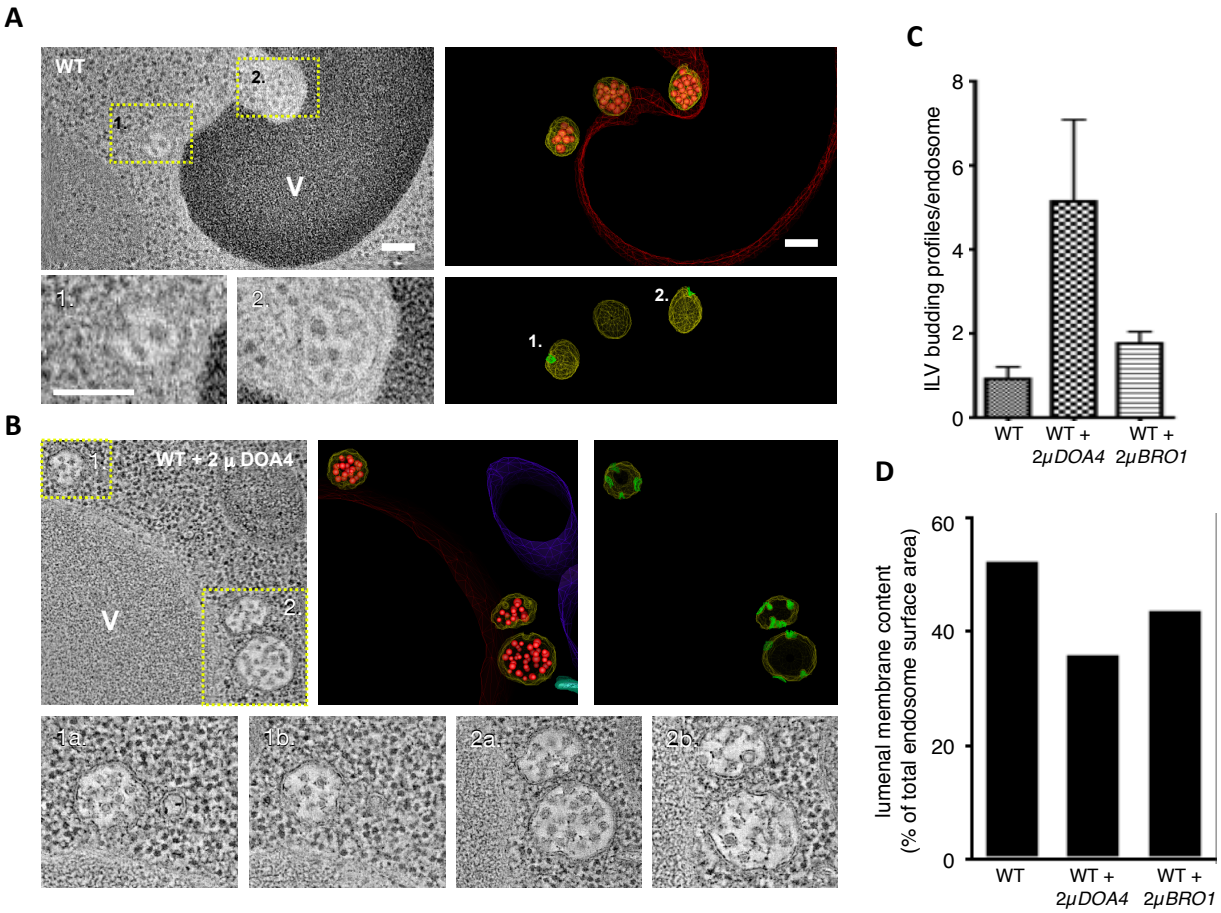

Figure 3.5. DOA4 overexpression inhibits ILV membrane scission. (A and B) 2-D cross-sectional tomographic slices and 3-D models from 250-nm-thick section electron tomographs. In each model, spherical endosomal limiting membranes are traced in yellow, freely detached ILVs are traced in red, and ILV budding profiles are traced in green. In some cases, the continuity of ILV budding profiles with the limiting endosomal membrane is out of plane in the tomographic slice but evident in the 3D reconstruction. Bars, 100 nm. ILV budding profiles were identified by recognizable negative curvature and a net surface area greater than half of the mean ILV surface (>750 nm2). (C) Quantitation from dual-axis tomographs and models of endosomes in wild-type cells alone (WT; N=12) versus wild-type cells transformed with a high-copy-number plasmid (2µ) encoding DOA4 (N=7) or BRO1 (N=17). Quantitative data for 2µ BRO1 transformants are derived from experiments published in Wemmer et al. (2011). (D) Quantitation of the lumenal versus limiting membrane surface areas in modeled endosomes.

DOA4 overexpression also caused a sharper reduction in the amount of lumenal membrane than did *BRO1* overexpression. In wild-type yeast, ILVs account for ~55% of the total membrane at each MVB, but *DOA4* overexpression caused a 40% reduction in this amount, whereas *BRO1* overexpression reduced the ILV content by only 20% (Figure 3.5D). *DOA4* overexpression, therefore, more strongly inhibits ILV membrane scission than does Bro1 overexpression. This more potent inhibitory effect mirrors the greater degree to which the overexpression of *DOA4* caused the accumulation of high-molecular-weight ESCRT-III complexes (Figure 3.4A-C), supporting a model in which Doa4 protects ESCRT-III from disassembly in order to control the rate at which ILV membrane scission occurs.

The Vps20 subunit of ESCRT-III inhibits complex stabilization by Doa4

The observations described above indicated that Doa4 regulates ESCRT-III stability and ILV membrane scission, and it appears to do so in a manner that does not depend upon its ubiquitin hydrolase activity. The lab had previously reported an unknown non-catalytic role for Doa4 that rescues ILV budding when *BRO1* is absent, and this function of Doa4 is inhibited through Doa4 binding to the MIM1 site in Vps20 (figure 3.1); thus, the ILV budding pathway was rescued in *bro1*Δ cells upon point-mutation of the Vps20 MIM1 sequence (*vps20*$^{\Delta MIM1}$; Richter et al., 2013). Figure 3.6 A and B show that the *vps20*$^{\Delta MIM1}$ mutation also rescued ESCRT-III complex stability in *bro1*Δ cells, whereas the *vps20*$^{\Delta MIM1}$ mutation on its own had no apparent effect toward ESCRT-III. Importantly, the rescue of ESCRT-III complex stability seen in *bro1*Δ*; vps20*$^{\Delta MIM1}$ cells required Doa4 but not its ubiquitin hydrolase activity because rescue still occurred upon replacing wild-type *DOA4* with the *doa4*^{C571S} allele, whereas deletion

of *DOA4* prevented rescue (figure 3.6 A and B). Therefore, the non-catalytic function Doa4 has toward stabilizing ESCRT-III complexes is inhibited through its interaction with the MIM1 sequence in the Vps20 subunit of ESCRT-III.

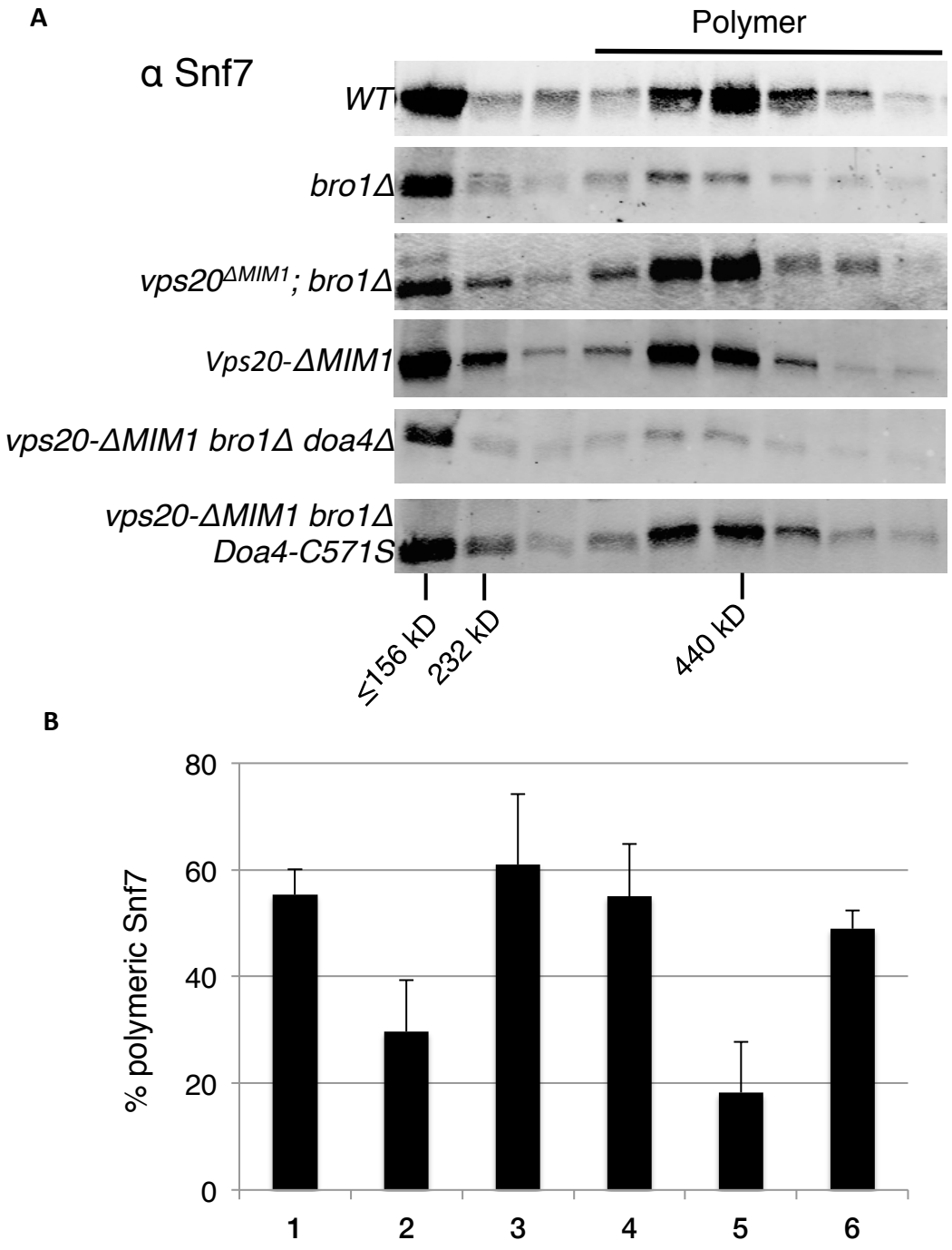

Figure 3.6. The Vps20 subunit of ESCRT-III inhibits complex stabilization by Doa4. Western-blot analysis (A) and quantification (B) of polymeric Snf7 as described in figure 3.3. The numbers to the right of the immunoblots in A correspond to the numerical categories along the X-axis in B.

Bro1 relieves Vps20 inhibitory binding to Doa4

Inhibitory binding of Vps20 to Doa4 is presumably dynamic in yeast to ensure that Doa4 regulation of ESCRT-III and ILV budding is spatiotemporally controlled. Such a transient interaction between Vps20 and Doa4 would explain why their coimmunoprecipitation from yeast could not be detected without disabling the Vps4 ATPase that disassembles ESCRT-III (Richter et al., 2013). Further evidence that Vps20 transiently binds Doa4 came from bimolecular fluorescence complementation (BiFC) studies in which we expressed either the amino- or carboxyl-terminal fragments of the Venus fluorescent protein (VN and VC, respectively) fused to the carboxyl terminus of Doa4 versus Vps20. Binding between Doa4 and Vps20 would bring the Venus fragments within proximity of one another, allowing the Venus reporter to assemble into its native three-dimensional structure and emit a fluorescent signal (Kerppola, 2006).

In wild-type cells coexpressing Doa4-VN and Vps20-VC, we observed BiFC fluorescence within the vacuole lumen, which was dependent upon Doa4 binding to Vps20 because fluorescence was absent when Doa4-VN was coexpressed with a mutant Vps20$^{\Delta MIM1}$- VC fusion protein lacking the Doa4-binding site (Figure 3.7A). Because reconstitution of the Venus fluorochrome through dimerization of its amino- and carboxyl-terminal fragments is irreversible, the normal association/dissociation cycle of proteins that interact dynamically with one another is disrupted (Kerppola, 2006). Therefore, the BiFC fluorescence in the vacuolar lumen of cells coexpressing Doa4-VN and Vps20-VC suggested that the stabilization of their interaction through Venus assembly caused aberrant packaging of both proteins into ILVs that are

subsequently delivered into the vacuole upon endolysosomal fusion. This route of delivery was confirmed by blocking the MVB pathway through expression of the catalytically inactive *vps4*^{E233Q} allele, which shifted the BiFC fluorescence between Doa4-VN and Vps20-VC to puncta that were labeled with the endocytic dye, FM 4-64 (Figure 3.7A, arrowhead).

The transient nature of Vps20 binding to Doa4 in yeast raised the question of how Doa4 is normally relieved from this inhibitory interaction. Given that the inhibitory effect Vps20 has toward Doa4 is most evident in *bro1*Δ cells (Richter et al., 2013; Figure3.6), we reasoned that Bro1 might be involved in relieving Doa4 from Vps20 inhibition, in which case, excess amounts of Bro1 could interfere with the Doa4-Vps20 interaction. Indeed, the BiFC fluorescence that had been observed in cells coexpressing Doa4-VN and Vps20-VC was absent from cells overexpressing *BRO1* (Figure 3.7B). We further queried which region of Bro1 blocks the Doa4-VN – Vps20-VC interaction by assaying BiFC fluorescence in cells overexpressing different functional domains of Bro1. The carboxyl-terminal proline-rich region of Bro1 binds directly to the Doa4 catalytic domain to stimulate its ubiquitin hydrolase activity (Richter et al., 2007). However, overexpression of this region (*2μ bro1*$^{388-844}$) had no apparent effect on BiFC between Doa4-VN and Vps20-VC. In contrast, BiFC fluorescence was abrogated by overexpression of the amino-terminal 'Bro1 domain' (*2μ bro1*$^{1-387}$; Figure 3.7B), which is the region of Bro1 that binds the Snf7 subunit of ESCRT-III (Kim et al., 2005).

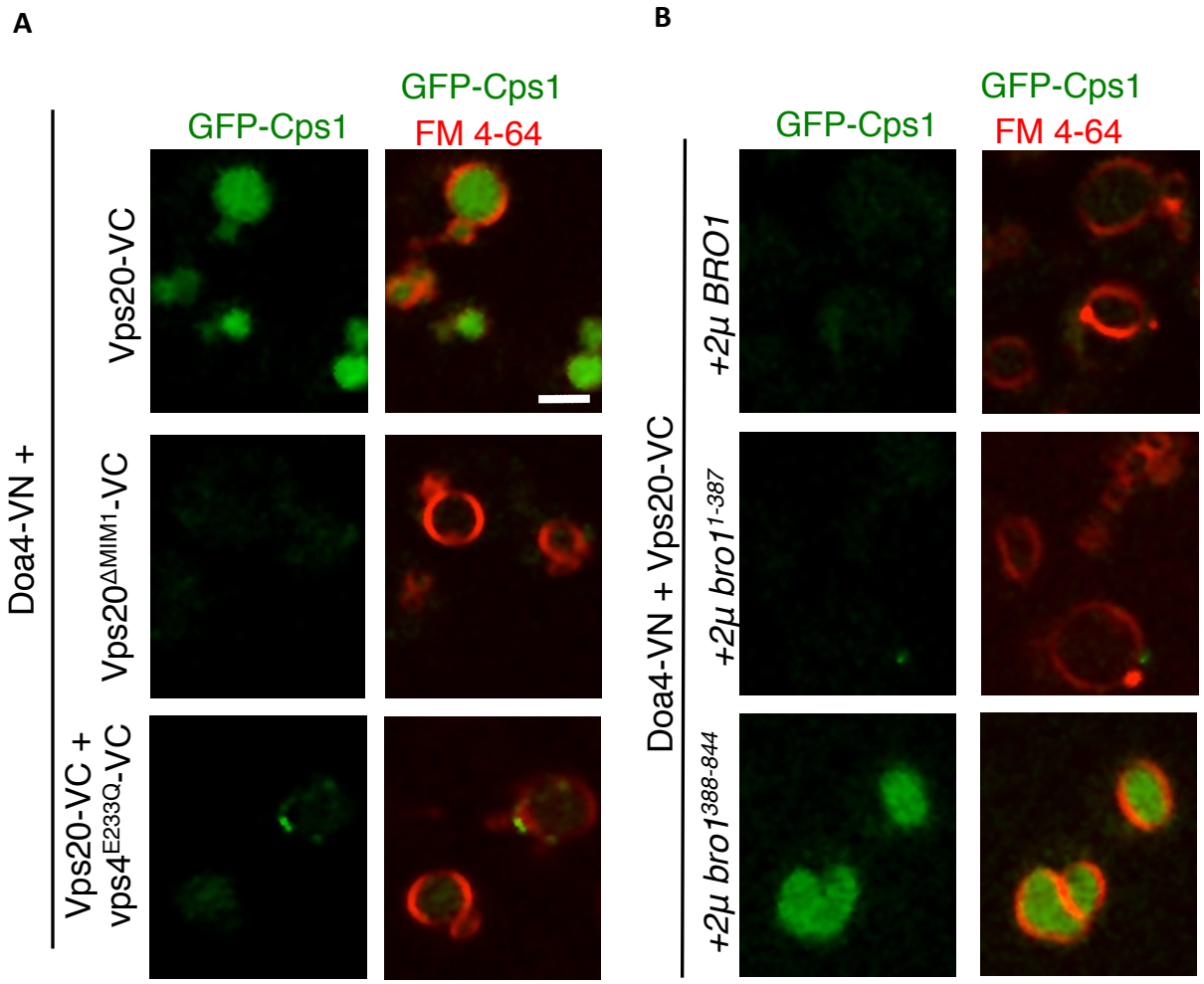

Figure 3.7. Bro1 relieves Vps20 inhibitory binding to Doa4. (A) Venus (optimized YFP) fluorescence derived from BiFC between Doa4-VN and either wild-type Vps20-VC or mutant Vps20$^{\Delta MIM1}$-VC. Endosome and vacuole membranes are stained with FM 4-64. The VN and VC fusions were coexpressed in wild-type yeast, except in the bottom row of cells, which were transformed with a low-copy-number plasmid (CEN) encoding the dominant-negative *vps4$^{E/Q}$* allele that blocks the MVB pathway. The arrowhead indicates colocalization of BiFC fluorescence at endosomes stained with FM 4-64. (B) YFP fluorescence derived from BiFC between Doa4-VN and Vps20-VC in FM 4-64-stained wild-type cells transformed with a high-copy-number plasmid (2μ) encoding wild-type *BRO1* versus the amino-terminal Bro1 domain (*bro1$^{1-387}$*) or the carboxyl-terminal proline-rich region of Bro1 (*bro1$^{388-844}$*). Bar = 2 μm.

Thus, Bro1 relieves Doa4 from its inhibitory interaction with Vps20, explaining why Vps20 inhibition of Doa4 is most evident in *bro1*Δ cells (Richter et al., 2013; Figure 3.3). The relief of inhibitory Vps20-binding to Doa4 by the Bro1 domain of Bro1 rather than the proline-rich region that stimulates Doa4 catalytic activity is consistent with a regulatory relationship between Doa4 and Bro1 that does not involve the ubiquitin hydrolase function of Doa4.

The open/active conformation of Vps20 binds Doa4

Biochemical studies previously showed that the yeast Vps20 protein has a closed/inactive conformation that must transition to an open/active state in order to nucleate Snf7 polymerization (Figure 3.8A; Saksena et al., 2009; Teis et al., 2010). Each conformational state of Vps20 can be stabilized by intragenic mutation (Saksena et al., 2013), which we exploited to test if either conformation of Vps20 preferentially binds Doa4. A fusion protein consisting of glutathione *S*-transferase (GST) fused to Doa4 amino acids 2-80 (which binds Vps20; Richter et al., 2013) was coexpressed in bacteria either with wild-type *VPS20*, with the constitutively closed/inactive *vps20*^{PW} allele (containing the P183W, P189W, and P192W substitutions), or with the constitutively open/active *vps20*^{loop} allele (containing a deletion of amino acids 48-59). Pulldowns from bacterial lysates using guathione-sepharose showed that GST- Doa4$^{2-80}$ interacted with the mutant vps20^{loop} protein as effectively as it did with wild-type Vps20, whereas the mutant vps20^{PW} protein failed to bind (Figure 3.8B). Doa4 is, therefore, specifically bound by the open/active conformation of Vps20 rather than the closed/inactive form, which suggests that inhibitory binding to Doa4 by Vps20 is

concurrent with Vps20 activation of ESCRT-III assembly.

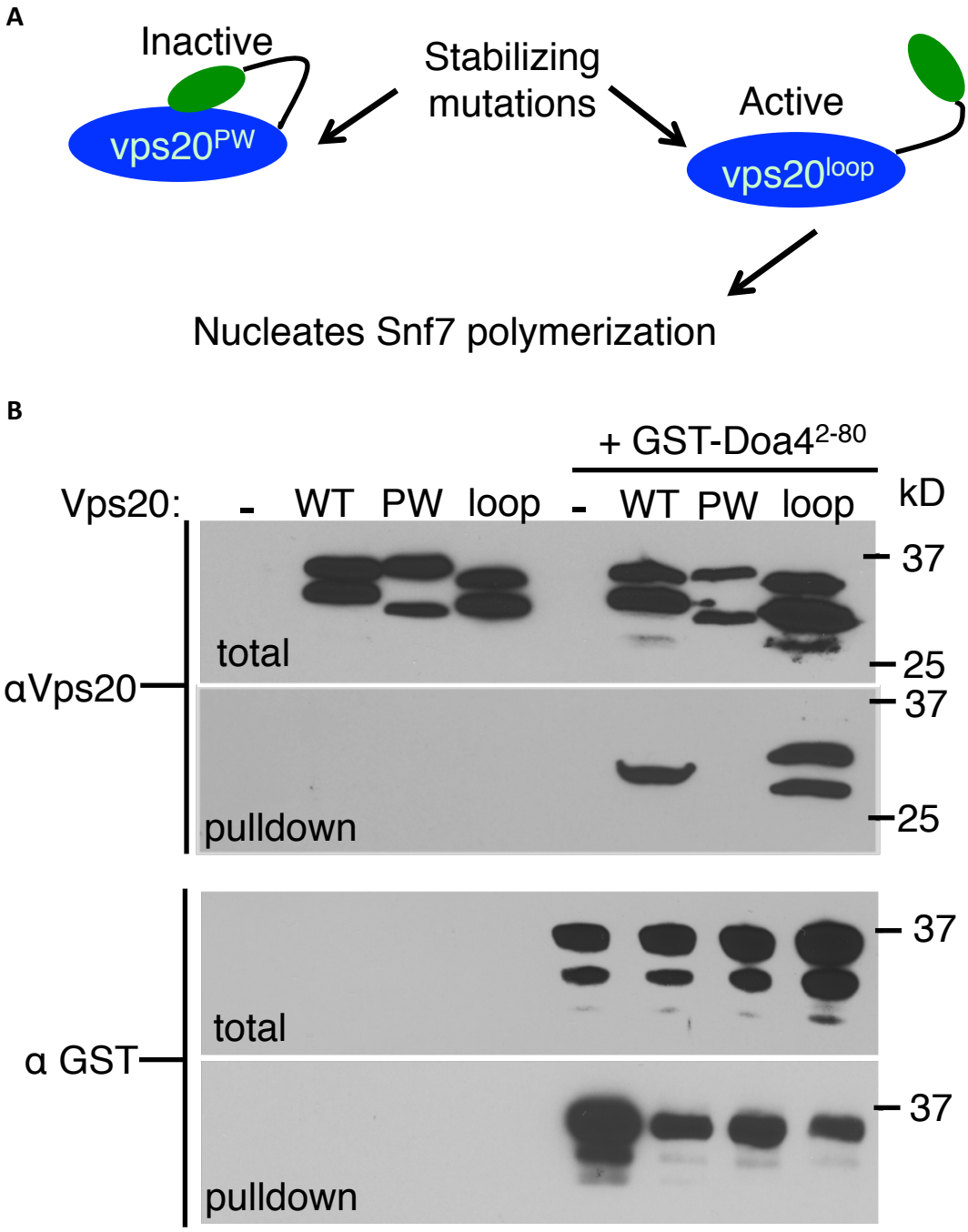

Figure 3.8. The open/active conformation of Vps20 binds Doa4. (A) Schematic diagram depicting the closed/inactive versus open/active conformations of Vps20, each of which is stabilized by mutations (*vps20^{PW}* and *vps20^{loop}*, respectively). (B) Glutathione-sepharose pulldowns from lysates of bacteria expressing wild-type or mutant Vps20 proteins; coexpression of GST-Doa4$^{2-80}$ is indicated above the top panel.

The open/active conformation of Vps20 inhibits Doa4 function in the MVB pathway

Having ascertained that Doa4 binds the open/active conformation of Vps20, we investigated whether constitutive expression of *VPS20* locked in this conformational state inhibits the MVB pathway. We first examined the localization of GFP fused to the cytosolic domain of Cps1, the archetypal ILV cargo protein used in chapter 2. In wild-type cells, ESCRT-mediated sorting of GFP-Cps1 into ILVs followed by MVB–vacuole fusion results in GFP localization to the vacuole lumen (Figure 3.9A; Odorizzi et al., 1998). Replacing wild-type *VPS20* with the open/active mutant *vps20^{loop}*, however, resulted in the mislocalization of GFP-Cps1 to vacuole membranes and to puncta adjacent to vacuoles (Figure 3.9A). This characteristic ESCRT-mutant phenotype is caused by a failure in MVB biogenesis and by the formation of class E compartments, which are aberrant stacks of flattened endosomes that lack ILVs (Rieder et al., 1996). ILV cargoes localize to the limiting membrane of class E compartments and also to vacuole membranes after class E compartments fuse with vacuoles (Odorizzi et al., 1998). Quantitative EM analysis of endosomal structures in 100 thin-cell sections confirmed that *vps20^{loop}* expression caused the formation of class E compartments at the expense of MVB biogenesis (Figure 3.9, B and E). However, mutation of the MIM1 sequence in the *vps20^{loop}* allele (resulting in *vps20$^{loop;\Delta MIM1}$*) rescued the sorting of GFP-Cps1 via the MVB pathway to result in the normal localization of GFP fluorescence in the vacuole lumen (Figure 3.9A). EM analysis confirmed the recovery of MVB

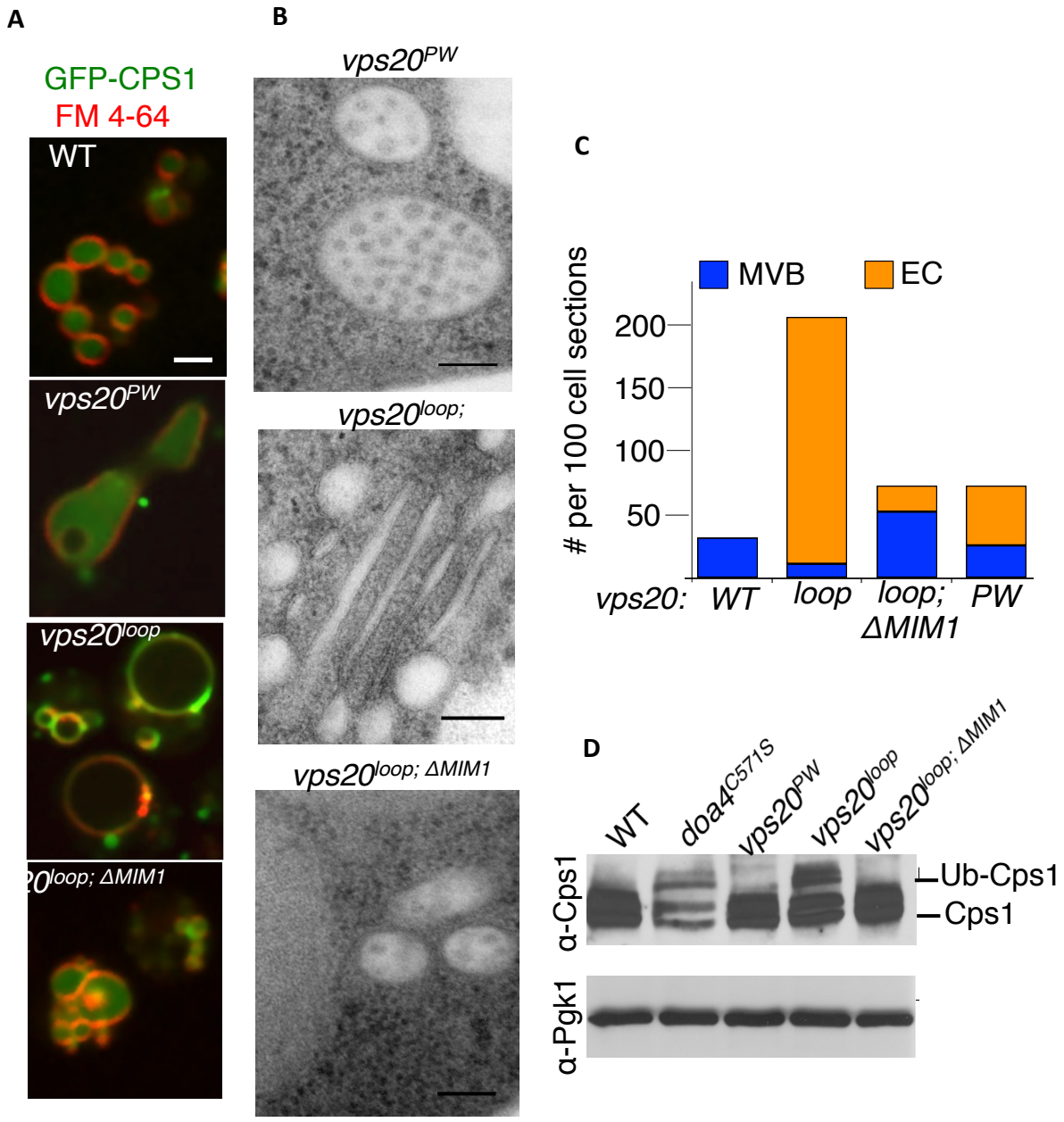

Figure 3.9. The open/active conformation of of Vps20 inhibits Doa4 function in the MVB pathway. (A) Fluorescence images of FM 4-64 stained yeast expressing GFP-Cps1. Bar = 2 μM. (B-D) EM of 80 nm thin sections of yeast cells. Bar = 100 nm. (E) Quantification of the number of MVBs and class E compartments (EC) in 100 cell profiles. (F) Western blot analysis of Cps1 and Pgk1 in total-cell lysates. The *PEP4* and *PRB1* genes were deleted in each strain to prevent spurious cleavage of ubiquitinated Cps1 (Ub-Cps1) upon vacuolar disruption during cell lysis.

biogenesis in *vps20*$^{loop;\Delta MIM1}$ cells (Figure 3.9, C and E), signifying that ILV budding had been restored. That the liberation of Doa4 from inhibitory Vps20-binding reversed the defects in ILV budding and cargo sorting caused by *vps20*^{loop} expression indicates that Vps20 locked in its open/active conformation impairs the MVB pathway through its interaction with Doa4.

Unexpectedly, we observed normal localization of GFP-Cps1 to the vacuole lumen in yeast expressing the mutant *vps20*^{PW} allele in place of wild-type *VPS20* (Figure 3.9A). Quantitative EM confirmed the biogenesis of MVBs in *vps20*^{PW} cells, although class E compartments still represented the majority of endosomal structures in this strain (Figure 3.9, D and E). Continued function of the MVB pathway in *vps20*^{PW} cells was surprising because in vitro studies had shown the mutant vps20^{PW} protein locked in its closed/inactive conformation is unable to nucleate Snf7 polymerization (Saksena et al., 2009). The Vps20^{PW} protein might, therefore, retain some degree of functionality under native conditions at endosomes.

Inhibition of the MVB pathway caused by expression of the *vps20*^{loop} allele prompted me to test its effect toward ILV cargo deubiquitination by Doa4. In principle, we expected that deubiquitination would not be impaired because data obtained thus far indicated that Vps20-binding inhibits Doa4 from functioning non-catalytically to regulate ESCRT-III (Figure 3.6; Richter et al., 2013). However, we found that the ILV cargo protein, Cps1, accumulated in its ubiquitinated state in *vps20*^{loop} cells as strongly as it did in cells expressing the catalytically inactive *doa4*^{C571S} allele (Figure 3.9F). As we had seen in the case of ILV budding and cargo sorting, mutation of the *MIM1* sequence

in *vps20*^{loop} (resulting in *vps20*$^{loop;\Delta MIM1}$) restored Cps1 deubiquitination, indicating that the constitutively open/active form of Vps20 that binds Doa4 inhibits Doa4-mediated deubiquitination in the MVB pathway. In contrast, Cps1 deubiquitination was unaffected in *vps20*^{PW} cells (Figure 3.9F), which was expected based on our finding that this mutation did not block GFP-Cps1 sorting (Figure 3.9A) or ILV budding (Figure 3.9D). Thus, inhibitory binding to Doa4 by Vps20 not only prevents Doa4 from stabilizing ESCRT-III but also restricts Doa4 function in the deubiquitination of ILV cargoes.

Discussion

ESCRT-III is an ancient and versatile membrane scission machine that functions in a growing list of membrane remodeling pathways (Hurley, 2015). Although the biophysical mechanism of membrane scission is unknown, in vitro and in vivo studies conducted in different model systems indicate that the scission activity of ESCRT-III is dictated by its cycle of assembly and disassembly (Sachse et al., 2004; Hanson et al., 2008; Wollert et al., 2009; Wemmer et al., 2011; Adell et al., 2014; Cashikar et al., 2014; Shen et al., 2014). Regulating this cycle is, therefore, expected to be important for determining the timing with which membrane scission is executed by ESCRT-III. The mechanisms that regulate ESCRT-III, however, are poorly understood.

In this study, we show the cycle of ESCRT-III assembly/disassembly at yeast endosomes is regulated by Doa4, the ubiquitin hydrolase that deubiquitinates transmembrane proteins sorted into ILVs in the MVB pathway. By stabilizing ESCRT-III, Doa4 inhibits ILV membrane scission. Assigning this regulatory role to Doa4 endows it with the ability to coordinate the timing of ILV membrane scission with cargo

deubiquitination, thereby guarding against premature enclosure of ubiquitinated cargoes within ILVs that have been severed by ESCRT-III from the limiting endosomal membrane (Figure 3.10). The importance this coordination has toward cellular physiology is manifested in yeast lacking *DOA4* expression: *doa4Δ* cells are sensitive to a variety of stresses due to the depletion of free, non-conjugated ubiquitin (Swaminathan et al., 1999). That this sensitivity is a consequence of ubiquitin depletion via the MVB pathway is indicated by the recovery of stress resistance in *doa4Δ* cells having extragenic mutations that disable ESCRT-III function (Amerik et al., 2000).

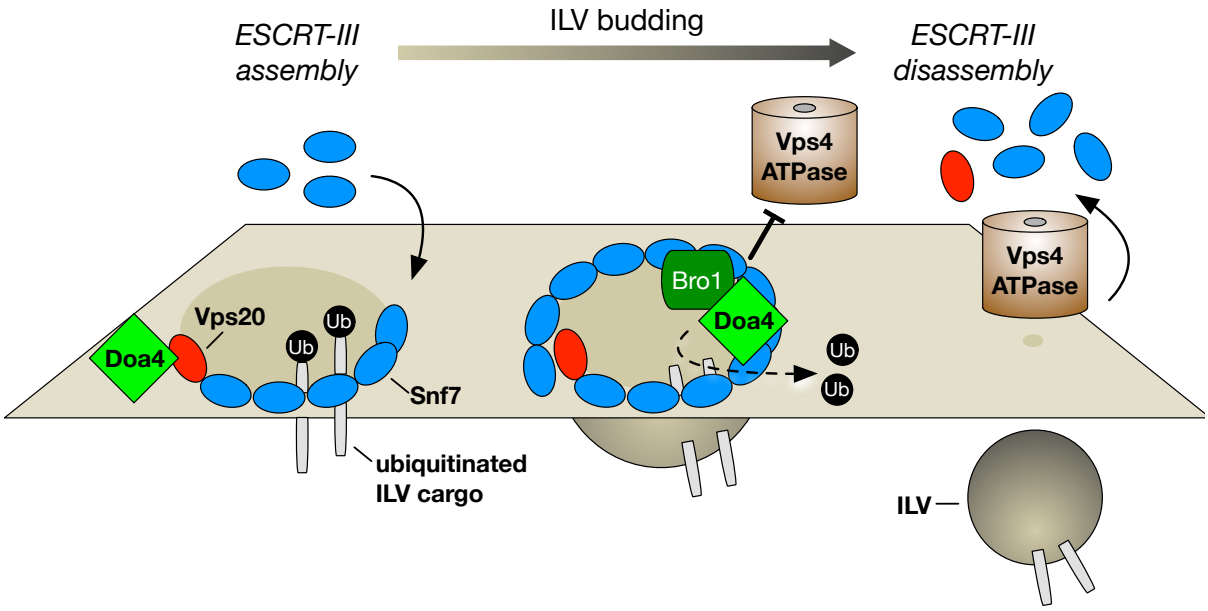

Figure 3.10. Model for Doa4 regulation and function during ILV budding. At the initiation of ESCRT-III assembly, Vps20 in its open/active conformation nucleates Snf7 polymerization and binds Doa4 to restrict its access to ubiquitinated ILV cargoes. Bro1 relieves inhibitory binding to Doa4 by Vps20, which presumably occurs after polymeric Snf7 has encircled cargoes to prevent their escape from the site of ILV budding. Bro1 also stimulates Doa4 ubiquitin hydrolase activity, and during the period of cargo deubiquitination, Doa4 and Bro1 stabilize ESCRT-III by inhibiting disassembly of the complex by Vps4. Once ESCRT-III disassembly occurs, ESCRT-III membrane scission activity completes the ILV budding process.

The role Doa4 has toward stabilizing ESCRT-III is inhibited through its interaction with the open/active conformation of Vps20 that nucleates Snf7 polymerization (Saksena et al., 2009). This finding seems paradoxical because it suggests that Vps20 works simultaneously to increase and decrease ESCRT-III abundance. However, inhibitory binding of Doa4 by Vps20 would facilitate another function ESCRT-III has upstream of ILV membrane scission: the spiral polymerization of Snf7 that occurs during ESCRT-III assembly encircles ubiquitinated transmembrane proteins that have been concentrated by ESCRT-0, -I, and -II (Teis et al., 2010). Premature deubiquitination of cargoes before ESCRT-III has sufficiently assembled would permit their escape from the site of ILV budding. Inhibitory binding of Doa4 by Vps20 might, therefore, be irrelevant to the function Doa4 has toward ESCRT-III stabilization and, instead, serve to limit Doa4 access to ubiquitinated ILV cargoes at the initial stage of ESCRT-III assembly so that the cargoes are not deubiquitinated before being trapped by the growing Snf7 polymer (Figure 3.9). This model is consistent with our observation that ILV cargo deubiquitination is inhibited by binding of Doa4 to the *vps20*^{loop} mutant protein and that deubiquitination is restored in this context by mutation of the Doa4-binding *MIM1* sequence in *VPS20*.

Inhibitory binding of Doa4 by Vps20 reduces ESCRT-III stability and disables ILV budding, indicating the importance of terminating Doa4 binding to Vps20. How might this repressive interaction normally be relieved? BiFC analysis of Doa4-Vps20 binding in yeast revealed that their interaction is disrupted by overproduction of either full-length Bro1 or the Bro1 domain. This finding extends our understanding of the functional cooperation between Doa4 and Bro1 in the MVB pathway. Earlier studies indicated that

the proline-rich carboxyl terminus of Bro1 binds the Doa4 catalytic domain to stimulate its ubiquitin hydrolase activity (Richter et al., 2007). We now show that the amino-terminal Bro1 domain of Bro1 facilitates Doa4-mediated stabilization of ESCRT-III by promoting Doa4 release from its inhibitory interaction with Vps20. That the proline-rich region of Bro1 responsible for stimulating Doa4 catalytic activity has no apparent role in Doa4-mediated stabilization of ESCRT-III is in accordance with our observations that Doa4 ubiquitin hydrolase activity is not required for its regulation of ESCRT-III. How the Bro1 domain relieves Doa4 from its inhibitory interaction with Vps20 is unclear. The Bro1 domain binds the MIM1 sequence in Snf7 (Wemmer et al., 2011), raising the possibility that Bro1 similarly binds to the MIM1 sequence in Vps20 to displace Doa4. However, we have yet to detect binding between Vps20 and Bro1 (N.J. and G.O., unpublished results).

Bro1 also functions to stabilize ESCRT-III through its interaction with Snf7 (Wemmer et al., 2011), and it does so independently of its role in relieving Doa4 from inhibitory binding to Vps20 because the reduction in ESCRT-III abundance seen in cells lacking Doa4 is reversed upon overexpression of the BRO1 gene. Bro1 inhibits Vps4-mediated disassembly of ESCRTIII at yeast endosomes, and as a consequence, the amount of ESCRT-III seen in wild-type cells is increased in response to *BRO1* overexpression (Wemmer et al., 2011). Our finding that *DOA4* overexpression in wild-type cells led to a greater accumulation of higher molecular weight ESCRT-III complexes suggests that Doa4 more potently inhibits ESCRT-III disassembly than does Bro1. Neither *DOA4* nor *BRO1* overexpression rescued ESCRT-III abundance in *vps20Δ* cells (this study and Wemmer et al., 2011), consistent with both proteins

functioning downstream of Vps20-mediated nucleation of ESCRT-III assembly. However, purified Bro1 can promote Snf7 polymerization in vitro (Tang et al., 2016), suggesting that Bro1 might boost the levels of ESCRT-III in vivo by stimulating its assembly in addition to stabilizing ESCRT-III polymers directly through binding to Snf7 (Wemmer et al., 2011) and indirectly by promoting the relief of inhibitory binding between Doa4 and Vps20 (this study).

Given the central role ESCRT-III has in ILV budding, the function we describe for Doa4 in regulating ESCRT-III would seem at odds with our previous work showing that ILV budding does not require Doa4 (Richter et al., 2007). However, the depletion of free, non-conjugated ubiquitin seen in the absence of Doa4 (Swaminathan et al., 1999) constricts the influx of ubiquitinated transmembrane proteins into the MVB pathway (Katzmann et al., 2004). Since ILV budding is dependent upon ubiquitinated ILV cargoes (MacDonald et al., 2012), the loss of Doa4 would be inconsequential to ESCRT-III function in ILV budding, especially given our results showing that Bro1 functions in parallel with Doa4 to regulate ESCRT-III. The absence of Doa4 would be expected to have a greater impact in the face of higher demand for ESCRTIII function in the MVB pathway. Indeed, increasing the influx of ubiquitinated cargoes by genetic repletion of free ubiquitin levels inhibits ILV budding in cells lacking Doa4 function (Richter et al., 2007). Our model positions Doa4 and Bro1 at the nexus of ESCRT-III function in the MVB pathway of yeast (Figure 3.9), but several questions remain. For instance, what triggers Bro1 to relieve Doa4 (directly or indirectly) from inhibitory binding by Vps20? Knowing this information would give insight into the state of ESCRT-III assembly at which Doa4 and Bro1 functionally cooperate. Conversely, what terminates

Doa4/Bro1 regulation of ESCRT-III? Based on the inhibition of ILV membrane scission seen upon overexpression of either *DOA4* (this study) or *BRO1* (Wemmer et al., 2011), their negative regulation seems necessary for completion of the ILV budding process. How Doa4 and Bro1 regulate ESCRT-III stability is also unknown. Like Bro1, Doa4 can bind Snf7 (Bowers et al., 2004; Wolters and Amerik, 2015), raising the possibility that Doa4 and/or Bro1 restrict access of polymeric Snf7 to the disassembly ATPase, Vps4; but testing this model has been complicated by difficulty in detecting Vps4 binding to Snf7 due to their low affinity for one another in isolation (Kojima et al., 2016).

Our results offer insight into the mechanism by which certain plus-stranded RNA viruses replicate in plants. Proteins encoded by the tomato bushy stunt virus (TBSV) and brome mosaic virus (BMV) recruit ESCRT-III to the cytosolic surface of peroxisomes and the endoplasmic reticulum, respectively, where the viruses exploit ESCRT-III to create membrane invaginations that protect the viral replication machinery away from the cytosol (Barajas et al., 2009; Diaz et al., 2015). These budded replication compartments, however, are not severed. Our finding that Doa4 and Bro1 can inhibit membrane scission by regulating ESCRT-III stability raises the possibility that a similar mechanism might be employed by TBSV and BMV to maintain their budded replication compartments as non-severed invaginations. Consistent with this proposal, both TBSV and BMV can replicate in yeast, and this process requires Doa4 and Bro1 (Panavas et al., 2005; Kushner et al., 2003). For BMV, the activities Doa4 and Bro1 have in maintaining ubiquitin homeostasis through ILV cargo deubiquitination are important for viral replication (Wang et al., 2011), but, as in ILV budding, the functions Doa4 and Bro1 have in deubiquitination and ESCRT-III regulation need not be

mutually exclusive.

Do orthologs of Doa4 and Bro1 in other organisms also regulate ESCRT-III function? The mammalian Bro1 ortholog, ALIX, seems to operate in this capacity at the plasma membrane, where it recruits CHMP4B, a Snf7 ortholog that functions in ESCRT-III-mediated membrane scission during the abscission step of cytokinesis (Carlton et al., 2012). ALIX also recruits the CHMP4C paralog, which is a checkpoint component that interferes with CHMP4B function to delay abscission until chromatin is cleared from the intercellular bridge connecting daughter cells (Christ et al., 2016). Like Bro1 in yeast, therefore, ALIX can regulate the timing of ESCRT-III membrane scission activity, albeit through a different mechanism and at a different membrane domain. Future studies might reveal whether ESCRT-III is also regulated at endosomes in mammalian cells either by ALIX or by UBPY, the apparent functional ortholog of Doa4.

Materials and methods

Yeast strains and plasmid construction

Standard techniques were used for the growth and genetic manipulation of *S. cerevisiae* strains (Table 2) and for the construction of plasmids (Table 3). Yeast strains created for this study were constructed by one-step PCR-based integration using cassettes described in Longtine et al. (1998) and Webster et al. (2014). The 2μ *bro1*$^{388\text{-}844}$ plasmid was constructed using the gene splicing by overlap extension method of PCR (geneSOE; Higuchi et al., 1988) to fuse 500 bp of the *BRO1* 5' untranslated region plus the start codon in frame with the coding sequence for Bro1 amino acids 388-844, and the full sequence was cloned into the SpeI/SalI site of

pRS426 (Christianson et al., 1992), resulting in the plasmid pGO642. To construct plasmids encoding the *vps20*^{PW} and *vps20*^{loop} alleles, the epitope-tagged versions of each allele described in Teis et al. (2010) were used as templates for PCR to generate copies that replaced the epitope tag with a stop codon, and the resulting full sequences of each non- tagged allele was cloned into the SacI site of pRS414 (Christianson et al., 1992), resulting in the plasmids pGO829 and pGO830. To construct bacterial expression plasmids, PCR products consisting of a Shine-Dalgarno sequence followed by the coding sequences for were *VPS20*, *vps20*^{PW}, or *vps20*^{loop} were created from wild-type genomic DNA, pGO829, or pGO830 templates, respectively, then cloned into the SacI/KpnI site of pST39 (Tan, 2001), resulting in the plasmids pGO511, pGO816, and pGO817. Into the BspEI/MluI site of pST39 or the Vps20- encoding pST39 plasmids, the coding sequence for GST-Doa4$^{2-80}$ from template pCR152 (Richter et al., 2013) was cloned, resulting in the plasmids pGO818, pGO819, pGO820, and pGO826.

Rate-zonal density gradient analysis of ESCRT-III

Performed as described in chapter 2 (glycerol density gradient centrifugation assay). Detection of Snf7 in each fraction was performed by incubating nitrocellulose with Alexa Fluor 680 secondary antibody (Invitrogen), then visualizing with an infrared imager (Odyssey; LI-COR Biosciences), and the amount of Snf7 was quantitated in triplicate experiments with Odyssey software (version 2.1). Calibration of the gradient was performed using Aldolase (158 kD), Catalase (232 kD), and Ferritin (440 kD) (GE Healthcare; United Kingdom).

Electron microscopy and tomography

Samples were prepared and TEM performed as described in chapter 2. For tomography, grids were labeled on both sides with fiduciary 15-nm colloidal gold (British Biocell International; United Kingdom). Typically, Z-shrinkage of semi-thick sections was 20% volume and corrected in final models and measurements. Dual-axis tilt series were collected from 660˚with 1˚increments at 200 kV using a Tecnai F20 (FEI-Company; Netherlands) at a magnification of 29,000x using SerialEM (Mastronarde, 2005). 2x binning on the recording 4K 6 4K CCD camera (Gatan; United Kingdom) creates a 2,000 x 2,000 image with a pixel size of 0.764 nm. Dual-axis electron tomograms (Mastronarde, 1997) of endosomes and ILVs required the IMOD package (Kremer et al., 1996) for tomogram construction and modeling (3DMOD 4.0.11). Manually assigned contours of the endosomal limiting membrane at the inner leaflet were used to measure the surface of the bilayers periodically every 3.85 nm and calculated using imodmesh. Best-fit sphere models were used to measure the diameters of nearly spherical lumenal vesicles from the outer leaflet of the membrane bilayers (O'Toole et al., 2002). IMODINFO provided surface area and volume data of contour models. Data were sorted, analyzed, and graphed using Microsoft Excel (Redmond, WA) and Prism 5 (GraphPad Software; La Jolla, CA).

Fluorescence microscopy

Liquid cultures of yeast strains were grown to logarithmic phase at 30℃ before observation at room temperature using a Nikon TE2000-U inverted fluorescence microscope equipped with a Yokogawa spinning disc confocal unit CSU-Xm2 and a

100x oil objective with a numerical aperture of 1.4 (Nikon Instruments; Melville, NY). Fluorescence images were acquired with a Photometrics Cascade II EM-CCD camera (Tucson, AZ) using MetaMorph (v7.0) software (Molecular Devices; Sunnyvale, CA), then processed with NIH ImageJ and Photoshop CS4 software (Adobe Systems, Mountain View, CA). Endosomal membranes were stained with FM 4-64 (Invitrogen; Carlsbad, CA) using a 20 minute pulse and 90 minute chase (Odorizzi et al., 2003).

Affinity purification of recombinant proteins expressed in bacteria

Vps20, Vps20^{PW}, and Vps20^{loop} proteins were expressed without or with GST-Doa4$^{2-80}$ in 5-ml liquid cultures of *Escherichia coli* BL21-CodonPlus (DE3) cells (Agilent Technologies; Santa Clara, CA) by induction with 0.5 mM isopropyl β-D-1-thiogalactopyranoside at 20℃ for 18 hr. Bacterial cells were then harvested by centrifugation at 1,800 x *g* for 10 min at 4℃, then lysed by resuspension on ice in 1 ml PBS supplemented with 1 mg/ml lysozyme (Roche Diagnostics), 0.25 units Benzonase Nuclease (Sigma-Aldrich; St. Louis, MO), and 1 mM phenylmethanesulfonyl fluoride (Sigma-Aldrich). Lysates were subjected to probe sonication at 15W for 20 sec, then 0.2% Triton X-100 (TX-100) was added, and the lysates were rotated at 4℃ for 10 min before being clarified by centrifugation at 16,100 x *g* for 10 min at 4℃. The resulting supernatants were mixed with glutathione-sepharose beads (GE Healthcare) and rotated at 4℃ for 1 hr. The beads were then washed thrice by centrifugation at 5,000 x *g* for 1 min and resuspension in 1 ml ice-cold PBS containing 0.2% TX-100, then washed twice in 1 ml ice-cold PBS. Washed beads were dried by rotary evaporation, bound proteins were eluted by boiling for 5 min in 100 µl Laemmli buffer, and 10 µl of each sample was resolved by SDS- PAGE, transferred to nitrocellulose, and analyzed

by western blot using mouse anti-GST monoclonal antibodies (Invitrogen) or using custom rabbit anti-Vps20 polyclonal antiserum (Invitrogen) that was raised against the yeast Vps20 peptide sequences E_{19}VKRSKDEIHKF$_{30}$ and L_{113}KKLNKEFSNVDE$_{125}$.

Detection of ubiquitinated CPS1 in yeast cell lysates

Yeast cells lacking vacuolar hydrolase activity (*pep4*Δ *prb1*Δ) were grown logarithmically in liquid culture at 27℃, then 10 OD_{600} units were harvested by centrifugation at 1,800 x *g* for 5 min at room temperature, resuspended in 5 mM *N*-ethylmaleimide (Sigma-Aldrich), and precipitated by the addition of 10% (vol/vol) TCA followed by incubation on ice for 20 min. Cellular material was re-precipitated twice in acetone as described above, dried by rotary evaporation, then resuspended by sonication in 100 µl Laemmli buffer. The cell walls in precipitates were disrupted by adding acid-washed glass beads (150-212 µm; Sigma) and mixing vigorously by vortex at room temperature for 15 min, then boiling for 5 min. Ten microliters of the protein sample was resolved by SDS-PAGE and analyzed by western blotting with rabbit polyclonal anti-Cps1 antiserum (Cowles et al., 1997) and mouse anti-Pgk1 monoclonal antibodies (Invitrogen).

Chapter 4: Summary and future directions

Summary

Endosomes collectively comprise a system of membrane-bound compartments that participate in vesicular membrane trafficking between the plasma membrane, the *trans*-Golgi network (TGN), and the major hydrolytic organelle, the lysosome (or the homologous organelle in yeast, the vacuole). Cytosolic machinery recruited to subcellular compartments remodel membranes to form vesicles or other scission products. The endosomal sorting complexes required for transport (ESCRTs) execute membrane remodeling and scission (reviewed in Hurley, 2015). ESCRTs were originally characterized on the basis of their activities at endosomes in *S. cerevisiae*, where they function in the biogenesis of multivesicular bodies (MVBs). MVBs are late endosomes that contain intralumenal vesicles (ILVs), which are degraded in the hydrolytic interior of vacuolar lysosomes upon endolysosomal fusion (Katzmann et al., 2001; Babst et al., 2002a; Babst et al., 2002b). A functional requirement for ESCRTs in the MVB pathway is conserved throughout eukaryotes (Hanson and Cashikar, 2012). Studies in vitro indicated that ESCRT-I and -II initiate ILV budding by inducing membrane invagination, and ESCRT-III completes the process by constricting the membrane and catalyzing the scission reaction that detaches nascent ILV buds into the MVB lumen (Wollert and Hurley, 2009; Wollert et al., 2010).

ESCRT-II regulates ESCRT-III assembly at cargo enriched microdomains on the endosomal limiting membrane

Ubiquitinated transmembrane proteins targeted for lysosomal degradation are sorted into ILVs by ESCRT-0, -I, and -II, each of which has one or more ubiquitin-binding domains (Katzmann et al., 2001; Bilodeau et al., 2002; Alam et al., 2004), while ESCRT-III and Vps4 function downstream to sever the necks of the forming ILVs. Loss of any ESCRT results in loss of ILV formation, and an unresolved question in the field has been what upstream ESCRTs contribute to membrane remodeling. ESCRT-II coordinates cargo sorting with ILV scission by initiating ESCRT-III formation. In this work, we identify a constitutively active ESCRT-II mutant that can partially suppress the phenotype of ESCRT-0 or ESCRT-I deletions by driving enhanced ESCRT-III complex formation. Although this hyper-active ESCRT-II mutant could drive ESCRT-III polymerization independently of all upstream ESCRT activity, either ESCRT-0 or -I were required to form ILVs, which suggests that upstream ESCRT activity is required for ESCRT-III polymers to be functional in ILV formation.

One question that emerges from this study is what effect upstream ESCRTs have on the endosomal limiting that supports ILV formation. Do cargo sorting ESCRTs lipid properties of the endosomal limiting membrane in some way? One conceivable model is that the abundance of ubiquitin binding domains present in ESCRT-0, -I, and -II concentrate ubiquitylated-transmembrane proteins to the extent that this 'cargo crowding' leads to asymmetry in the lipid bilayer which favors ILV budding (Jarsch et al., 2016). Another question is what stimulates upstream ESCRTs to initiate ILV budding? Binding ubiquitylated transmembrane proteins is one obvious possibility, but interactions

with other protein trafficking machinery or specific lipids are also possible. ESCRT-0 binds clathrin, which is the coat component of vesicles trafficked to endosomes. Given that endosomes are at a unique crossroads between the endocytic and secretory pathways, perhaps early acting ESCRTs stimulate endosome membrane remodeling in response to general vesicular trafficking demands. We have observed by electron tomography that ILV budding profiles are often on a side of the endosomal limiting membrane that faces Golgi cisternae or ER tubules, and these secretory pathway organelles are generally in close proximity to class E-compartments (N.J., M.W., and G.O. unpublished results). Do these endosome approaches by the secretory pathway represent communication between these organelles, and if so, what is the nature of this communication and what factors mediate it?

Regulation of ESCRT-III and ILV scission by Doa4

ESCRT-III executes membrane scission at endosomes during intralumenal vesicle (ILV) budding. The mechanism of ILV membrane scission is linked to the dynamic cycle of ESCRT-III assembly and disassembly. Vps20, Snf7, Vps24, and Vps2 make up the ESCRT-III complex, but the bulk of the polymer is comprised of Snf7 (Babst et al., 2002a; Teis et al., 2008). We show in *S. cerevisiae* that Snf7 disassembly and membrane scission at endosomes is inhibited by Doa4, a ubiquitin hydrolase that deubiquitinates transmembrane proteins sorted as cargoes into ILVs. Bro1, an ESCRT-III associated protein, and Vps20 regulate Doa4 function at endosomes (Luhtala and Odorizzi 2004; Richter et al., 2007; Richter et al., 2013). An MIT-"like" domain in the

amino terminus of Doa4 binds the open/active conformation of Vps20 (figure 3.1), which nucleates Snf7 polymerization (Richter et al., 2013; Teis et al., 2008). We show that Doa4 regulation of the Snf7 polymer state is inhibited by this Vps20 interaction. A proline rich domain in the carboxyl terminus of Bro1 directly stimulates Doa4 catalytic activity at endosomes (Figure 3.1; Richter et al., 2007). We show that Doa4 catalytic activity is not required for its regulation of ESCRT-III, but Bro1 relieves the inhibitory binding of Vps20 to Doa4. Our results reveal a mechanism to delay ILV membrane scission while cargoes undergo deubiquitination.

There are many things yet to be learned about Doa4 function at endosomes, including the molecular interactions that recruit Doa4 to endosomes. Bro1 and Snf7 are necessary, but direct interaction between either protein and the N-terminal localization domain of Doa4 has not been shown. Vps20 binds the N-terminus of Doa4, but the interaction is not required for Doa4 endosome localization. Perhaps ubiquitin is involved in Doa4 endosome recruitment, but this has been difficult to test as ubiquitin depletion in *S. cerevisiae* is detrimental to cell viability (Swaminathan et al., 1999). Chapter three shows that *DOA4* overexpression causes an accumulation of high molecular weight Snf7 polymers, but how Doa4 has such a dramatic stabilizing influence over the polymer has yet to be determined. The Odorizzi lab has not been able to detect in vitro binding between Doa4 and Snf7, but it is possible that this interaction occurs directly in vivo under conditions that we have not yet reproduced in vitro. Alternatively, Doa4 could indirectly influence Snf7 oligomerization state by regulating its interactions with ESCRT-III capping proteins, Vps4, or regulators of Vps4. ESCRT-III disassembly may also be regulated by ubiquitin hydrolases in mammals, as

the AMSH ubiquitin hydrolase competes with VPS4 for binding CHMP1, which is an ESCRT-III associated protein that stimulates VPS4 catalytic activity (Agromayor and Martin-Serrano, 2006).

Coordination of cargo sorting and deubiquitination with ILV budding and scission

Future studies will reveal more about how activities of the ESCRT complexes are regulated to coordinate sorting of ubiquitinated transmembrane cargoes with ILV bud formation, cargo deubiquitination, and membrane scission. ESCRT-0 initiates the cascade of ESCRT functions at endosomes, but little is known about ESCRT-0 regulation beyond a requirement for PI3P (Katzmann et al., 2003). What drives the ubiquitin binding ESCRTs to interact, and how do they work together to sort cargo? What stimulates ESCRT-II to activate Vps20? We show that activated Vps20 binds Doa4, but when does this interaction occur relative to Vps20 nucleation of Snf7? By what mechanism and at what phase of the ILV budding process are the ubiquitin binding ESCRTs released from ESCRT-III?

There is some data to suggest that crosstalk exists between upstream and downstream ESCRTs. The efficiency of ESCRT mediated trafficking would logically benefit from a checkpoint that could accommodate dynamic cargo sorting demands prior to remodeling the membrane for scission, and Bro1 is in a unique position to mediate this checkpoint. Bro1 stimulates the catalytic activity of Doa4 and interacts with Rsp5, the ubiquitin ligase that targets ILV substrates in *S. cerevisiae* (Nikko and Andre, 2007). In addition to binding Snf7 (Kim et al., 2005), Bro1 has a ubiquitin binding

domain of unknown relevance except that it is genetically redundant with ubiquitin binding by ESCRT-0 (Pashkova et al., 2013). Bro1 stalls ESCRT-III disassembly and ILV scission by Vps4, both independently (Wemmer et al., 2011) and by relieving Vps20 inhibition of Doa4. Thus, Bro1 is conveniently positioned to "sense" the cargo load presented by Rsp5 and engaged by ESCRT-0, and Bro1 ensures that ILV membrane scission does not proceed until ILV cargo deubiquitination is complete. Alix, the closest mammalian ortholog to Bro1, binds ESCRT-I and -III, but the relevance of these interactions towards ILV formation remain unclear (Fisher et al., 2007; Strack et al., 2003; Martin-Serrano et al., 2003; von Schwedler et al., 2003).

How does Bro1 binding Snf7 releive the interaction between Vps20 and Doa4? Can Bro1 detect when Snf7 is sufficiently polymerized such that ILV cargoes are prevented from diffusing out of the ILV bud site? What regulates the transformation of ESCRT-III from a two-dimensional cargo entrapment complex to a three-dimensional membrane-remodeling complex? Vps4 is central to both of these questions, as is regulation of Vps4 by Bro1 and Doa4. In cells with Vps4 depleted, mammalian ESCRT-III filaments accumulate at the plasma membrane as three-dimensional coiled helices. The filaments transform into two-dimensional rings around the model ESCRT cargo, the HIV-1 Gag protein, when the viral protein is transiently expressed (Cashikar et al., 2014). Viral Gag proteins recruit ESCRTs in a ubiquitin dependent manner through ALIX, the closest mammalian ortholog to Bro1 (Martin-Serrano et al., 2003; Morita and Sundquist, 2004). Future studies are needed to address how the presence of ubiquitinated cargoes and deubiquitination influence the architecture of ESCRT-III filaments at endosomes, the plasma membrane, and elsewhere around the cell.

Table A.1. Yeast strains used in chapter 2

strain	Description	genotype	reference
SEY6210	WT	*MATα leu2-3112 ura3-52 his3-Δ200 trp1-Δ901 lys2-801 suc2-Δ9 GAL*	Robinson *et al.* (1988)
KFY7	*vps36Δvps20Δ*	SEY6210.1, *VPS36::URA3, VPS20::HIS3*	This study
SKY8	*vps23Δvps36Δvps20Δ*	SEY6210, *VPS23::HIS3, VPS36::URA3, VPS20::G418*	This study
MBY30	*vps36Δ*	SEY6210, *VPS30::HIS3*	Babst *et al.* (2002b)
SKY1	*vps23Δvps36Δ*	SEY6210, *VPS23::HIS3, VPS36::URA3*	This study
MBY21	*vps27Δ*	SEY6210, *VPS27::HIS3*	Odorizzi *et al.* (1998)
EEY6-2	*vps23Δ*	SEY6210, *VPS23::HIS3*	Babst *et al.* (2000)
MBY3	*vps4Δ*	SEY6210, *VPS4::TRP1*	Babst *et al.* (1997)
EEY2-1	*vps20Δ*	SEY6210, *VPS20::HIS3*	Babst *et al.* (2002a)
SKY15	*vps23Δvps36Δsnf7Δ*	SEY6210, *VPS23::HIS3, VPS36::URA3, SNF7::G418*	This study
SKY14	*vps23Δvps36Δvps27Δ*	SEY6210, *VPS23::HIS3, VPS36::URA3, VPS27::G418*	This study
MCY23	*vps28Δ*	SEY6210, *VPS28::HIS3*	Curtiss *et al.* (2007)
DKY48	*vps37Δ*	SEY6210, *VPS37::HIS3*	Katzmann *et al.* (2001)
MBY65	*mvb12Δ*	SEY6210, *MVB12::HIS3*	Curtiss *et al.* (2007)
MBY31	*vps22Δ*	SEY6210.1, *VPS22::HIS3*	Babst *et al.* (2002b)
BWY101	*vps25Δ*	SEY6210, *VPS25::HIS3*	Babst *et al.* (2002b)
EEY2-1	*vps20Δ*	SEY6210, *VPS20::HIS3*	Babst *et al.* (2002a)
EEY9	*snf7Δ*	SEY6210, *SNF7::HIS3*	Babst *et al.* (2002a)
BWY102	*vps24Δ*	SEY6210, *VPS24::HIS3*	Babst *et al.* (1998)
MBY28	*vps2Δ*	SEY6210, *VPS2::HIS3*	Babst *et al.* (2002a)

Table A.2. plasmids used in chapter 2

plasmids	Description	genotype	reference
pSK212	*VPS36*-V5-EGFP	*VPS36*-V5-EGFP (pRS414)	This study
pSK243	*vps36(ΔPI3P)*-V5-GFP	*vps36(K38E,R89A,R261E)*-V5-EGFP (pRS414)	This study
pSK253	*vps36(R89A,R261A)*-V5-GFP	*vps36(R89A,R261A)*-V5-EGFP (pRS414)	This study
pSK239	*vps36(ΔUb)*-V5-GFP	*vps36(T187G,F188A)*-V5-EGFP (pRS414)	This study
pSK240	*vps36(ΔUbΔPI3P)*-V5-GFP	*vps36(K38E,R89A,R261E,T187G,F188A)*-V5-EGFP (pRS414)	This study
pSK241	*vps36(S)*-V5-GFP	*vps36(F492S)*-V5-EGFP (pRS414)	This study
pSK215	*vps36(ΔGLUE)*-V5-GFP	*vps36(Δ1-289)*-V5-EGFP (pRS414)	This study
pMB187	*vps4(E233Q)*	*vps4(E233Q)* (pRS415)	Babst *et al.* (1998)
pSK179	*VPS36-V5*	*VPS36*-V5 (pRS414)	This study
pSK213	*vps36(ΔPI3P)*	*vps36(K38E,R89A,R261E)*-V5 (pRS414)	This study
pSK250	*vps36(R89A,R261A)*	*vps36(R89A,R261A)*-V5 (pRS414)	This study
pSK183	*vps36(ΔUb)*	*vps36(T187G,F188A)*-V5 (pRS414)	This study
pSK222	*vps36(ΔUbΔPI3P)*	*vps36(K38E,R89A,R261E,T187G,F188A)*-V5 (pRS414)	This study
pSD2	GFP-Cps1	GFP-Cps1 (pRS415)	Odorizzi *et al.* (1998)
pMB131	*VPS36*	*VPS36* (pRS414)	Alam *et al.* (2004)
pSK163	*vps36(S)*	*vps36(F492S)* (pRS414)	This study
pSK180	*vps36(S)*-V5	*vps36(F492S)*-V5 (pRS414)	This study
pMB196	CFP-Cps1	CFP-Cps1 (pRS425)	This study
pSK143	p2μ[EII-V5]	*VPS36*-V5, *VPS22*-HA, *VPS25* (pRS425)	This study
pMB175	p2μ[EII]	*VPS36*, *VPS22*-HA, *VPS25* (pRS425)	Babst *et al.* (2002b)
pSK165	p2μ[EII(ΔGLUE)]	*vps36(Δ1-289)*, *VPS22*-HA, *VPS25* (pRS425)	This study
pSK223	p2μ[EII(ΔGLUE,S)]	*vps36(Δ1-289,F492S)*-V5, *VPS22*-HA, *VPS25* (pRS425)	This study
pSK197	*vps36(Δ15)*	*vps36(Δ301-315)*-V5 (pRS414)	This study
pSK200	*vps36(Δ25)*	*vps36(Δ301-325)* (pRS414)	This study
pSK147	p2μ[EII(S)]	*vps36(F492S)*-V5, *VPS22*-HA, *VPS25* (pRS425)	This study

Table A.3. strains used in chapter 2

strain	genotype	reference
SEY6210	*MATα leu2-3,112 ura3-52 his3Δ200 trp1-Δ901 lys2-Δ801 suc2-Δ9*	Robinson et al., 1998
GOY65	SEY6210; *bro1Δ::HIS3*	Odorizzi et al., 2003
GOY248	SEY6210; *vps20$^{\Delta MIM1}$::KANMX6*	Richter et al., 2013
GOY250	SEY6210; *vps20$^{\Delta MIM1}$::KANMX6 bro1Δ::HIS3*	Richter et al., 2013
GOY307	SEY6210; *vps20$^{\Delta MIM1}$::KANMX6 bro1Δ::TRP1 doa4Δ::KANMX6*	Richter et al., 2013
DBY5	SEY6210; *doa4Δ::HIS3*	Richter et al., 2007
DBY6	SEY6210; *doa4Δ::HIS3 vps4Δ::TRP1*	Richter et al., 2007
MBY3	SEY6210; *vps4Δ::TRP1*	Babst et al., 1997
EEY2-1	SEY6210; *vps20Δ::HIS3*	Babst et al., 2002b
GOY445	SEY6210; *VPS20-VC::KANMX6 DOA4-VN::HIS3MX6*	This study
GOY454	SEY6210; *vps20$^{\Delta MIM1}$-VC::KANMX6 DOA4-VN::HIS3MX6*	This study
GOY471	SEY6210; *vps20^{PW}-VC::KANMX6 DOA4-VN::HIS3MX6*	This study
GOY472	SEY6210; *vps20^{loop}-VC::KANMX6 DOA4-VN::HIS3MX6*	This study
GOY477	SEY6210; *vps20$^{loop;\Delta MIM1}$*	This study
MMY14	SEY6210; *pep4Δ::LEU2 prb1Δ::LEU2 SNA3-GFP::KANMX6*	McNatt et al., 2007
MMY60	SEY6210; *pep4Δ::LEU2 prb1Δ::LEU2 SNA3-GFP::KANMX6 doa4^{C571S}*	McNatt et al., 2007
GOY474	SEY6210; *pep4Δ::LEU2 prb1Δ::LEU2 SNA3-GFP::KANMX6 vps20Δ::HIS3MX6*	This study
GOY476	SEY6210; *pep4Δ::LEU2 prb1Δ::LEU2 SNA3-GFP::KANMX6 vps20$^{loop;\Delta MIM1}$::HIS3MX6*	This study

Table A.4. plasmids used in chapter 2

plasmid	Description	genotype	reference
pRS416		*URA3* Ap^R *CEN*	Christianson et al., 1992
pRS414		*TRP1* Ap^R *CEN*	Christianson et al., 1992
pRS426		*URA3* Ap^R *2μ*	Christianson et al., 1992
pST39		Ap^R	Tan, 2001
pCR64	*CEN doa4$^{C/G}$*	*URA3* Ap^R *(pRS416) doa4^{C571G}*	Richter et al., 2007
pMB103	*2μ vps4$^{E/Q}$*	*URA3* Ap^R *(pRS426) vps4^{E233Q}*	Babst et al., 1997
pGO216	*2μ BRO1*	*URA3* Ap^R *(pRS426) BRO1*	Wemmer et al., 2011
pGO642	*2μ bro1$^{388-844}$*	*URA3* Ap^R *(pRS426) bro1$^{388-844}$*	This study
pMWM3	*2μ bro1$^{1-387}$*	*URA3* Ap^R *(pRS426) bro1$^{1-387}$*	Wemmer et al., 2011
pGO511	Vps20	Ap^R (pST39) *VPS20*	This study
pGO816	Vps20^{PW}	Ap^R (pST39) *vps20^{P183W,P189W,P192W}*	This study
pGO817	Vps20^{loop}	Ap^R (pST39) *vps20$^{Δ48-59}$*	This study
pGO818	GST-Doa4$^{2-80}$	Ap^R (pST39) *GST-doa4$^{2-80}$*	This study
pGO819	Vps20; GST-Doa4$^{2-80}$	Ap^R (pST39) *VPS20 GST-doa4$^{2-80}$*	Babst et al., 1997
pGO820	Vps20^{PW}; GST-Doa4$^{2-80}$	Ap^R (pST39) *ps20^{P183W,P189W,P192W} GST-doa4$^{2-80}$*	Babst et al., 2002b
pGO826	Vps20^{loop}; GST-Doa4$^{2-80}$	Ap^R (pST39) *vps20$^{Δ48-59}$ GST-doa4$^{2-80}$*	This study
pGO45	*2μ GFP-CPS1*	*URA3* Ap^R (pRS426) *GFP-CPS1*	Odorizzi et al., 1998
pGO829	*CEN vps20^{PW}*	*TRP1* Ap^R (pRS414) *vps20^{P183W,P189W,P192W}*	This study
pGO830	*CEN vps20^{loop}*	*TRP1* Ap^R (pRS414) *vps20$^{Δ48-59}$*	This study

Bibliography

Adell, M. A. Y., Vogel, G. F., Pakdel, M., Müller, M., Lindner, H., Hess, M. W., & Teis, D. (2014). Coordinated binding of Vps4 to ESCRT-III drives membrane neck constriction during MVB vesicle formation. *The Journal of Cell Biology*, *205*(1), 33–49.

Agromayor, M., & Martin-Serrano, J. (2006). Interaction of AMSH with ESCRT-III and deubiquitination of endosomal cargo. *The Journal of Biological Chemistry*, 281(32), 23803-23091.

Alam, S. L., Sun, J., Payne, M., Welch, B. D., Blake, B. K., Davis, D. R., et al. (2004). Ubiquitin interactions of NZF zinc fingers. *The EMBO Journal*, *23*(7), 1411–1421.

Amerik, A. Y., Nowak, J., Swaminathan, S., & Hochstrasser, M. (2000). The Doa4 deubiquitinating enzyme is functionally linked to the vacuolar protein-sorting and endocytic pathways. *Molecular Biology of the Cell*, *11*(10), 3365–3380.

Arighi, C. N., Hartnell, L. M., Aguilar, R. C., Haft, C. R., & Bonifacino, J. S. (2004). Role of the mammalian retromer in sorting of the cation-independent mannose 6-phosphate receptor. *The Journal of Cell Biology*, *165*(1), 123–133.

Ashrafi, K., Farazi, T.A., Gordon, J.I (1998). A role for Saccharomyces cerevisiae fatty acid activation protein 4 in regulating N-mryistoylation during entry into stationary phase. *J Biol Chem* 273, 25864-25874.

Azmi, I., Davies, B., Dimaano, C., Payne, J., Eckert, D., Babst, M., & Katzmann, D. J. (2006). Recycling of ESCRTs by the AAA-ATPase Vps4 is regulated by a conserved VSL region in Vta1. *The Journal of Cell Biology*, *172*(5), 705–717.

Babst, M. (2011). MVB vesicle formation: ESCRT-dependent, ESCRT-independent and everything in between. *Current Opinion in Cell Biology*, *23*(4), 452–457.

Babst, M. (2014). Quality control: quality control at the plasma membrane: one mechanism does not fit all. *The Journal of Cell Biology*, *205*(1), 11–20.

Babst, M., Katzmann, D. J., Estepa-Sabal, E. J., Meerloo, T., & Emr, S. D. (2002a). Escrt-III: an endosome-associated heterooligomeric protein complex required for mvb sorting. *Developmental Cell*, *3*(2), 271–282.

Babst, M., Katzmann, D. J., Snyder, W. B., Wendland, B., & Emr, S. D. (2002b). Endosome-associated complex, ESCRT-II, recruits transport machinery for protein sorting at the multivesicular body. *Developmental Cell*, *3*(2), 283–289.

Babst, M., Sato, T. K., Banta, L. M., & Emr, S. D. (1997). Endosomal transport function in yeast requires a novel AAA-type ATPase, Vps4p. *The EMBO Journal*, *16*(8), 1820–1831.

Babst, M., Wendland, B., Estepa, E. J., & Emr, S. D. (1998). The Vps4p AAA ATPase regulates membrane association of a Vps protein complex required for normal endosome function. *The EMBO Journal*, *17*(11), 2982–2993.

Bache, K. G., Raiborg, C., Mehlum, A., & Stenmark, H. (2003). STAM and Hrs are subunits of a multivalent ubiquitin-binding complex on early endosomes. *The Journal of Biological Chemistry*, *278*(14), 12513–12521.

Bankaitis, V. A., Johnson, L. M., & Emr, S. D. (1986). Isolation of yeast mutants defective in protein targeting to the vacuole. *Proceedings of the National Academy of Sciences of the United States of America*, *83*(23), 9075–9079.

Barajas, D., Jiang, Y., and Nagy, P.D. (2009). A unique role for the host ESCRT proteins in replication of Tomato bushy stunt virus. PLoS Pathog. 5, e1000705.

Bilodeau, P. S., Urbanowski, J. L., Winistorfer, S. C., & Piper, R. C. (2002). The Vps27p Hse1p complex binds ubiquitin and mediates endosomal protein sorting. *Nature Cell Biology*, *4*(7), 534–539.

Bodon, G., Chassefeyre, R., Pernet-Gallay, K., Martinelli, N., et al. (2011). Charged multivesicular body protein 2B (CHMP2B) of the endosomal sorting complex required for transport III (ESCRT-III) polymerizes into helical structures deforming the plasma membrane. *J Biol Chem* 286, 40276-40286.

Bonifacino, J. S. (2004). The GGA proteins: adaptors on the move. *Nature Reviews. Molecular Cell Biology*, *5*(1), 23–32.

Bonifacino, J. S., & Rojas, R. (2006). Retrograde transport from endosomes to the trans-Golgi network. *Nature Reviews. Molecular Cell Biology*, *7*(8), 568–579.

Bonifacino, J. S., & Traub, L. M. (2003). Signals for sorting of transmembrane proteins to endosomes and lysosomes. *Annual Review of Biochemistry*, *72*, 395–447.

Boura, R., Rozyzki, B., Chung, H.S., Herrick, D.Z., Canagarajah, B., Cafiso, D.S., Eaton, W.A., Hummer, G., & Hurley, J.H (2012). Solution structure of the ESCRT-I and -II supercomplex: implications for membrane budding and scission. *Structure* 20, 874-886.

Cao, T. T., Deacon, H. W., Reczek, D., Bretscher, A., & Zastrow, von, M. (1999). A kinase-regulated PDZ-domain interaction controls endocytic sorting of the beta2-adrenergic receptor. *Nature*, *401*(6750), 286–290.

Carlton, J.G., Caballe, A., Agromayor, M., Kloc, M., and Martin-Serrano, J. (2012). ESCRT-III governs the Aurora B-mediated abscission checkpoint through CHMP4C. Science 336, 220–225.

Carlton, J.G., and Martin-Serrano, J. (2007). Parallels between cytokinesis and retroviral budding: a role for the ESCRT machinery. Science 316, 1908–1912.

Cashikar, A. G., Shim, S., Roth, R., Maldazys, M. R., Heuser, J. E., & Hanson, P. I. (2014). Structure of cellular ESCRT-III spirals and their relationship to HIV budding. *eLife*, *3*, e02184.

Christ, L., Wenzel, E.M., Liestøl, K., Raiborg, C., Campsteijn, C., and Stenmark, H. (2016). ALIX and ESCRT-I/II function as parallel ESCRT-III recruiters in cytokinetic abscission. J. Cell Biol. 212, 499–513.

Christianson, T.W., Sikorski, R.S., Dante, M., Shero, J.H., and Hieter, P. (1992). Multifunctional yeast high-copy-number shuttle vectors. Gene 110, 119–122.

Clague, M. J., Liu, H., & Urbé, S. (2012). Governance of endocytic trafficking and signaling by reversible ubiquitylation. *Developmental Cell*, *23*(3), 457–467.

Cooper, A. A., & Stevens, T. H. (1996). Vps10p cycles between the late-Golgi and prevacuolar compartments in its function as the sorting receptor for multiple yeast vacuolar hydrolases. *The Journal of Cell Biology*, *133*(3), 529–541.

Cowles, C.R., Snyder, W.B., Burd, C.G., and Emr, S.D. (1997). Novel Golgi to vacuole delivery pathway in yeast: identification of a sorting determinant and required transport component. EMBO J. 16, 2769–2782.

Dai, J., Li, J., Bos, E., Porcionatto, M., Premont, R. T., Bourgoin, S., et al. (2004). ACAP1 promotes endocytic recycling by recognizing recycling sorting signals. *Developmental Cell*, *7*(5), 771–776.

Davies, B. A., Azmi, I. F., Payne, J., Shestakova, A., Horazdovsky, B. F., Babst, M., & Katzmann, D. J. (2010). Coordination of substrate binding and ATP hydrolysis in Vps4-mediated ESCRT-III disassembly. *Molecular Biology of the Cell*, *21*(19), 3396–3408.

Diaz, A., Zhang, J., Ollwerther, A., Wang, X., and Ahlquist, P. (2015). Host ESCRT proteins are required for bromovirus RNA replication compartment assembly and function. PLoS Pathog. 11, e1004742.

Doray, B., Bruns, K., Ghosh, P., & Kornfeld, S. (2002). Interaction of the cation-dependent mannose 6-phosphate receptor with GGA proteins. *The Journal of Biological Chemistry*, *277*(21), 18477–18482.

Dunn, K. W., Kamocka, M. M., & McDonald, J. H. (2011). A practical guide to evaluating colocalization in biological microscopy. *American Journal of Physiology. Cell Physiology*, *300*(4), C723–42.

Dupré, S., & Haguenauer-Tsapis, R. (2001). Deubiquitination step in the endocytic pathway of yeast plasma membrane proteins: crucial role of Doa4p ubiquitin isopeptidase. *Molecular and Cellular Biology*, *21*(14), 4482–4494.

Fisher, R.D., Chung, H., Zhai., Q., Robinson, H., Sundquist, W.I., and Hill, C.P. (2007). Structural and biochemical studies of ALIX/AIP1 and its role in retrovirus budding. *Cell*, 128, 841-852.

Garrus, J.E., von Schwedler, U.K., Pornillos, O.W., Morham, S.G., Zavitz, K.H., Wang, H.E., Wettstein, D.A., Stray, K.M., Côté, M., Rich, R.L., et al. (2001). Tsg101 and the vacuolar protein sorting pathway are essential for HIV-1 budding. *Cell*, 107, 55–65.

Gill, D.J., Teo, H., Sun, J., Perisic, O., Veprinstev, D.B., Emr, S,D., Williams, R.L (2007). Structural incite into the ESCRT-I/II link and its role in MVB trafficking. *EMBO J* 26, 600-612.

Guo, Y., Sirkis, D. W., & Schekman, R. (2014). Protein sorting at the trans-Golgi network. *Annual Review of Cell and Developmental Biology*, *30*, 169–206. http://doi.org/10.1146/annurev-cellbio-100913-013012

Hanson, P. I., & Cashikar, A. (2012). Multivesicular body morphogenesis. *Annual Review of Cell and Developmental Biology*, *28*, 337–362.

Hanson, P. I., Roth, R., Lin, Y., & Heuser, J. E. (2008). Plasma membrane deformation by circular arrays of ESCRT-III protein filaments. *The Journal of Cell Biology*, *180*(2), 389–402.

Henne, W.M., Buchkovich, N. J., Emr, S.D. (2011). The ESCRT pathway. *Dev Cell*, 21, 77-91.

Henne, W. M., Buchkovich, N. J., Zhao, Y., & Emr, S. D. (2012). The endosomal sorting complex ESCRT-II mediates the assembly and architecture of ESCRT-III helices. *Cell*, *151*(2), 356–371.

Hierro, A., Sun, J., Rusnak, A.S., Kim, J., Prag, G., Emr, S.D, & Hurley, J.H. (2004). Structure of the ESCRT-II endosomal trafficking complex. *Nature* 431, 221-225.

Higuchi, R., Krummel, B., and Saiki, R.K. (1988). A general method of in vitro preparation and specific mutagenesis of DNA fragments: study of protein and DNA interactions. Nucleic Acids Res. 16, 7351–7367.

Hsu, V. W., Bai, M., & Li, J. (2012). Getting active: protein sorting in endocytic recycling. *Nature Reviews. Molecular Cell Biology*, *13*(5), 323–328.

Hurley, J. H. (2010). The ESCRT complexes. *Critical Reviews in Biochemistry and Molecular Biology*, *45*(6), 463–487.

Hurley, J. H. (2015). ESCRTs are everywhere. *The EMBO Journal*, *34*(19), 2398–2407.

Hurley, J. H., & Stenmark, H. (2011). Molecular mechanisms of ubiquitin-dependent membrane traffic. *Annual Review of Biophysics*, *40*, 119–142.

Hurley, J. H., & Yang, B. (2014). Making sense of Vps4. *Journal of Molecular Biology*, *426*(3), 503–506.

Im, Y. J., & Hurley, J. H. (2008). Integrated structural model and membrane targeting mechanism of the human ESCRT-II complex. *Developmental Cell*, *14*(6), 902–913.

Jarsch, I. K., Daste, F., & Gallop, J. L. (2016). Membrane curvature in cell biology: An integration of molecular mechanisms. *The Journal of Cell Biology*, *214*(4), 375–387.

Jimenez, A.J., Maiuri, P., Lafaurie-Janvore, J., Divoux, S., Piel, M., and Perez, F. (2014). ESCRT machinery is required for plasma membrane repair. Science 343, 1247136.

Johannes, L., & Popoff, V. (2008). Tracing the retrograde route in protein trafficking. *Cell*, *135*(7), 1175–1187.

Katzmann, D. J., Babst, M., & Emr, S. D. (2001). Ubiquitin-dependent sorting into the multivesicular body pathway requires the function of a conserved endosomal protein sorting complex, ESCRT-I. *Cell*, *106*(2), 145–155.

Katzmann, D. J., Sarkar, S., Chu, T., Audhya, A., & Emr, S. D. (2004). Multivesicular body sorting: ubiquitin ligase Rsp5 is required for the modification and sorting of carboxypeptidase S. *Molecular Biology of the Cell*, *15*(2), 468–480.

Katzmann, D. J., Stefan, C. J., Babst, M., & Emr, S. D. (2003). Vps27 recruits ESCRT machinery to endosomes during MVB sorting. *The Journal of Cell Biology*, *162*(3), 413–423.

Keener, J. M., & Babst, M. (2013). Quality control and substrate-dependent downregulation of the nutrient transporter Fur4. *Traffic (Copenhagen, Denmark)*, *14*(4), 412–427.

Kelly, B. T., & Owen, D. J. (2011). Endocytic sorting of transmembrane protein cargo. *Current Opinion in Cell Biology*, *23*(4), 404–412.

Kerppola, T.K. (2006) Design and implementation of bimolecular fluorescence complementation (BiFC) assays for the visualization of protein interactions in living cells. Nature Protocols 1, 1278-1286.

Kieffer, C., Skalicky, J. J., Morita, E., De Domenico, I., Ward, D. M., Kaplan, J., & Sundquist, W. I. (2008). Two distinct modes of ESCRT-III recognition are required for VPS4 functions in lysosomal protein targeting and HIV-1 budding. *Developmental Cell*, *15*(1), 62–73.

Kim, J., Sitaraman, S., Hierro, A., Beach, B. M., Odorizzi, G., & Hurley, J. H. (2005). Structural basis for endosomal targeting by the Bro1 domain. *Developmental Cell*, *8*(6), 937–947.

Kostelansky, M. S., Schluter, C., Tam, Y. Y. C., Lee, S., Ghirlando, R., Beach, B., et al. (2007). Molecular architecture and functional model of the complete yeast ESCRT-I heterotetramer. *Cell*, *129*(3), 485–498.

Kostelansky, M. S., Sun, J., Lee, S., Kim, J., Ghirlando, R., Hierro, A., et al. (2006). Structural and functional organization of the ESCRT-I trafficking complex. *Cell*, *125*(1), 113–126.

Kremer, J.R., Mastronarde, D.N., and McIntosh, J.R. (1996). Computer visualization of three-dimensional image data using IMOD. J. Struct. Biol. 116, 71–76.

Kushner, D.B., Lindenbach, B.D., Grdzelishvili, V.Z., Noueiry, A.O., Paul, S.M., and

Ahlquist, P. (2003). Systematic, genome-wide identification of host genes affecting replication of a positive-strand RNA virus. Proc. Natl. Acad. Sci. USA 100, 15764–15769.

Li, M.Z., & Elledge, S.J. (2007). Harnessing homologous recombination in vitro to generate recombinant DNA via SLIC. *Nat Methods* 4, 251-256.

Lin, C. H., MacGurn, J. A., Chu, T., Stefan, C. J., & Emr, S. D. (2008). Arrestin-related ubiquitin-ligase adaptors regulate endocytosis and protein turnover at the cell surface. *Cell*, *135*(4), 714–725.

Longtine, M.S., McKenzie, A., Demarini, D.J., Shah, N.G., Wach, A., Brachat, A., Philippsen, P., and Pringle, J.R. (1998). Additional modules for versatile and economical PCR-based gene deletion and modification in Saccharomyces cerevisiae. Yeast 14, 953–961.

Luhtala, N., & Odorizzi, G. (2004). Bro1 coordinates deubiquitination in the multivesicular body pathway by recruiting Doa4 to endosomes. *The Journal of Cell Biology*, *166*(5), 717–729.

MacDonald, C., Buchkovich, N.J., Stringer, D.K., Emr, S.D., and Piper, R.C. (2012). Cargo ubiquitination is essential for multivesicular body intralumenal vesicle formation. EMBO Rep.13, 331–338.

MacGurn, J. A., Hsu, P.-C., & Emr, S. D. (2012). Ubiquitin and membrane protein turnover: from cradle to grave. *Annual Review of Biochemistry*, *81*, 231–259.

Mageswaran, S. K., Johnson, N. K., Odorizzi, G., & Babst, M. (2015). Constitutively active ESCRT-II suppresses the MVB-sorting phenotype of ESCRT-0 and ESCRT-I mutants. *Molecular Biology of the Cell*, *26*(3), 554–568.

Marcusson, E. G., Horazdovsky, B. F., Cereghino, J. L., Gharakhanian, E., & Emr, S. D. (1994). The sorting receptor for yeast vacuolar carboxypeptidase Y is encoded by the VPS10 gene. *Cell*, *77*(4), 579–586.

Martin-Serrano, J., Yarovoy, A., Perez-Caballero, D., Bieniasz, P. D., & Yaravoy, A. (2003). Divergent retroviral late-budding domains recruit vacuolar protein sorting factors

by using alternative adaptor proteins. *Proceedings of the National Academy of Sciences of the United States of America*, *100*(21), 12414–12419.

Mastronarde, D.N. (1997). Dual-axis tomography: an approach with alignment methods that preserve resolution. J. Struct. Biol. 120, 343–352.

Mellman, I. (1996). Endocytosis and molecular sorting. *Annual Review of Cell and Developmental Biology*, *12*, 575–625.

Meyer, H.H., Wang, Y., Warren, G (2002). Direct binding of ubiquitin conjugates by the mammalian p97 adapter complexes, p47 and Ufd1-Npl14. *EMBO J* 21, 5645-5652.

Misra, S., Puertollano, R., Kato, Y., Bonifacino, J. S., & Hurley, J. H. (2002). Structural basis for acidic-cluster-dileucine sorting-signal recognition by VHS domains. *Nature*, *415*(6874), 933–937.

Mizuno, E., Kawahata, K., Kato, M., Kitamura, N., Komada, M. (2003). STAM proteins bind ubiquitinated proteins on the early endosome vis the VHS domain and ubiquitin-interacting motif. *Mol Biol Cell* 14, 3675-3689.

Mizuno, E., Iura, T., Mukai, A., Yoshimori, T., Kitamura, N., & Komada, M. (2005). Regulation of epidermal growth factor receptor down-regulation by UBPY-mediated deubiquitination at endosomes. *Molecular Biology of the Cell*, *16*(11), 5163–5174.

Morita, E., & Sundquist, W. I. (2004). Retrovirus budding. *Annual Review of Cell and Developmental Biology*, *20*, 395–425.

Nickerson, D. P., West, M., & Odorizzi, G. (2006). Did2 coordinates Vps4-mediated dissociation of ESCRT-III from endosomes. *The Journal of Cell Biology*, *175*(5), 715–720.

Nickerson, D. P., West, M., Henry, R., & Odorizzi, G. (2010). Regulators of Vps4 ATPase activity at endosomes differentially influence the size and rate of formation of intralumenal vesicles. *Molecular Biology of the Cell*, *21*(6), 1023–1032.

Nikko, E., & André, B. (2007). Split-ubiquitin two-hybrid assay to analyze protein-protein interactions at the endosome: application to Saccharomyces cerevisiae Bro1 interacting with ESCRT complexes, the Doa4 ubiquitin hydrolase, and the Rsp5 ubiquitin ligase. *Eukaryotic Cell*, *6*(8), 1266–1277.

Nothwehr, S. F., Ha, S. A., & Bruinsma, P. (2000). Sorting of yeast membrane proteins into an endosome-to-Golgi pathway involves direct interaction of their cytosolic domains with Vps35p. *The Journal of Cell Biology*, *151*(2), 297–310.

Obita, T., Saksena, S., Ghazi-Tabatabai, S., Gill, D. J., Perisic, O., Emr, S. D., & Williams, R. L. (2007). Structural basis for selective recognition of ESCRT-III by the AAA ATPase Vps4. *Nature*, *449*(7163), 735–739.

Odorizzi, G., Babst, M., & Emr, S. D. (1998). Fab1p PtdIns(3)P 5-kinase function essential for protein sorting in the multivesicular body. *Cell*, *95*(6), 847–858.

Odorizzi, G., Katzmann, D. J., Babst, M., Audhya, A., & Emr, S. D. (2003). Bro1 is an endosome-associated protein that functions in the MVB pathway in Saccharomyces cerevisiae. *Journal of Cell Science*, *116*(Pt 10), 1893–1903.

Olmos, Y., Hodgson, L., Mantell, J., Verkade, P., and Carlton, J.G. (2015). ESCRT-III controls nuclear envelope reformation. Nature 522, 236–239.

O'Toole, E.T., Winey, M., McIntosh, J.R., and Mastronarde, D.N. (2002). Electron tomography of yeast cells. Meth. Enzymol. 351, 81–95.

PALADE, G. E. (1955). A small particulate component of the cytoplasm. *The Journal of Biophysical and Biochemical Cytology*, *1*(1), 59–68.

Panavas, T., Serviene, E., Brasher, J., and Nagy, P. (2005). Yeast genome-wide screen reveals dissimilar sets of host genes affecting replication of RNA viruses. Proc. Natl. Acad. Sci. USA 102, 7326–7331.

Pashkova, N., Gakhar, L., Winistorfer, S. C., Sunshine, A. B., Rich, M., Dunham, M. J., et al. (2013). The yeast Alix homolog Bro1 functions as a ubiquitin receptor for protein sorting into multivesicular endosomes. *Developmental Cell*, *25*(5), 520–533.

Polo, S., Sigismund, S., Faretta, M., Guidi, M., Capua, M. R., Bossi, G., et al. (2002). A single motif responsible for ubiquitin recognition and monoubiquitination in endocytic proteins. *Nature*, *416*(6879), 451–455.

Pornillos, O., Alam, S.L., Rich, R.L., Myszka, D.G., Davis, D.R., and Sundquist, W.I. (2002). Structure and functional interactions of the TSG101 UEV domain. *EMBO J,* 21, 2397-2406.

Puertollano, R., Aguilar, R. C., Gorshkova, I., Crouch, R. J., & Bonifacino, J. S. (2001). Sorting of mannose 6-phosphate receptors mediated by the GGAs. *Science (New York, N.Y.)*, *292*(5522), 1712–1716.

Raiborg, C., Bremnes, B., Mehlum, A., Gillooly, D. J., D'Arrigo, A., Stang, E., & Stenmark, H. (2001). FYVE and coiled-coil domains determine the specific localisation of Hrs to early endosomes. *Journal of Cell Science*, *114*(Pt 12), 2255–2263.

Raymond, C. K., Howald-Stevenson, I., Vater, C. A., & Stevens, T. H. (1992). Morphological classification of the yeast vacuolar protein sorting mutants: evidence for a prevacuolar compartment in class E vps mutants. *Molecular Biology of the Cell*, *3*(12), 1389–1402.

Ren, X., Hurley, J.H. (2010). VHS domains of ESCRT-0 cooperate in high-avidity binding to polyubiquitinated cargo. *EMBO J* 29, 1045-1054.

Richter, C. M., West, M., & Odorizzi, G. (2013). Doa4 function in ILV budding is restricted through its interaction with the Vps20 subunit of ESCRT-III. *Journal of Cell Science*, *126*(Pt 8), 1881–1890.

Richter, C., West, M., & Odorizzi, G. (2007). Dual mechanisms specify Doa4-mediated deubiquitination at multivesicular bodies. *The EMBO Journal*, *26*(10), 2454–2464.

Rieder, S.E., Banta, L.M., Köhrer, K., McCaffery, J.M., and Emr, S.D. (1996). Multilamellar endosome-like compartment accumulates in the yeast vps28 vacuolar protein sorting mutant. Mol. Biol. Cell 7, 985–999.

Robinson, J. S., Klionsky, D. J., Banta, L. M., & Emr, S. D. (1988). Protein sorting in Saccharomyces cerevisiae: isolation of mutants defective in the delivery and processing of multiple vacuolar hydrolases. *Molecular and Cellular Biology*, *8*(11), 4936–4948.

Rothman, J. H., & Stevens, T. H. (1986). Protein sorting in yeast: mutants defective in vacuole biogenesis mislocalize vacuolar proteins into the late secretory pathway. *Cell*, *47*(6), 1041–1051.

Row, P. E., Liu, H., Hayes, S., Welchman, R., Charalabous, P., Hofmann, K., et al. (2007). The MIT domain of UBPY constitutes a CHMP binding and endosomal localization signal required for efficient epidermal growth factor receptor degradation. *The Journal of Biological Chemistry*, *282*(42), 30929–30937.

Row, P. E., Prior, I. A., McCullough, J., Clague, M. J., & Urbé, S. (2006). The ubiquitin isopeptidase UBPY regulates endosomal ubiquitin dynamics and is essential for receptor down-regulation. *The Journal of Biological Chemistry*, *281*(18), 12618–12624.

Różycki, B., Boura, E., Hurley, J. H., & Hummer, G. (2012). Membrane-elasticity model of Coatless vesicle budding induced by ESCRT complexes. *PLoS Computational Biology*, *8*(10), e1002736.

Sachse, M., Strous, G.J., and Klumperman, J. (2004). ATPase-deficient hVPS4 impairs formation of internal endosomal vesicles and stabilizes bilayered clathrin coats on endosomal vacuoles. J. Cell. Sci. 117, 1699–1708.

Saksena, S., Wahlman, J., Teis, D., Johnson, A. E., & Emr, S. D. (2009). Functional reconstitution of ESCRT-III assembly and disassembly. *Cell*, *136*(1), 97–109.

Samson, R.Y., Obita, T., Freund, S.M., Williams, R.L., and Bell, S.D. (2008). A role for the ESCRT system in cell division in Archaea. Science 322, 1710–1713.

Seaman, M. N. J. (2004). Cargo-selective endosomal sorting for retrieval to the Golgi requires retromer. *The Journal of Cell Biology*, *165*(1), 111–122.

Seaman, M. N. J. (2008). Endosome protein sorting: motifs and machinery. *Cellular and Molecular Life Sciences : CMLS*, *65*(18), 2842–2858.

Seaman, M. N. J. (2012). The retromer complex - endosomal protein recycling and beyond. *Journal of Cell Science*, *125*(Pt 20), 4693–4702.

Seaman, M. N., McCaffery, J. M., & Emr, S. D. (1998). A membrane coat complex essential for endosome-to-Golgi retrograde transport in yeast. *The Journal of Cell Biology*, *142*(3), 665–681.

Shen, Q.-T., Schuh, A. L., Zheng, Y., Quinney, K., Wang, L., Hanna, M., et al. (2014). Structural analysis and modeling reveals new mechanisms governing ESCRT-III spiral filament assembly. *The Journal of Cell Biology*, *206*(6), 763–777.

Sherman, F., Fink, G.R., Hick, J.B (1979). Methods in yeast genetics: A laboratory manual, Cold Spring Harbor, NY: Cold Spring Harbor Laboratory Press.

Shestakova, A., Hanono, A., Drosner, S., Curtiss, M., Davies, B. A., Katzmann, D. J., & Babst, M. (2010). Assembly of the AAA ATPase Vps4 on ESCRT-III. *Molecular Biology of the Cell*, *21*(6), 1059–1071.

Shields, S. B., Oestreich, A. J., Winistorfer, S., Nguyen, D., Payne, J. A., Katzmann, D. J., & Piper, R. (2009). ESCRT ubiquitin-binding domains function cooperatively during MVB cargo sorting. *The Journal of Cell Biology*, *185*(2), 213–224.

Shih, S.C., Katzmann, D.J., Schnell, J.D., Sutano, M., Emr, S.D., Hicke, L. (2002). Epsins and Vps27/Hrs contain ubiquitin-binding domains that function in receptor endocytosis. *Nat Cell Biol* 4, 389-393.

Shim, S., Kimpler, L. A., & Hanson, P. I. (2007). Structure/function analysis of four core ESCRT-III proteins reveals common regulatory role for extreme C-terminal domain. *Traffic (Copenhagen, Denmark)*, *8*(8), 1068–1079.

Slagsvold, T., Aasland, R., Hiranos, S., Bache, K.G., Raiborg, C., Trambaiolo, D., Wakatsuki, S., Stenmark, H (2005) Eap45 in mammalian ESCRT-II binds ubiquitin via a phosphoinositide-interacting GLUE domain. *J Biol Chem* 280, 19600-19606.

SOTELO, J. R., & PORTER, K. R. (1959). An electron microscope study of the rat ovum. *The Journal of Biophysical and Biochemical Cytology*, *5*(2), 327–342.

Spormann, D.O., Heim, J., and Wolf, D.H. (1992). Biogenesis of the yeast vacuole (lysosome). The precursor forms of the soluble hydrolase carboxypeptidase yscS are associated with the vacuolar membrane. J. Biol. Chem. 267, 8021–8029.

Stahelin, R. V., Long, F., Diraviyam, K., Bruzik, K. S., Murray, D., & Cho, W. (2002). Phosphatidylinositol 3-phosphate induces the membrane penetration of the FYVE domains of Vps27p and Hrs. *The Journal of Biological Chemistry*, *277*(29), 26379–26388.

Strack., B., Calistri, A., Craig, S., Popova, E., & Gottlinger, H.G. (2003). AIP1/ALIX is a binding partner for HIV-1 p6 and EIAV p9 functioning in virus budding. *Cell*, 114, 689-699.

Stuchell-Brereton, M. D., Skalicky, J. J., Kieffer, C., Karren, M. A., Ghaffarian, S., & Sundquist, W. I. (2007). ESCRT-III recognition by VPS4 ATPases. *Nature*, *449*(7163), 740–744.

Swaminathan, S., Amerik, A. Y., & Hochstrasser, M. (1999). The Doa4 deubiquitinating enzyme is required for ubiquitin homeostasis in yeast. *Molecular Biology of the Cell*, *10*(8), 2583–2594.

Tan, S. (2001). A modular polycistronic expression system for overexpressing protein complexes in Escherichia coli. Protein Expr. Purif. 21, 224–234.

Tang, S., Buchkovich, N. J., Henne, W. M., Banjade, S., Kim, Y. J., & Emr, S. D. (2016). ESCRT-III activation by parallel action of ESCRT-I/II and ESCRT-0/Bro1 during MVB biogenesis. *eLife*, *5*, e15507.

Tang, S., Henne, W. M., Borbat, P. P., Buchkovich, N. J., Freed, J. H., Mao, Y., et al. (2015). Structural basis for activation, assembly and membrane binding of ESCRT-III Snf7 filaments. *eLife*, *4*, e12548.

Teis, D., Saksena, S., & Emr, S. D. (2008). Ordered assembly of the ESCRT-III complex on endosomes is required to sequester cargo during MVB formation. *Developmental Cell*, *15*(4), 578–589.

Teis, D., Saksena, S., Judson, B. L., & Emr, S. D. (2010). ESCRT-II coordinates the assembly of ESCRT-III filaments for cargo sorting and multivesicular body vesicle formation. *The EMBO Journal*, *29*(5), 871–883.

Temkin, P., Lauffer, B., Jäger, S., Cimermancic, P., Krogan, N. J., & Zastrow, von, M. (2011). SNX27 mediates retromer tubule entry and endosome-to-plasma membrane trafficking of signalling receptors. *Nature Cell Biology*, *13*(6), 715–721.

Teo, H., Gill, D. J., Sun, J., Perisic, O., Veprintsev, D. B., Vallis, Y., et al. (2006). ESCRT-I core and ESCRT-II GLUE domain structures reveal role for GLUE in linking to ESCRT-I and membranes. *Cell*, *125*(1), 99–111.

Teo, H., Perisic, O., González, B., & Williams, R. L. (2004). ESCRT-II, an endosome-associated complex required for protein sorting: crystal structure and interactions with ESCRT-III and membranes. *Developmental Cell*, *7*(4), 559–569.

Vietri, M., Schink, K. O., Campsteijn, C., Wegner, C. S., Schultz, S. W., Christ, L., et al. (2015). Spastin and ESCRT-III coordinate mitotic spindle disassembly and nuclear envelope sealing. *Nature*. 522, 231-235.

von Schwedler, U.K., Stuchell, M., Muller, B., Ward, D.M., Chung, H.Y., Morita, E., Wang, H.E., et al. (2003). The protein network of HIV budding. *Cell*, 114, 701-713.

Wang, X., Diaz, A., Hao, L., Gancarz, B., den Boon, J.A., and Ahlquist, P. (2011). Intersection of the multivesicular body pathway and lipid homeostasis in RNA replication by a positive-strand RNA virus. J. Virol. 85, 5494–5503.

Webster, B. M., Colombi, P., Jäger, J., & Lusk, C. P. (2014). Surveillance of nuclear pore complex assembly by ESCRT-III/Vps4. *Cell*, *159*(2), 388–401.

Wemmer, M., Azmi, I., West, M., Davies, B., Katzmann, D., & Odorizzi, G. (2011). Bro1 binding to Snf7 regulates ESCRT-III membrane scission activity in yeast. *The Journal of Cell Biology*, *192*(2), 295–306.

Wollert, T., & Hurley, J. H. (2010). Molecular mechanism of multivesicular body biogenesis by ESCRT complexes. *Nature*, *464*(7290), 864–869.

Wollert, T., Wunder, C., Lippincott-Schwartz, J., & Hurley, J. H. (2009). Membrane scission by the ESCRT-III complex. *Nature*, *458*(7235), 172–177.